TOPICAL REVIEW • OPEN ACCESS

Graphene related materials for thermal management

To cite this article: Yifeng Fu *et al* 2020 *2D Mater.* **7** 012001

2D Materials

OPEN ACCESS

TOPICAL REVIEW

Graphene related materials for thermal management

RECEIVED
13 June 2019

REVISED
21 August 2019

ACCEPTED FOR PUBLICATION
27 September 2019

PUBLISHED
22 October 2019

Yifeng Fu[1], Josef Hansson[1], Ya Liu[1,2], Shujing Chen[3], Abdelhafid Zehri[1], Majid Kabiri Samani[1], Nan Wang[4], Yuxiang Ni[5], Yan Zhang[3], Zhi-Bin Zhang[6], Qianlong Wang[7], Mengxiong Li[2], Hongbin Lu[2], Marianna Sledzinska[8], Clivia M Sotomayor Torres[8,9], Sebastian Volz[10], Alexander A Balandin[11], Xiangfan Xu[12] and Johan Liu[1,3]

[1] Electronics Materials and Systems Laboratory, Department of Microtechnology and Nanoscience (MC2), Chalmers University of Technology, SE-412 96 Göteborg, Sweden
[2] State Key Laboratory of Molecular Engineering of Polymers, Department of Macromolecular Science, Collaborative Innovation Center of Polymers and Polymer Composites, Fudan University, 2005 Songhu Road, Shanghai 200433, People's Republic of China
[3] SMIT Center, School of Mechatronics Engineering and Automation, Shanghai University, Shanghai 200444, People's Republic of China
[4] SHT Smart High Tech AB, Kemivägen 6, SE-412 58, Gothenburg, Sweden
[5] School of Physical Science and Technology, Southwest Jiaotong University, 610031, Chengdu, People's Republic of China
[6] Division of Solid-State Electronics, Department of Engineering Sciences, Uppsala University, SE-751 21, Uppsala, Sweden
[7] Shenzhen Shen Rui Graphene Technology Co., Ltd, Huike Industrial Park, Baoan District, Shenzhen, People's Republic of China
[8] Catalan Institute of Nanoscience and Nanotechnology (ICN2), CSIC and BIST, Campus UAB, Bellaterra, Barcelona, 08193, Spain
[9] ICREA-Institucio Catalana de Recerca i Estudis Avancats, E-08010 Barcelona, Spain
[10] Laboratory for Integrated Micro-Mechatronic Systems LIMMS/CNRS-IIS(UMI2820), Institute of Industrial Science, The University of Tokyo, 4-6-1 Komaba, Meguro-ku, Tokyo, 153-8505, Japan
[11] Nano-Device Laboratory, Department of Electrical and Computer Engineering, Materials Science and Engineering Program, University of California, Riverside, California 92521, United States of America
[12] Center for Phononics and Thermal Energy Science School of Physics Science and Engineering, Tongji University, Shanghai 200092, People's Republic of China

E-mail: yifeng.fu@chalmers.se, johanliu@shu.edu.cn and xuxiangfan@tongji.edu.cn

Keywords: graphene, 2D materials, thermal management, material fabrication, thermal characterization

Abstract

Almost 15 years have gone ever since the discovery of graphene as a single atom layer. Numerous papers have been published to demonstrate its high electron mobility, excellent thermal and mechanical as well as optical properties. We have recently seen more and more applications towards using graphene in commercial products. This paper is an attempt to review and summarize the current status of the research of the thermal properties of graphene and other 2D based materials including the manufacturing and characterization techniques and their applications, especially in electronics and power modules. It is obvious from the review that graphene has penetrated the market and gets more and more applications in commercial electronics thermal management context. In the paper, we also made a critical analysis of how mature the manufacturing processes are; what are the accuracies and challenges with the various characterization techniques and what are the remaining questions and issues left before we see further more applications in this exciting and fascinating field.

Contents

1. Introduction 2
2. Basic theory of thermal transport 4
3. Materials development 4
3.1. Graphene based heat spreaders 4
3.1.1. Mono- and few-layer graphene based heat spreader 5
3.1.2. Graphene film as heat spreader 6
3.1.3. LPE graphene based heat spreader 8
3.2. Graphene enhanced thermal composites 11
3.3. Graphene fibers 13
3.4. Graphene laminates 13
3.5. Graphene based 3D structures 14
3.5.1. Graphene foam 14
3.5.2. Vertically aligned graphene sheets 15
3.5.3. Hybrid graphene structures 15
3.6. Graphene nanofluids 15

3.7. Other 2D materials 17
3.8. Summary 19
4. Modeling of thermal transport in graphene 19
4.1. Molecular dynamics simulations of interfacial thermal resistance involving graphene 20
4.1.1. The impact of graphene layer number 20
4.1.2. The effects of interfacial coupling and substrate property 22
4.1.3. The effects of doping on graphene thermal performance 24
4.2. Functionalization of graphene to increase heat spreading performances 24
5. Thermal characterization 25
5.1. Thermal bridge 25
5.2. Electron beam self-heating method 26
5.3. Scanning thermal microscopy 27
5.4. Optothermal Raman spectroscopy 28
5.5. Pulsed photothermal reflectance 29
5.6. Dependence of resistance on temperature 30
5.7. Joule heating 30
5.8. 3ω method 31
5.9. Transient plane source 31
5.10. Laser flash 31
5.11. Summary 33
6. Current and future potential applications 34
7. Concluding remarks 34
References 35

1. Introduction

Thermal management and heat dissipation are generic problems that exist in many large power and heat exchange systems. Intensive heat density has been observed not at least in the electronics systems. The heart of the electronics sector, i.e. the semiconductor industry has followed Moore's law since 1965. In the past decades, chip manufacturers have been increasing the number of transistors with shrinked size to achieve higher component density and clock frequency. The pursuing for high performance dramatically increased power consumption in integrated circuits, which led to great challenge on heat dissipation in electronics systems. In recent years, Moore's law has slowed down and is expected to hit the wall very soon due to the physical limits imposed by quantum effect. Instead of further miniaturization of transistors, multi-core design has been proposed and applied to continue the performance evolution. This will release the stress on thermal management to some extend but the problem of non-uniform local over-heating inside chips remains unsolved. For instance, heat flux at local hotspots has exceeded 1000 W cm^{-2} in insulated gate bipolar transistors (IGBT) [1] which is a big threat to the reliability of the component and will significantly shorten their lifetime.

2D materials are a group of materials possessing layered structures with a thickness of a few atoms. The most representative 2D material is graphene, which was mechanically exfoliated for the first time by Novoselov *et al*, using Scotch tape [2]. Graphene consists of carbon atoms bonded in a hexagonal lattice and exhibits unique structural, electrical, thermal, mechanical and chemical properties [3–5], therefore it has become one of the hottest research fields for various applications in both academia and industry. For instance, a record high electron mobility of 3×10^7 cm^2 V^{-1} s^{-1} has been theoretically predicted for graphene [6] and a mobility of 350 000 cm^2 V^{-1} s^{-1} has been experimentally reported from chemical vapor deposition (CVD)-grown graphene [7], which could meet the requirement of high-end electronic devices. The extremely strong yet flexible feature of graphene also holds the promise of many demanding applications such as sport equipments [8, 9], flexible batteries [10, 11], solar cells [12–14], etc. With the rise of graphene, other 2D materials also attracted great interest for potential applications in electronics [15–17].

Among the unique properties of graphene and related 2D materials, their high thermal conductivity [18–25] shows great potential to address the thermal management challenge in electronics systems. Taking graphene for example, the first measurements of suspended graphene using optothermal Raman technique by Balandin *et al* (as shown in figure 1) revealed that the thermal conductivity values substantially exceeding that of the bulk graphite which is ~2000 W m^{-1} K^{-1} at room temperature (RT) [18, 19]. Independent follow-up measurements confirmed this conclusion [20, 26, 27]. Ruoff *et al* used the optothermal method to measure the suspended monolayer graphene with various sizes in vacuum and gaseous environments [20, 26], and they found that the thermal conductivity values range from (2.6 ± 0.9) to $(3.1 \pm 1.0) \times 10^3$ W m^{-1} K^{-1} near 350 K. Yoon *et al* used the thermal microscopy with improved signal-to-noise ratio to measure the thermal conductivity of residue-free graphene and obtained thermal conductivity values range from 2430 ± 190 to 2100 ± 160 W m^{-1} K^{-1} for suspended graphene bridges at 335–366 K [27]. The intriguing thermal properties of graphene were explained by the specifics of the long-wavelength phonon transport in 2D crystal lattices [19, 21, 28]. The long-wavelength phonons in graphene have exceptionally long mean free path which is limited by the size of the sample even if the thermal transport is diffusive [19, 29]. The latter can be explained by noting that the three-phonon Umklapp scattering alone is not suffcient for restoration of the thermal equilibrium in 2D crystal lattice unlike in 3D crystal lattices [30]. One of the implications of this effect is an anomalous dependence of the thermal conductivity of few-layer graphene with the number of atomic planes in the samples [21, 28, 31].

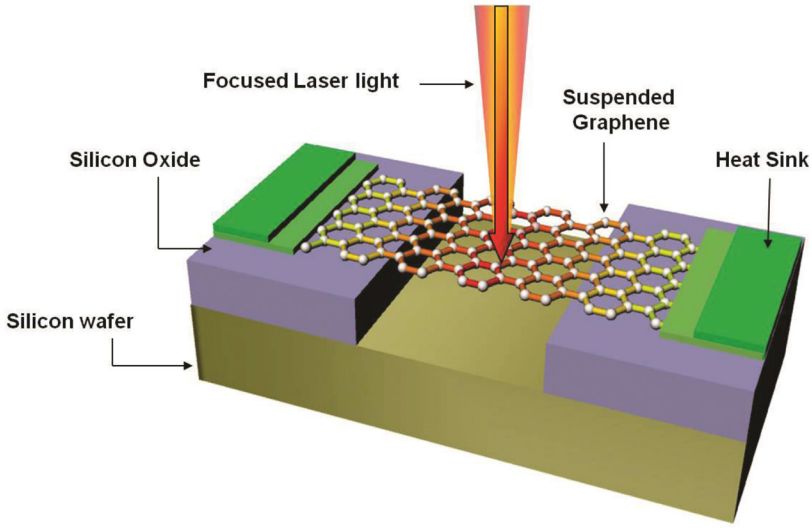

Figure 1. Illustration of the first measurement of the thermal conductivity of graphene using the Raman optothermal method. Reproduced with permission from [19], © Nature Publishing Group.

Other interesting features of phonon thermal conduction in graphene include non-monotonic dependence on the ribbon width [32], and strong isotope and point-defect scattering [33].

The exceptional thermal properties of graphene coupled with its flexibility motivated extensive research on its derivatives, including graphene oxide, graphene films, graphene fibers, graphene foams, graphene laminates, graphene thermal interface materials (TIMs), etc, for thermal management applications. Various composites in which graphene and its derivatives play a role of fillers [34–38] have been developed. A mixture of liquid phase exfoliated (LPE) graphene and few-layer graphene flakes perform excellently as fillers in thermal pastes [34, 35] and thermal phase change materials [39]. Graphene is a better filler than carbon nanotubes (CNTs) in thermal composites owing to its excellent thermal coupling to matrix materials and substantially lower cost. Meter-sized graphene films fabricated from exfoliated graphene flakes in suspension exhibited excellent thermal performance and showed great potential as heat spreaders [40–42].

Another 2D material which is very promising for thermal management is boron nitride (BN), which has similar lattice to graphene but with boron and nitride atoms alternatively arranged in the hexagon structure (hBN). Theoretically, hBN possesses high thermal conductivity up to 1700–2000 W m^{-1} K^{-1} [43], so it has been used to develop TIMs [44–49] and heat spreaders [50–52]. More importantly, hBN is an electrical-insulating material which makes it a strategically important and very good complementary to graphene and their derivatives where electrical conduction is not allowed.

In this paper, we will review the recent progress on thermal management using graphene based materials as well as other 2D materials such as hBN. The fundamental heat transfer mechanisms will briefly be introduced first. After that, various graphene constellations including its derivatives and related 2D materials demonstrated for thermal management applications will be reviewed and summarized in detail. Theoretical analysis on the performance of the thermal management materials will be compared and summarized to understand the phonon and thermal transport in the 2D material systems. In addition, different thermal characterization methods applied for these materials will be presented and their advantages and limits as well as accuracies will be summarized and commented. At the end of this review, the challenges and opportunities to use graphene and other 2D materials for thermal management will be discussed and commented.

2. Basic theory of thermal transport

Heat conduction is realized by the collision of microscopic particles and movement of heat carriers in matters. In a material, heat conduction is governed by Fourier's law, as expressed below:

$$q = -\kappa \cdot \nabla T \tag{1}$$

where q is the local heat flux with an unit of W m^{-2}, κ is thermal conductivity of the material with an unit of W m^{-1} K^{-1}, and ∇T is the local temperature gradient with an unit of K m^{-1}. The Fourier's law describes how efficiently heat can be conducted from a high temperature region to a low temperature region in a material. However, for thermal management in electronics where heat has to be conducted through different materials across contact interfaces, thermal resistance is commonly applied to evaluate the efficiency of thermal transport because it is additive and convenient to measure. The thermal resistance is calculated by:

$$R = \frac{\Delta T}{Q}. \tag{2}$$

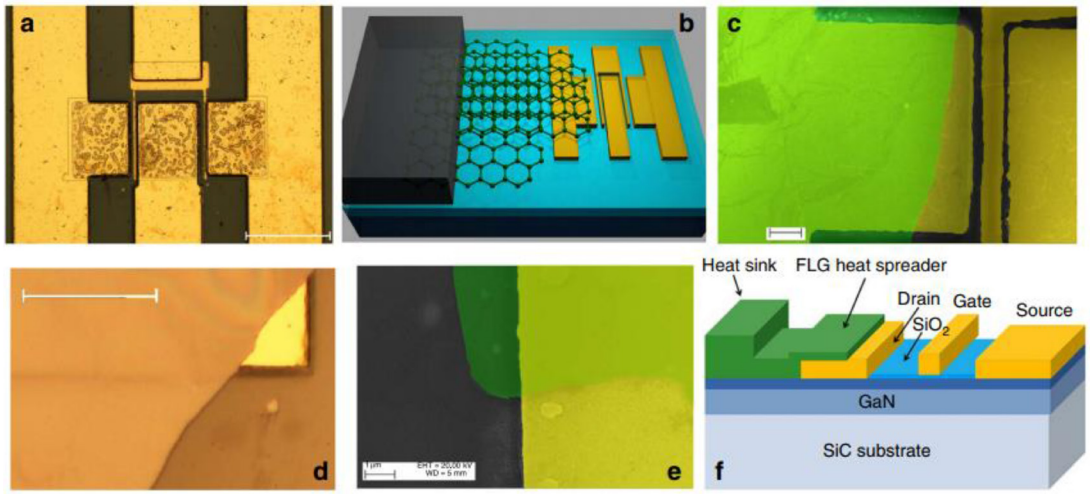

Figure 2. Graphene quilt as heat spreader for AlGaN/GaN HFETs. (a) Optical image of the AlGaN/GaN HFETs before placing the graphene heat spreader. (b) Schematic of the FLG heat spreader placed on the drain contact of the AlGaN/GaN HFET. (c) SEM image of the graphene heat spreader transferred onto the drain contact. (d) Optical image of the graphene quilt overlapping the metal drain contact and the GaN substrate. (e) SEM image of the heat spreader-metal contact region and GaN surface. (f) Schematic of the graphene quilt and the device structure. The scale bars are 100 μm in (a) and (d). The scale bars are 10 μm and 1 μm in (c) and (e), correspondingly. (a)–(f) Are reproduced with permission from [62], © Nature Publishing Group.

In equation (2), ΔT is the temperature difference (K) between two surfaces and Q is the thermal energy (W) conducted between these two surfaces. The total thermal resistance R consists of thermal resistance of the materials along the heat conduction path which is dependent on the thermal conductivity and thickness of the materials, and the contact resistance at the interface of two different materials which is dependent on many factors including bonding pressure, surface roughness, surface cleanliness, etc.

In order to improve the heat dissipation from electronics systems to the ambient, high thermal conductivity of materials, small material thickness and efficient interaction at material interfaces are desired. Different from material thickness and interfacial conditions that can be engineered in specific applications, thermal conductivity is the intrinsic property of a material which is dependent on the transport of electrons and phonons. In 2D materials where free electrons are limited, the heat conduction is dominated by phonons. It is also noticed that thermal conductivity in a 2D material varies significantly in different directions due to their anisotropic atomic structures [53, 54]. In the x-y plane, atoms interact with each other through covalent bonding so the in-plane thermal conductivity is very high, whereas in the z-direction van der Waals force (which is very weak) governs the inter-layer interaction therefore the through-plane thermal conductivity of 2D materials is normally very low [19].

3. Materials development

In this section, we will comment and summarize the state of the art of the graphene based materials in different forms and configurations as they contribute with enhancement of thermal conductivity in different ways.

3.1. Graphene based heat spreaders

Heat spreader plays a key role in thermal management in, for instance, electronics systems. It enables much bigger surface area than the original surface on components for heat exchange, therefore dramatically facilitating the heat dissipation to cool down electronics systems. Traditional heat spreaders are typically made of metals such as aluminum and copper which are quite heavy [55, 56]. The 2D structure and huge surface-to-volume ratio make graphene and related 2D materials ideal candidates as heat spreaders.

3.1.1. Mono- and few-layer graphene based heat spreader

The in-plane thermal conductivity of exfoliated and suspended graphene has been reported as high as 2000–5300 W m^{-1} K^{-1} in the literature [18, 19, 23, 29, 34, 57]. The values are comparable to CNTs [19, 58, 59], as well as higher than the values reported for graphite [60] and diamond [61]. Balandin *et al* demonstrated the first graphene based heat spreader using few-layer graphene mechanically exfoliated from highly oriented pyrolytic graphite (HOPG) [62]. The graphene-graphite quilts were firstly exfoliated and then transferred onto SiC substrates to cool down high-power GaN transistors as shown in figure 2. Results showed that temperature at the hotspots can be lowered by ~20 °C when the transistor was operating at ~13 W mm^{-1} which can be translated into a heat density of about 250 W cm^{-2}. This indicates that the graphene enhanced structure here as the hotspot could extend the lifetime of the device by an order-of-magnitude. Further modeling results indicated

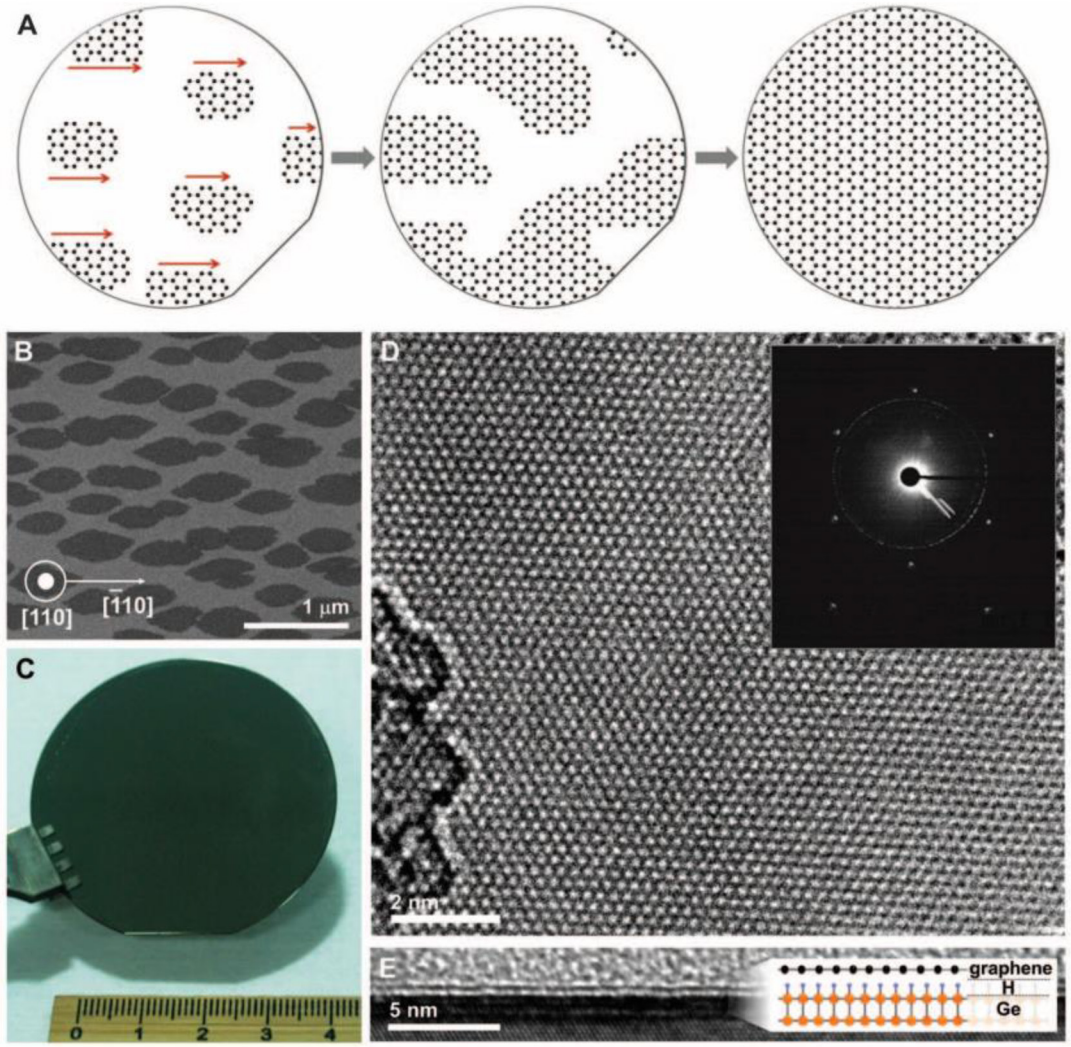

Figure 3. Single-crystal monolayer graphene grown on Ge surface [73]. (A) Schematic of single-crystal monolayer graphene grown from unidirectionally aligned multiple seeds. (B) A typical SEM image of graphene seeds at the early stage of growth. (C) A photograph of graphene grown on a 5.08 cm Ge/Si wafer. (D) A HR-TEM image of the single-crystal monolayer graphene. (Inset) Four overlaid SAED patterns. (E) A cross-sectional TEM image demonstrating that the as-grown graphene is monolayer. (Inset) A schematic illustration of the monolayer graphene grown on the H-terminated Ge surface. Reproduced with permission from [73].

that the efficiency of the graphene heat spreader is dependent on the device structure and geometry [63]. Gao *et al* used CVD method to grow mono- and few-layer graphene as heat spreader [64, 65]. It was found that the hotspot with a heat flux of 430 W cm^{-2} on Si chips can be cooled down by ~13 °C (from 121 °C to 108 °C) using mono-layer graphene as a heat spreader, whereas multi-layer graphene can only cool down the hotspot by ~8 °C. This is attributed to the smaller grain size of graphene grown on Ni foils than those grown on Cu foils, which resulted to more grain boundaries and consequently lower thermal performance of the graphene material. Bae *et al* used multi-layer graphene grown on Ni surface as heat spreaders on flexible substrates [66]. Results showed that graphene based heat spreader brings more uniform temperature distribution on the substrate compared to gold based heat spreaders. Shih *et al* used mono-layer graphene grown from CVD method to cool down a photonic crystal (PhC) cavity [67]. Experimental results showed that the graphene heat spreader can lower the PhC cavity by 45 K under an optical power of 100 μW. CVD graphene was also applied by Lee *et al* to cool down GaAs/InGaAs/InGaP collector-up heterojunction bipolar transistors, where 30% reduction of thermal resistance was observed [68].

Compared to the mechanically exfoliated graphene, the CVD method to grow graphene is becoming more and more mature so the CVD graphene based heat spreader shows better process scalability and compatibility [69–71]. On the other hand, graphene synthesized from CVD method contains much more defects and grain boundaries (i.e. domain size is much smaller) in its crystalline structure and therefore exhibits lower thermal conductivity than their mechanically exfoliated counterparts [19]. Lee *et al* reported that thermal conductivity values of suspended CVD graphene are around 2660, 1890, and 680 W m^{-1} K^{-1} for average grain sizes of 4.1, 2.2, and 0.5 μm, respectively [72], showing clear dependence of

Table 1. Comparison between material fabrication processes and thermal properties of GFs.

Assembled structures	Raw material	Exfoliation /dispersion methods	Film formation methods	Heat treatment (°C)	Thermal conductivity (W m^{-1} K^{-1})	Ref
Graphene film	GO	Not mentioned	Self-assembling	1000	60	[90]
Graphene film	GO	Ultrasonication	Vacuum filtration	1200	1043.5	[82]
Graphene film	GO	Ultrasonication	Self-assembling	2000	1100	[91]
Graphene film	Graphene	Ball-milling	Vacuum filtration	2850	1434	[92]
Graphene film	Thermally exfoliated graphene	Ultrasonication	Electro-spray deposition	2850	1434	[85]
Graphene film	Graphite oxide	Not mentioned	Self-assembling	3000	1950	[93]
Graphene film	GO	Shear mixing	Self-assembling	2850	3214	[40]

thermal conductivity on graphene grain size. In addition, fitting data showed that the thermal conductivity of suspended single-crystal graphene is around 5500 W m^{-1} K^{-1} which is very close to mechanically exfoliated graphene [72].

The limitation from crystalline defects in CVD grown graphene is being addressed by recent advances in material synthesis. In the past few years, great progress has been achieved on CVD graphene, large grain size up to wafer level single crystal graphene has been reported. For instance, Lee *et al* successfully grown single-crystal mono-layer graphene on Ge substrate without any wrinkles [73], as shown in figure 3. Due to the extremely weak interaction between graphene and the underlying Ge surface, etch-free dry transfer of the graphene was realized which makes it possible to recycle the Ge substrate for continual graphene growth. This method requires complex preparation of the substrate, for instance the single-crystal Ge underlayer has to be epitaxially grown on Si substrate prior to the graphene growth. Recently, fast growth of large single-crystal graphene has been reported [74–79]. For instance, Wu *et al* [74] realized fast growth of inch-sized single-crystal graphene on CuNi alloy substrates, 1.5-inch large graphene mono-layer can be grown in 2.5 h using locally feeding carbon precursors at a single nucleation site. Lin *et al* also reported the growth of super-clean graphene with enhanced optical, electrical and thermal properties [80].

The progress in CVD technology pushed the graphene heat spreader closer towards practical application. However, other challenges such as handling of CVD graphene at industry scale, process compatibility, and limited total thermal energy that mono-layer and few-layer graphene can conduct are still obstacles to be removed before CVD graphene can be applied as heat spreaders in industry [62, 64].

3.1.2. *Graphene film as heat spreader*

Although the thermal conductivity of suspended graphene is very high at RT, the in-plane thermal conductivity of graphene decreases significantly when it is in contact with a substrate [53]. For instance, the in-plane thermal conductivity of SLG supported on amorphous silicon dioxide (SiO_2) was found to be ~600 W m^{-1} K^{-1} at RT owing to phonon coupling and scattering [23, 84]. Due to this and the limitations mentioned above, graphene films (GFs) assembled from chemically or thermally exfoliated graphene sheets were developed as new heat dissipation materials.

Many different assembly processes have been developed, such as vacuum filtration [82–84], electrospinning [85], wet-spun method [42], dip coating [86], inkjet printing [87], and spin coating [88]. The assembling mechanisms of graphene or graphene oxide (GO) flakes are based on different physical and chemical interactions among flakes, such as Van der Waals force and hydrogen bonds. During the flake assembly, individual particles can be spontaneously or passively aligned to form well-oriented layer structures. For example, the evaporation of GO suspensions leads to a phase change of GO from random to liquid crystal at gas–liquid interfaces, which provides the driving force to form film structures [89].

The reported thermal performance of GFs varied widely depending on different fabrication methods [40, 82–93]. As shown in table 1, the in-plane thermal conductivity values of most fabricated GFs are below 1500 W m^{-1} K^{-1}, which are much lower than that of the commercial pyrolytic graphite sheets (PGS) with the highest value of 1950 W m^{-1} K^{-1}.

The poor thermal conductivity of GF is strongly related to the structural defects both at atomic level and microscale. Previous studies have revealed that the heat conduction in graphene is essentially governed by phonon transport inside the sp^2 bonded hexagonal carbon lattice [94–96]. Molecular dynamics (MD) simulation has shown that the thermal conductivity of graphene can be reduced by 90% with oxygen content of 5% [94]. Therefore, a high crystallinity and large grain size of graphene is critical for achieving GFs with outstanding thermal conductivities along the in-plane direction. To restore the crystallinity of graphene, different approaches have been reported, including chemical and thermal reductions to get rid of oxygen in the materials. For example, GFs were treated by different chemical reducing agents, such

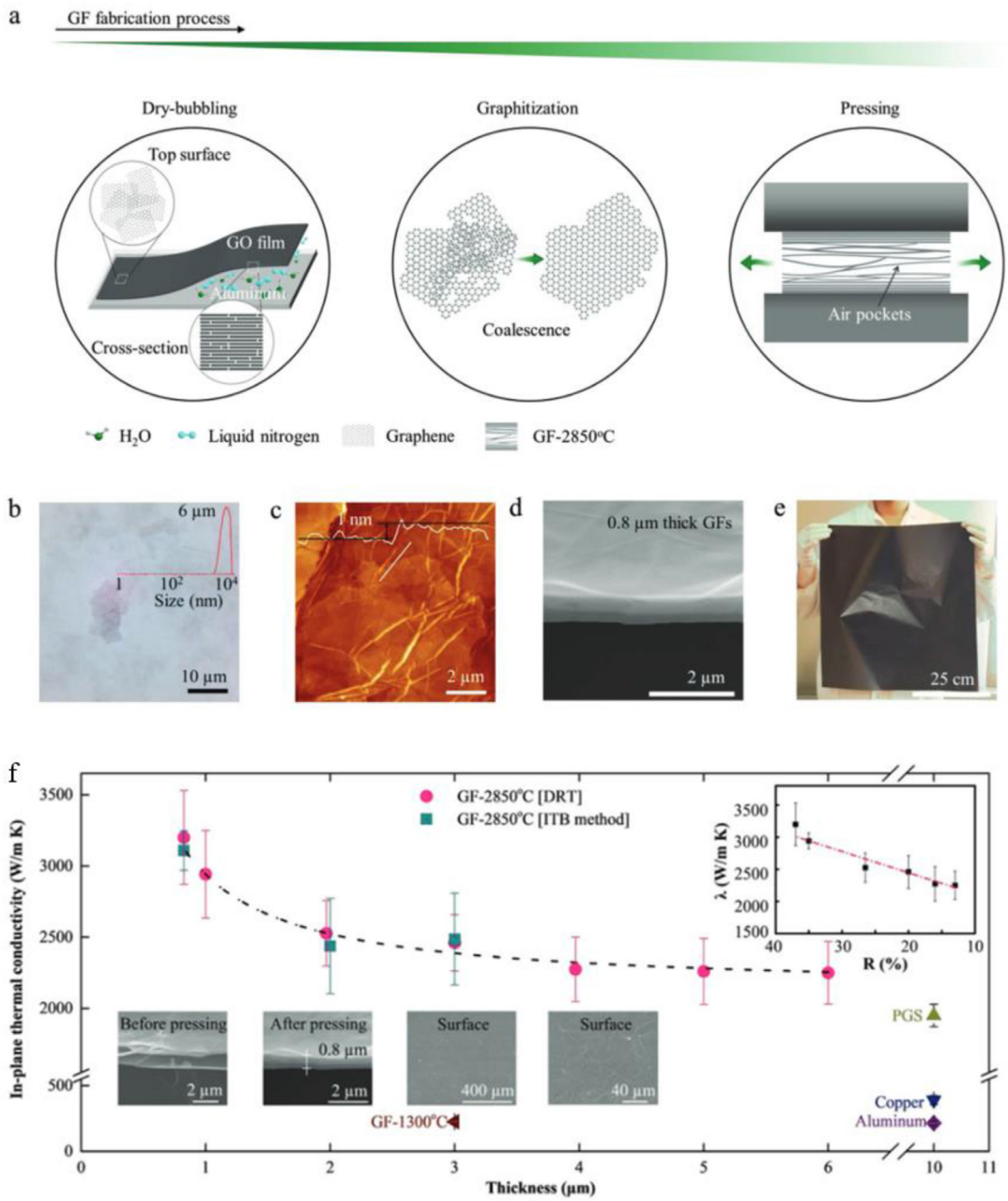

Figure 4. Fabrication process of GFs. (a) Sketch of the fabrication process. (b) Optical image of GO flakes with an average size of about 6 μm. (c) AFM image of GO flakes with a thickness of less than 1 nm. (d) SEM image of cross-section of the fabricated GFs. (e) Optical image of the fabricated large-area GFs. (f) In-plane thermal conductivity of GFs before and after pressing after annealing under 2850 °C. Reproduced with permission from [40].

as L-ascorbic acid [97] and hydroiodic acid [98, 99]. Thermal annealing at the carbonization temperature of 1300 °C [82, 90, 100] and the graphitization temperature of 2200 °C [85] have also been reported for reduction. The quality of GFs varies a lot depending on the reduction process. It has been widely accepted that high temperature annealing of GFs above 2000 °C enables defect healing and improves the crystallinity in graphene materials [101, 102]. By careful control of the graphitization temperature and pressure, it is possible to achieve similar thermal conductivity of GFs as in PGS [40]. In spite of all the merits of high temperature annealing, there are also some issues in the GF annealing process that need to be addressed. For instance, the decomposition of oxygen groups leads to the formation of CO_2 or CO gases which can increase the layer distance and even forms air pockets (as shown in figure 4) that will decrease the alignment of graphene flakes in the film [40].

Currently, the advantages of high temperature annealed GFs is not obvious as compared to PGS. To further improve the thermal conductivity of GFs, structural optimization becomes highly essential, such as improving grain size, achieving good alignment, fabricating large and smooth structures and reducing the interlayer binding energy. A recent study concluded that the increase in grain size from ~200 nm to ~10 μm leads to an exponentially increased thermal con-

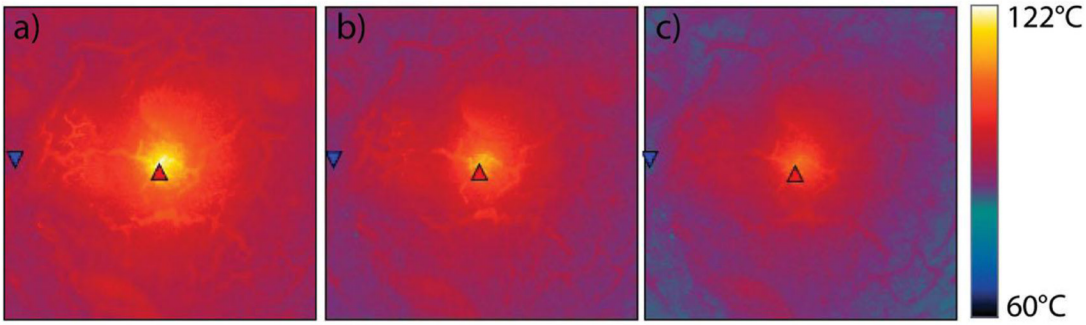

Figure 5. Infrared images of the chip surface. (a) Temperature distribution on the bare chip. (b) Temperature distribution on the chip with graphene heat spreader but without FGO. (c) Temperature distribution on the chip with graphene heat spreader and FGO. Reproduced with permission from [110].

ductivity of graphene from ~610 to ~5230 W m^{-1} K^{-1} [103]. A large grain size can greatly benefit the transfer of low-frequency ballistic phonons inside the grain as well as their good transmittance across the grain boundaries, thereby leading to the ultrahigh in-plane thermal conductivity of GF. The thermal conductivity of GFs is also dependent on the lattice structure of graphene layers at the through-plane direction. Phonon interfacial scattering among graphene layers is the main roadblock to the improvement of thermal conductivity. Previous studies showed that changing the order of graphite from AB Bernal stacking graphene to turbostratic-stacking graphene led to an obvious decrease of interlayer binding energy [104], which can significantly decrease the phonon interfacial scattering and benefit the heat transfer at the in-plane direction [105]. A recent study proved this theory and showed that thermal conductivity of GFs had significant improvement up to 3200 W m^{-1} K^{-1} with the presence of 37% of turbostratic-stacking graphene.

In addition, the assembling methods of GFs give more flexibility to design the film structure compared to the fabrication of PGS. For example, the thickness of commercial PGS is limited within 10–100 μm which gives fewer choices for customers. For GFs, different thicknesses from a few hundreds of nanometers up to millimeters can be realized easily, which can meet all kinds of requirements from different applications ranging from microelectronics to military and space exploration. In addition, commercial PGSs have gradually decreased densities when the film thickness increases. Previous studies about the polyimide (PI) pyrolytic process also reported that the orientation of graphite layer texture became much worse in the case of thick PGS (above 25 μm) due to the increased amount of curvatures and layer misfit [106]. Therefore, the thickness of PGS fabricated in industry is usually limited within 25 μm when the film density reaches to 2.1 g cm^{-3} to get a well-oriented graphite layer texture. Different from the PGS, the GFs are preassembled by individual GO sheets and have much better orientations in the horizontal direction. Therefore, the thickness increase would not lead to the increase of layer misfit in GFs. The well-oriented graphene layer structure and high density of GFs contributes significantly to a much higher thermal conductivity than that of PGS when the thickness is more than 25 μm.

The scientific question that still needs to be addressed is whether we can further increase the thermal conductivity of graphene film towards even higher values. Theoretical study indicates that in a perfect and defect-free structure, thermal conductivity of graphene can reach close to 10 000 W m^{-1} K^{-1} [107]. It seems that careful control of the turbostratic state, defect and wrinkle free and well aligned structures together with large grain size are the right strategy to push the thermal conductivity of graphene film even higher.

3.1.3. LPE graphene based heat spreader

Liquid phase exfoliation (LPE) is a very important complementary to tape assisted mechanical exfoliation, CVD, and sublimation method to produce graphene in suspension form. The method starts from graphite particles and allows large scale production of graphene at low cost. Therefore, it holds the promise of many applications including coating, composites, inks, fibers, heat spreading materials, etc. There are two types of LPE process, one is pure mechanical exfoliation in liquid using shear or nominal forces, e.g. by sonication, to overcome the van der Waals force in graphite to directly produce pristine graphene flakes. The other involves chemical reaction during the exfoliation, that means the graphite particles are firstly expanded and oxidized and then exfoliated to produce graphene oxide (GO) suspension which can be subsequently reduced to generate so called reduced graphene oxide (rGO). Most LPE processes reported today are originated from Hummer's method [108] with modifications such as using different oxidants and temperature to make the production process safer and more environmental friendly. Compared to the pure mechanical exfoliation in liquid, the production of graphene from reduced GO flakes has advantages of large lateral size, good dispersibility, and large-scale industrial productivity but suffers from more defects in the graphene lattice and more impurities in the graphene material.

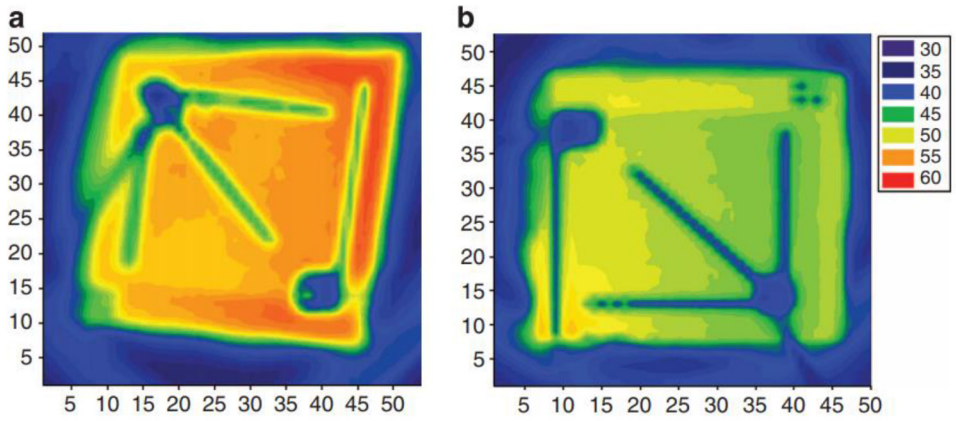

Figure 6. Infrared images of the chip surfaces. (a) Temperature distribution on the conventional LED chip. (b) Temperature distribution on the LED chip with embedded rGO pattern. Reproduced with permission from [110].

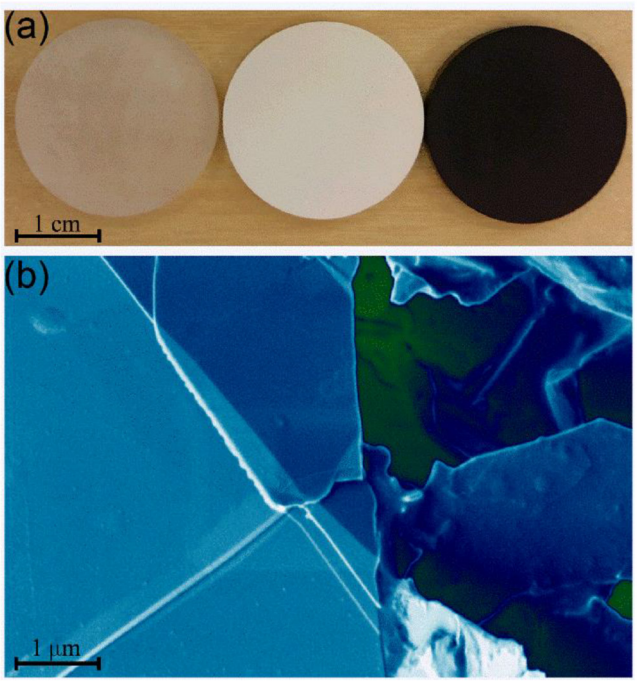

Figure 7. (a) Optical image of the pristine epoxy, and epoxy with the loading of 18 vol.% and 19 vol.% of graphene and *h*-BN fillers, respectively. Note a distinctively black color of graphene composite as opposed to the white color of *h*-BN composite. (b) Scanning electron microscopy image of the epoxy composite with 45 vol.% of graphene fillers. The microscopy image of the high-loading composites shows clearly the overlapping of graphene fillers inside the epoxy matrix. The overlapping fillers confirmed the formation of the percolation network at this high loading fraction of graphene. Reproduced with permission from [111], © American Chemistry Society.

Heat spreaders based on LPE graphene have been demonstrated to cool down hotspots up to 1750 W cm^{-2} [109]. Zhang *et al* applied both vacuum filtration and drop coating methods to fabricate graphene films as heat spreaders from pure mechanical LPE graphene suspension [109]. 3ω measurement showed that the thermal conductivity of the drop coated graphene film is around 110 W m^{-1} K^{-1} in the in-plane direction, which is much lower than the graphene exfoliated by tape due to the defects in the graphene crystal and the huge contact resistance between the graphene flakes. A temperature drop of 6 °C and 4 °C is detected at the hotspot using vacuum filtrated graphene heat spreader and drop coated graphene heat spreader, respectively. Finite element method (FEM) modeling revealed that the alignment of graphene flakes in the heat spreader and the thermal boundary resistance between graphene and the chip surface are the key parameters determining the performance of the heat spreader.

Zhang *et al* also reported a heat spreader using reduced GO films [110]. In order to decrease the thermal boundary resistance, a silane functionalized GO (FGO) layer was coated as thermal coupler between the heat spreader and the chip. Molecular dynamics simulation (MDS) showed that thermal conductivity of the graphene heat spreader can be increased by

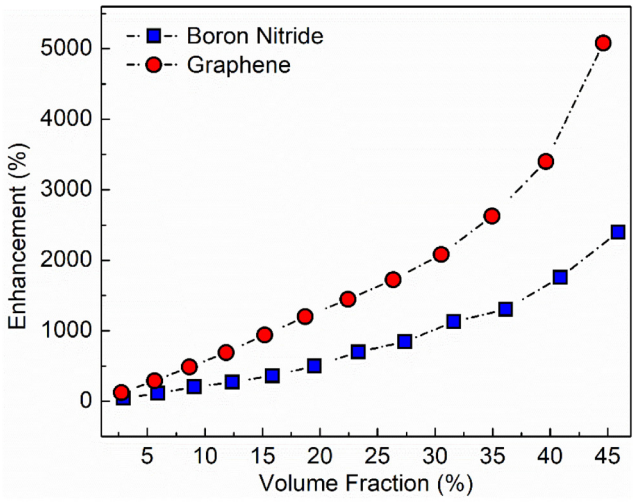

Figure 8. Thermal conductivity enhancement $\eta\% = 100 \times ((K - K_m))/K_m$ as a function of filler loading fraction (here K_m is the thermal conductivity of the base material and K is the thermal conductivity of resulting composite). The red circles and blue squares are the experimental data points for epoxy with graphene and *h*-BN fillers, respectively. Graphene filled epoxies outperform *h*-BN filled epoxies primarily because the intrinsic thermal conductivity of the graphene is higher than that of *h*-BN. Reproduced with permission from [124], © American Chemistry Society.

15%–56% after functionalization due to the decreased cross-plane phonon scattering between the graphene heat spreader and the chip. Thermal characterization results showed that the heat spreader with silane FGO decreased the hotspot temperature by 12 °C in contrast to a temperature drop of 6 °C by the graphene heat spreader without silane FGO, as shown in figure 5.

Improved heat dissipation in GaN light-emitting diodes (LEDs) was also observed by Han *et al* using embedded GO pattern [110]. GO dispersion was firstly coated on sapphire substrate and followed by thermal reduction in hydrogen under 1100 °C. Afterwards the rGO was patterned by lithography and GaN layer was grown on top by epitaxial growth. Following this step the LED structure was fabricated so that the patterned rGO was embedded underneath. Experiment results show that the peak temperature of the chip surface is about 5 °C lower on the rGO embedded LED compared to the conventional LED, as shown in figure 6.

The thermal performance of LPE graphene heat spreader is dependent on a few factors. Firstly, the presence of dispersant and other constituents most of time degrades the properties of the thin films. Secondly, the arrangement in the individual graphene flakes in a thin film plays an important role in determining the film performance. It has shown that, by means of filtration, highly aligned graphene films show strong anisotropic thermal conductivities, i.e. 120 $W\,m^{-1}\,K^{-1}$ in in-plane direction versus 0.5–2 $W\,m^{-1}\,K^{-1}$ in cross-plane direction [112]. The final but not the least factor concerns lateral size of graphene flakes. It was shown that thermal conductivity increases linearly with the increase of flake size which indicates that heat conduction is mainly limited by flake boundaries [113]. Therefore, it is possible to prepare high performance graphene films as heat spreaders from GO suspensions, provided that the GO flakes turn to graphene of good quality. It has been repeatedly reported that complete reduction and graphene lattice restoration of GO can be realized by means of super-high temperature annealing, i.e. 1700 °C to 3000 °C [114]. A previous study reports thermal conductivity at 1400 $W\,m^{-1}\,K^{-1}$ was achieved from solution-processed GO films after annealing at 2850 °C and mechanical pressing which shows great potential for heat spreading application [115].

3.2. Graphene enhanced thermal composites

The unique heat conduction properties of graphene motivated experimental studies of graphene and FLG in TIM, thermal composites and coatings [20, 24, 25, 34, 39, 62, 116, 117]. The first studies of graphene composites found that even a small loading fractions of random graphene fillers can result in increased thermal conductivity of epoxy composites [34, 118, 119]. The large variations of the thermal conductivity of graphene thermal composites originates from differences in the methods of preparation, matrix materials, quality of graphene, lateral sizes and thickness of graphene fillers and other factors [19, 31, 33, 120–123]. Most of the early investigations of thermal composites with graphene fillers were limited to the low loading fractions of fillers, $f < 10$ vol.%. The situation has changed recently when composites with large loading of graphene became available owing to the technological developments and substantial cost reduction (see figure 7).

Thermal properties of composites with the high loading fraction of graphene or FLG fillers is interesting from both fundamental science and practical applications points of view. The high loading results in achieving the thermal percolation in the compos-

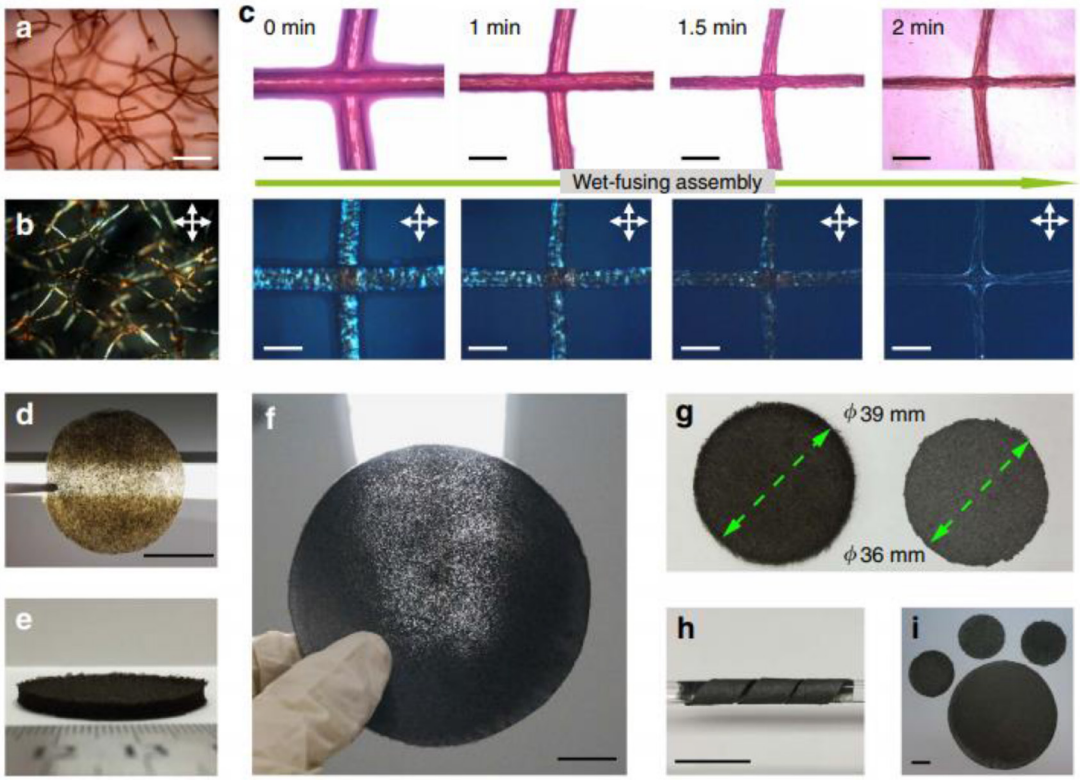

Figure 9. Mechanism of wet-fusing assembly and morphology of as-prepared graphene oxide fiber fabrics (GOFFs) and graphene fiber fabrics (GFFs). (a) Optical microscopy (OM) and (b) polarized-light optical microscopy (POM) images of GO fibers. (c) Wet-fusing of GO fibers. (d) A piece of thin GOFF (0.05 mm). (e) A piece of thick GOFF (3 mm). (f) A thermally annealed GFF with porous feature. (g) GOFF (left) and GFF (right), indicating the slight shrinkage of lateral dimension and color change. (h) A stripe of GFF coiled around a glass rod. (i) Four GFFs of different sizes and thicknesses. Scale bars, (a) and (b) 500 μm, (c) 150 μm, (d), (f), (h) and (i) 20 mm. Reproduced with permission from [163].

ites [125–132]. The thermal percolation is less understood phenomenon that the electrical percolation [133–140]. The electrical percolation is described by the scaling law $\sigma \sim (f - f_E)^t$, where σ is the electrical conductivity of the composite, f is the filler loading volume fraction, f_E is the filler loading fraction at the electrical percolation threshold, and t is the critical exponent. Unlike the electrical conductivity, in most of cases, the thermal conductivity of composites does not reveal such noticeable changes as the loading fraction increases. Controlling electrical and thermal percolation in composites with graphene using filler optimization and perhaps combining graphene with other electrically insulating 2D fillers such as hexagonal boron nitride (*h*-BN) remains an important challenge for further development of graphene thermal composites.

There is a strong practical motivation for research of composites with the high loading of graphene for instance for better TIMs for heat removal in electronics [22, 141–143]. Commercially available TIMs with the bulk thermal conductivity below 5 W m^{-1} K^{-1} no longer meet the industry requirements. Composites with the high loading of graphene have the potential to deliver high thermal conductivity. Recent technological developments demonstrated that the LPE graphene can be produced in large quantities inexpensively [144, 145]. There have been significant progress in the methods of reduction of graphene oxide (GO) [139, 146–148]. These developments made graphene fillers practical even for the composites with the high loading fraction. A recent study reported thermal properties of composites with the high loading (up to $f = 45$ vol.%) of graphene and *h*-BN [124]. The electrically insulating *h*-BN was used for comparison with graphene in order to establish the general trends in thermal conductivity of composites with 2D filler materials (see figure 8). It was found that the thermal percolation happens at higher loading than the electrical percolation in graphene composites. The thermal conductivity of graphene epoxy composites exceeded ~12.5 W m^{-1} K^{-1}, which is higher than that of commercially available TIMs [124, 149].

Besides, graphene composite material also showed great potential as a heat sink material. Conventional heat sinks are made of metals, such as copper or aluminum, with fins to increase its surface area. However, carbon based heat sink attracts lot of interests due to its light weight, anisotropic and high thermal conductivity. Graphite has a long history of being considered as material for heat sink. In 2003, Norley *et al* proposed to make graphite-based heat sinks with controllable isotropy [150]. In their design, flat and well oriented graphite sheet was bonded together to

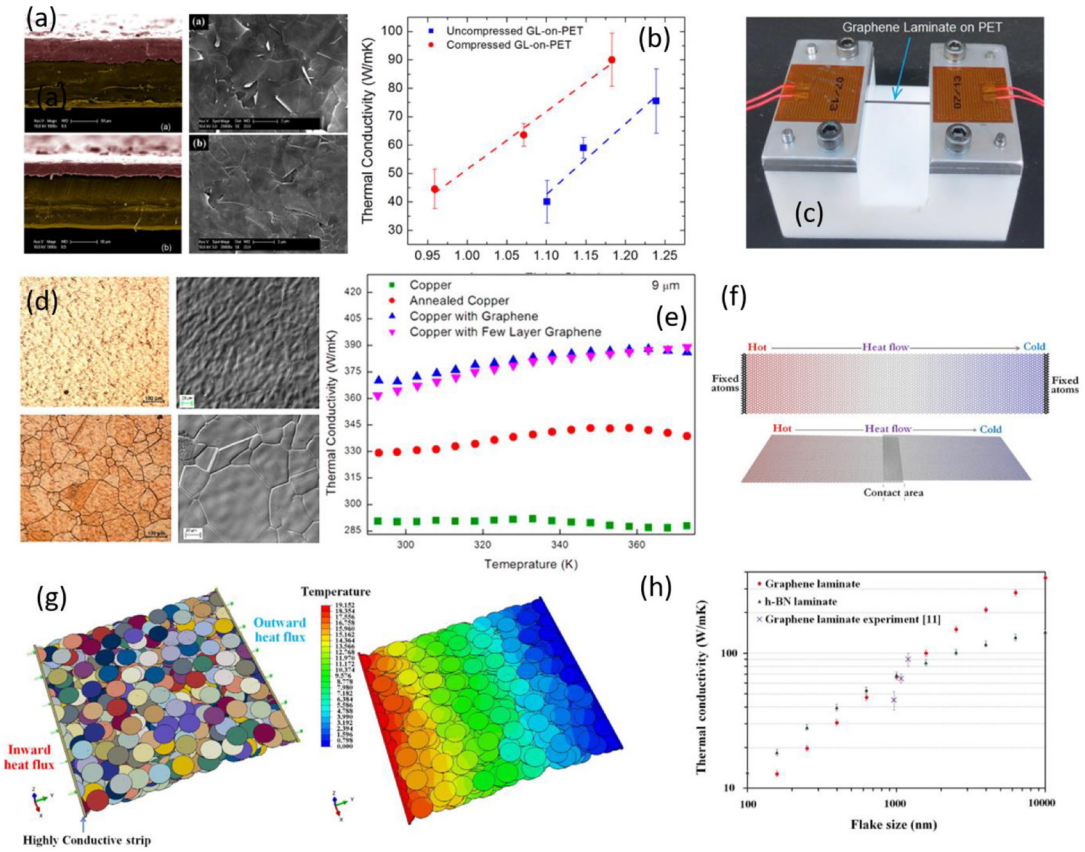

Figure 10. (a)–(c) Images and thermal conductivity of graphene/PEI laminate. Reproduced with permission from [113]; (d) and (e) images and thermal conductivity of graphene/copper laminate. Reproduced with permission from [116]; (f) constructed molecular models of graphene for the thermal transfer performance valuation. Reproduced with permission from [171]; (g) a typical developed 3D representative volume element of graphene laminate constructed in Abaqus/Standard. Reproduced with permission from [171]; (h) multiscale results for effective thermal conductivity of graphene and *h*-BN laminates as a function of flake size. Reproduced with permission from [171].

make a graphite heat sink. It was found that the thermal conductivity of this graphite heat sink in the horizontal direction is higher than the vertical direction. In the next year, Getz *et al* fabricated a heat sink made from different size of graphite sheets based on similar concept [151]. Recently, heat sink performance of graphene and its composites has been studied. Wu *et al* used Cu nanoparticle coated graphene sheets to fabricate a composite film with thermal conductivity up to 1912 W m^{-1} K^{-1} at 50 °C. Simulation revealed that the graphene/Cu composite film exhibits more efficient thermal transport ability compared to Cu and graphene film [152]. Wai *et al* developed a facile mechanical cleavage method to synthesize graphene nanosheets and graphene nanosheets/Cu (GN/Cu) composite film. Heat sink made from this GN/Cu composite film reached a thermal conductivity as high as 2142 W m^{-1} K^{-1}, showing an increase of 26% compared to the graphene sheet heat sink [153]. Lu *et al* coated 1900 nm graphene sheets on aluminum heat sink to obtain a 7 °C temperature decrease compared to uncoated heat sink under a heat flux of 1.8 W cm^{-1} [154]. In recent years, patents based on graphene enhanced heat sinks have been filed [155, 156] due to the advantages of light weight and high thermal performance. Moreover, graphene/graphite based heat sink is able to control the thermal conductivity in different directions, which provides the possibility of preferentially heat transport.

3.3. Graphene fibers

Graphene fibers are, similarly to graphene films, macroscopic assembled structures of interlocking layers of reduced graphene oxide flakes. They have so far mainly been studied for their mechanical and electrical properties [157], for replacing carbon fibers and application within smart textiles. However, they also hold great promise for use in thermal applications [158].

Graphene oxide (GO) fibers can be fabricated through wet-spinning of liquid crystal GO dispersions into a coagulant bath [157]. The assembled GO fibers are then reduced to form graphene fibers, and possibly annealed as well. The process has a plethora of parameters, both within the GO dispersion, coagulant bath, spinning setup, reduction process and annealing, This enables a very high variability in graphene fiber properties, and the possibility to further optimize the properties. For instance, Xin *et al* [158] showed how an optimized mixture of small

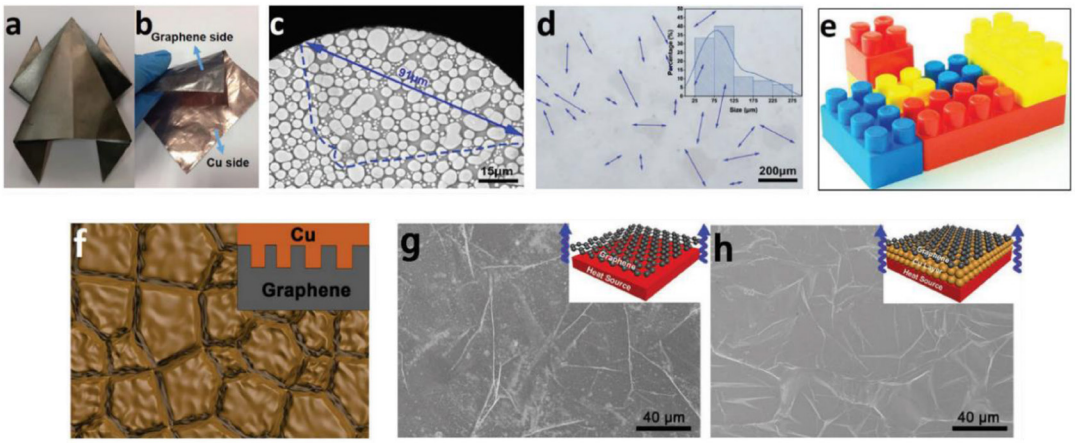

Figure 11. (a) Flexible graphene film was folded into a frog; (b) graphene/Cu laminate in the status of bending; (c) TEM image of a graphene sheet; (d) optical microscopy image and (inset in (d)) corresponding size distributions of graphene sheets; (e) optical image of building bricks; (f) diagrammatic sketch and schematic diagram (the inset) of graphene/Cu laminate surface; (g) SEM image of the surface of graphene film with many granular bubbles and microfolds and (h) graphene/Cu laminate, the insets are schematic diagram of heat conduction from heat resource through graphene film and graphene/Cu laminate, respectively. Reproduced with permission from [175].

and large GO flakes leads to an improvement in thermal conductivity (1290 W m^{-1} K^{-1}) and mechanical strength compared to only large flakes. Xu *et al* [159] systematically eliminated defects at all levels to achieve a Young's modulus of up to 282 GPa [159], strength of 1.45 GPa which was recently improved even further by Xin *et al* [160] which used microfluidics to control the flake orientation during the spinning process. This resulted in, rather than circular fibers, belt-like structures with a record high thermal conductivity of 1575 W m^{-1} K^{-1}, Young's modulus of 309 GPa and tensile strength of 1.9 GPa. While the best mechanical properties of graphene fibers were still not on par with the strongest carbon fibers [161], the thermal conductivity has surpassed carbon fibers that have undergone similar thermal annealing [162].

The wet-spinning fabrication route is highly scalable, with possible spinning speeds of kilometers per hour [159] per nozzle, opening the possibility of large-scale application as filler in polymer matrices, or as freestanding structures within flexible electronics or textiles. Toward these applications, Li *et al* [163] demonstrated a flexible and porous non-woven fabric of fused graphene fibers, with an in-plane thermal conductivity of 301.5 W m^{-1} K^{-1} at a density of 0.22 g cm^{-3}, as shown in figure 9.

3.4. Graphene laminates

Graphene laminates have been demonstrated for surface protective, water desalination [164], gas impermeable barrier [165] and electromagnetic interference shielding [166]. But applying graphene laminates for thermal coating applications is becoming more and more popular. Generally, in a graphene laminate, graphene is deposited on various substrates, including polymers (polyethylene terephthalate (PET)) [113] and metals (copper [167, 168], Aluminum [154]). In a graphene laminate, graphene sheets are combined by binders or Van der Waals force. Until now, a few simple fabrication techniques for graphene laminates have been developed, including CVD [169], drop-casting, spin-coating, spray-coating and dip-coating [170].

Improvement of thermal conductivity up to 600 times for plastic substrate and 24% for Cu film has been achieved by coating graphene to fabricate the laminate structure (figures 10(d) and (e)) [113, 116]. Except for the extremely high thermal conductivity of pristine graphene, reduced surface roughness and improved grain size on the substrate also contributed to the thermal performance of metal based graphene laminate [171]. Moreover, it is widely believed that the alignment and flake size of graphene influence the thermal conductivity more than the density of graphene fillers in a graphene laminate. After compressed with large flake-size graphene, linear improvement of thermal conductivity from 40 to 90 W m^{-1} K^{-1} was achieved by Balandin *et al* for graphene laminate [113], as seen in figures 10(a)–(c). In particular, multiscale modeling of heat conduction in graphene laminates demonstrated that flake size is one of the main factors affecting the thermal conductivity of graphene laminates (figures 10(f)–(h)) [171]. For the small graphene flakes, inter-flake contact resistance makes a big difference to the thermal conductivity. Consequently, increasing graphene flake size [57], building covalent bonds between graphene flakes [172, 173] and orientating graphene sheets [54] are effective routes to further improve the thermal conductivity of graphene laminates.

So far, the volume fraction of graphene in the graphene laminates is very low, therefore many researchers are trying to increase the percentage of graphene in the laminates to improve their thermal conductivity. However, the surface of graphene film is chemically inert and it is difficult to combine the graphene

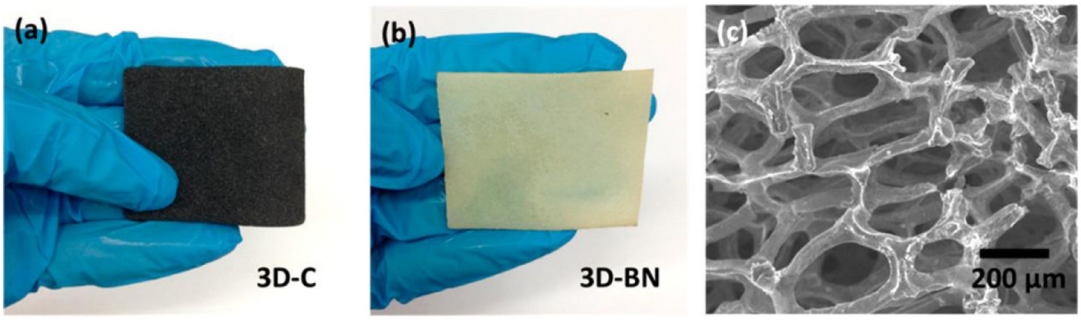

Figure 12. Macroscale Ni-templated (a) 3D graphene foam, (b) *h*-BN foam, (c) SEM image of graphene foam cross-section. Reproduced with permission from [176].

film with metal. Initially, graphene/metal laminates or graphite/metal laminates were fabricated by vacuum hot pressing [174]. Owing to the rough surface of the graphene films and metals, the contact resistance at the bonding interface is typically very high [175]. In order to reduce the contact resistance, interfacial materials, such as indium, thermal conductive adhesive (TCA) and commercial double-side tape, were used to assemble graphene films and Cu foils (figure 11) [175]. Results showed that the thermal conductivity of graphene/Cu laminates can be 3 times higher than that of Cu after the optimization at the interface [175]. On the other hand, the thickness of interfacial materials is difficult to control which will lower the performance of the laminates. To further improve the thermal conductivity of the laminates, Cu thin layer (about 1 μm thick) was sputtered on the surface of graphene films [175]. Similar to the interlock system within building blocks, granular bubbles and microfolds on the surface of graphene film make it tightly anchored on the coated Cu layer. Since the large flake size in graphene can reduce the number of contacts and the introduction of Cu makes the heat capacity of the laminate higher than pristine graphene film, this graphene/Cu laminate has high thermal conductivity up to 1932 W m^{-1} K^{-1} [175].

3.5. Graphene based 3D structures

In addition to the previously mentioned graphene structures, there are a number of graphene based 3D structures that have been proposed for use in thermal management.

3.5.1. *Graphene foam*

Graphene foam consists of graphene assembled in a porous macroscale foam-like structure. The porosity of the foam makes the effective thermal conductivity of graphene foam very low, with a thermal conductivity of 0.26 to 1.7 W m^{-1} K^{-1} at a solid concentration of around 0.45 vol% [177]. Nonetheless, graphene foams exhibit a thermal conductivity close to that of metal foams, at an order of magnitude higher degree of porosity [178]. In addition, graphene foams have a very high degree of compressibility, making them attractive for TIM applications. Graphene foams are primarily synthesized through graphene CVD on Ni foams and the subsequent etching of the Ni template, leaving a free-standing graphene structure. [179]. A similar structure can also be formed using freeze casting of or hydrothermal reduction of GO suspensions [180, 181]. As free standing structures, both graphene foam and a graphene/CNT aerogel has been demonstrated for TIM applications, with thermal conductivity of around 88 W m^{-1} K^{-1} for compressed graphene foam (figure 12) [176, 181] and low thermal interface resistances at very low pressures [179]. Similar structures have also been demonstrated using *h*-BN [176, 182], with a cross-plane thermal conductivity of up to 62 W m^{-1} K^{-1} for compressed *h*-BN foam [176]. Both graphene and *h*-BN foams can be infiltrated to form polymer composites [182, 183]. An *et al* created a vertically aligned graphene foam epoxy composite with a through-plane thermal conductivity of 35.5 W m^{-1} K^{-1} at a graphene loading fraction of 19 vol%, significantly higher than randomly dispersed graphene enhanced composites. Recently, Zhamu *et al*, synthesized a highly elastic and resilient graphene foam by a chemical-free method. This graphene-carbon hybrid foam showed super effective potential application as a heat sink [184].

3.5.2. *Vertically aligned graphene sheets*

Graphene sheets have excellent in-plane thermal conductivity, but is normally limited to heat spreading application due to the low through-plane thermal conductivity. A potential solution to this limitation is to stack multiple graphene sheets to form a bulk material which can be used for TIM and other thermal applications. Liang *et al* [185] introduced the concept, creating a material with a through-plane thermal conductivity of 112 W m^{-1} K^{-1}. Graphene films are stacked and bonded together with solder or polymer, and then cut perpendicular to the heat conducting axis into thin slices applicable as TIM. The concept has further been improved and optimized by Zhang *et al* [186] and by Wang *et al* [187, 188], with a thermal conductivity of 615 W m^{-1} K^{-1} and 1379 W m^{-1} K^{-1} respectively. The exceptionally high thermal

conductivity compared to conventional TIM, and even higher than heat sink materials, eliminates the normal drawbacks for TIM with a thick bond line. Instead, the thermal contact resistances between TIM and joining surfaces are the limiting factors rather than the thermal conductivity. Indeed, as seen by Wang *et al* [188], the overall performance depends mainly on the contacts, and through bonding with a thin indium layer the performance rivals that of thin solder joints, while retaining good flexibility and thickness which is crucial for gap filling applications.

3.5.3. *Hybrid graphene structures*

The unique properties of 2D materials can be further taken advantage of together with other materials in hybrid combinations. Normally, the through-plane thermal conductivity of graphene structures is a limitation. A possible way to increase the *Z*-direction thermal conductivity is to introduce more thermal paths through covalent bonding of graphene layers using an intermediary material. This has been demonstrated using carbon nanorings [189] and more recently using *in situ* grown vertically aligned SiC nanorods [190]. By this approach, the through-plane thermal conductivity was increased from 4 to 17 W m^{-1} K^{-1} in a TIM application.

Another application of hybrid graphene structures is together with CNTs. CNT arrays have been widely investigated for use as TIMs [191], but are severely limited by the thermal contact resistance between CNT and substrate. However, simulations suggests that CNTs covalently bonded to graphene has the potential for a significantly lower resistance [192–195]. Realizing this structure experimentally has proven difficult, but has been demonstrated using novel CVD approaches [196, 197]. Furthermore, Sun *et al* [198] showed that covalent anchoring of CNTs to graphene could lower the thermal contact resistance by several orders of magnitude. Hybrid graphene/CNT structures with CNT arrays grown on graphene films can be used for efficient heat dissipation [198] or novel TIM structures [199].

3.6. Graphene nanofluids

Nanofluids attract increasing research interest due to their advanced heat transfer properties compared to conventional fluids. The benchmark study on the effect of nanoparticles on the thermal conductivity of fluids showed positive correlations between nanoparticles and thermal conductivity of fluids [200] that was stipulated by classical theory. Graphene, with its high thermal conductivity, has also been studied in the effort aiming at integrating graphene as fillers in heat transfer fluids for a large spectrum of applications. Graphene suspensions were found to effectively enhance the thermal properties of the host fluids. For example, the graphene nanofluid showed an enhancement in the thermal conductivity at more than 36% compared to the pure fluid, and the effect increases with the concentration of graphene nanosheets [201, 202]. Functionalized graphene exhibited more pronounced increase in the heat transfer of water-based nanofluids (i.e. up to 171 increase in heat transfer coefficient at 0.01% loading) [203]. Ghozatloo *et al* [201] showed an increase of 31.83% in the thermal conductivity of deionized water used in heat exchanger at 0.075 wt% of Potassium persulfate (KPS) oxidized graphene with an increase in the heat transfer coefficient with the concentration of the loading. When used in heat pipe, the graphene could improve the heat transfer by increasing the surface wettability between the fluid and solid surface of the pipe [204], while an increase in the dynamic viscosity has to be considered [205]. The addition of up to 0.3 vol.% graphene nanoplatelets resulted in a decrease of the contact angle of the nanofluid than that of the distilled water by 20% [206]. A thermal resistance reduction of 48.4% was obtained as the deposition of the graphene nanoplatelets that formed a coating on the wick surfaces and improved the surface wettability [204]. Study on the effect of graphene presence on the viscosity behaviour of the base fluid suggested a Newtonian behaviour, where the thermal conductivity, dynamic viscosity and density were found to increase [207]. The temperature was also reported to have an effect on the dynamic viscosity and density but not on the thermal conductivity under turbulent conditions. Meanwhile, some study exhibited a non-Newtonian behaviour of distilled water nanofluids with functionalized hydrogen-exfoliated graphene [208]. The lack of temperature dependency in theoretical formulation neglected particle-particle interactions [209], where a viscosity increase of over 30 times was reported as the particle-particle interaction was taken into consideration, together with a maximum enhancement of thermal conductivity by 1.43 times at 1.5% volume fractions in external flows in laminar regime. The particle-particle interaction was also emphasized by Anoop *et al* [210], and the particle aggregation and the electroviscous effect at the particle-fluid interface were also non-negligible. An increase in the thermal conductivity and specific heat capacity of up to 48% and 18%, respectively, was reported by Rodríguez-Laguna *et al* [211]. As for the case of high boiling point organic solvent, the resulted thermal conductivity was attributed to a long-range effect of the dispersed graphene on the solvent molecules and a local orientation of the solvent molecules parallel to the graphene sheet. Studies regarding graphene nanomaterial have shown a positive correlation between the thermal properties and the graphene loading in the carrier medium.

The improvement of the thermo-physical properties of the nanofluid can be expected by the aid of graphene additives. At the meantime, challenges raise from the complex phenomenon at the graphene-liquid interface and the understanding of the mechanism of graphene contribution to the ther-

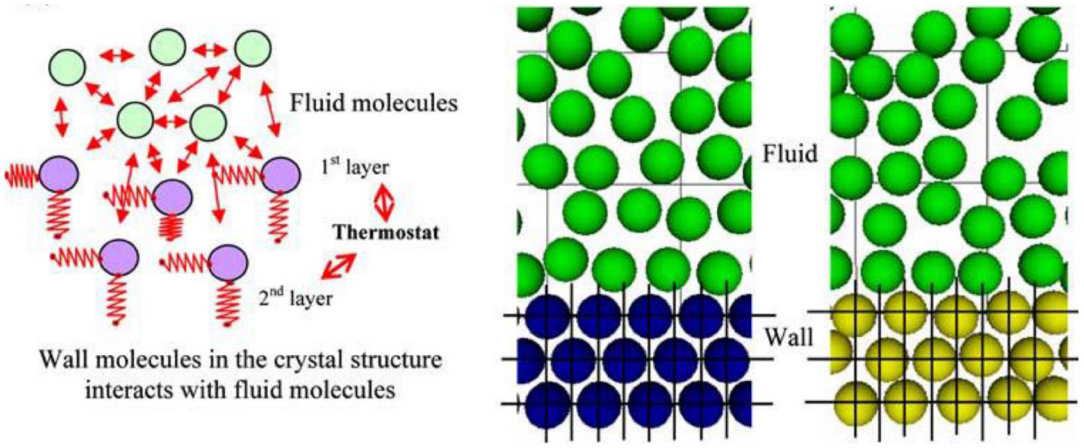

Figure 13. Schematic representation of thermal wall–fluid interactions. Reproduced with permission from [215].

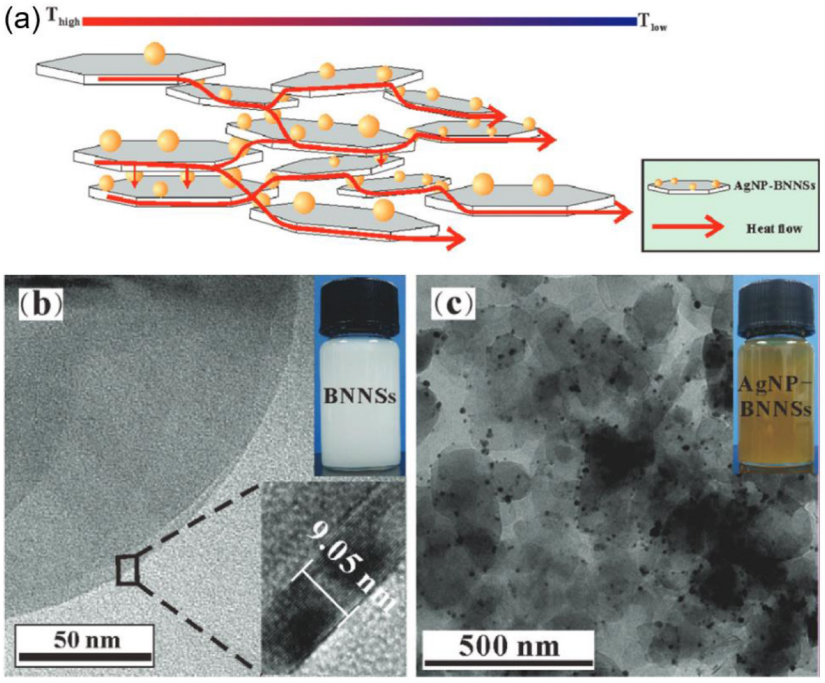

Figure 14. (a) Proposed model of AgNP–BNNSs for thermal conducting paths. (b) TEM images of a slice of the BNNSs. (c) TEM image of AgNP–BNNSs. Reproduced with permission from [229].

mal transport. Extensive investigations are needed to understand how the graphene increased the stability of the liquid [212]. When applying graphene nanofluids in heat dissipation, the thermal resistance at the interface is a key issue in the heat transport. Modelling and simulations have been carried out to study the interfacial thermal resistance. The acoustic mismatch model (AMM) attributed the thermal resistance to phonon radiation and acoustic impedance [213], and the diffuse mismatch model (DMM) focused on the phonon density mismatch [214]. Molecular dynamics simulations (MDS) provided insights into the thermal transport across the interfaces. Kim *et al* studied the thermal resistance at the solid–liquid interface, as shown in figure 13, and suggested the dependence of interface thermal resistance on the fluid velocity and state [215–217]. The resistance at the solid–liquid interface of a nanochannel coated by graphene layers was studied, and results showed that an influence of fluid-wall interface strength on the interfacial thermal resistance [218].

Computational fluid dynamics (CFD) methods were also available in investigations on the thermohydraulic performance of nanofluids. Both single-phase and two-phase models were developed for nanofluids consist of nano-sized additives and the base fluid [219, 220]. Simulation results showed that the graphene nanoplatelet enhanced the transport properties at turbulent convection heat transfer [221], while there was no advantage of the nanofluid at low concentration in laminar convective heat transfer. Reproduced with permission from [222].

3.7. Other 2D materials

In addition to graphene and its derivatives, hexagonal BN (hBN) is another 2D material possessing interesting electrical and thermal properties therefore shows great potential as heat spreaders and composite fillers. Theoretical calculation shows that the thermal conductivity of hBN nano-ribbons is as high as 1700–2000 W m^{-1} K^{-1} [43]. In addition, hBN is an electrically insulating material with a bandgap of ~5.955 eV [223]. This allows hBN to directly contact with devices and circuits when it is applied as a heat spreader, therefore dramatically decreases the thermal boundary resistance and improve the heat spreading performance.

Sun *et al* used LPE method to synthesis hBN flakes and followed by the fabrication of hBN films as heat spreaders to cool down hotspots with a heat flux of 600 W cm^{-2} [50]. Thermal characterization showed that the temperature at the hotspot was decreased by 20 °C. Since the hBN flakes are too fragile to form a free-standing film, acetate cellulose solution was used to improve the mechanical strength of the hBN heat spreader. Bao *et al* used drop-coated few-layer hBN as heat spreaders [51]. Experimental results showed that the hBN heat spreader can decrease the hotspot temperature by 3.8 °C under 1000 W cm^{-2}. If the hBN film is enhanced by graphene, the hotspot temperature can be lowered by 9.2 °C under the same heat flux. Liu *et al* used plasma enhanced CVD method without catalyst to grow poly-crystalline hBN on SiO_2/Si, quartz, sapphire and silicon substrates [224]. Owing to the direct growth and conformal interface between hBN and the substrates, the interfacial thermal resistance has been decreased and much higher saturated power density on the field effect transistors can be achieved. Choi *et al* used 35 nm and 80 nm thick hBN films to cool down hotspots on Si substrates. They achieved a factor of 4.1 and 2.2 reduction of hotspot temperature, respectively [52].

Similar to graphene and their derivatives, hBN has also been used as composite fillers to develop TIMs. Jang *et al* used silane coupling agents to modify the BN surface to improve its dispersibility in epoxy [44]. They found that longer carbon chain in the coupling agent can lead to better interfacial adhesion between BN and epoxy in the composite, which consequently improved the thermal conductivity of the composite to about 3.5 W m^{-1} K^{-1}, i.e. an increase of 45.4% compared to pure BN enhanced thermal composite. The effect of the coupling agent is also verified by Wang *et al* who applied hBN, cubic BN (cBN) and conglomerated hBN as fillers in the composites [45]. The highest thermal conductivity of 10.1 W m^{-1} K^{-1} was obtained from the hBN based composite, and this can be further improved to 12.3 W m^{-1} K^{-1} by adding AlN particles to fill in the space between the BN flakes. Wong and Sun's group theoretically investigated the functionalization of hBN by -OH and $-O(CH_2)_4CH_3$ groups and found that the thermal conductivity of monolayer hBN was still over 100 W m^{-1} K^{-1} [225]. They also applied spray-assisted spherical hBN platelets [226] and hot-pressed BN [227, 228] to enhance the polymer composites, and a thermal conductivity of 2.3 W m^{-1} K^{-1} and 23.1 W m^{-1} K^{-1} was realized, respectively. It was reported that the hot-pressing induced orientation of the BN contributed significantly to the thermal performance of the composites [227, 228]. In order to decrease the interfacial thermal resistance between the BN flakes, nanoscale silver particles were added to bridge the BN flakes and an in-plane thermal conductivity of 65.7 W m^{-1} K^{-1} was achieved, as shown in figure 14 [229]. Shen *et al* used polydopamine (PDA) coated hBN as fillers in the composite and achieved in-plane thermal conductivity of 5.4 W m^{-1} K^{-1} [230]. Wattanakul *et al* also used hBN to formulate the thermal composite, but the hBN material was not functionalized and a maximum thermal conductivity of 1.97 W m^{-1} K^{-1} was demonstrated [48].

Hydrogen boride is a 2D material with hydrogen atoms bridging the hexagonal boron network. Recently, He *et al* calculated the thermal conductance of 2D hydrogen boride [231]. It was found that the lattice thermal conductance in hydrogen boride was comparable as in graphene (4.07 nW K^{-1} nm^2 versus 4.1 nW K^{-1} nm^2), but electron thermal conductance in hydrogen boride (3.6 nW K^{-1} nm^2) was almost ten times that of graphene. Therefore, the total thermal conductance of hydrogen boride could be two-fold of graphene, which is the highest value in all reported materials. But this needs further confirmation by experimental measurement.

2D transition metal dichalcogenides (TMDs) are also a member of the 2D material family. Generally, TMDs are atomically thin semiconductors typically in the form of MX_2, in which M is a transition metal atom (Mo, W, etc) and X is a chalcogen atom (S, Se, or Te). Theoretical predictions based on the phonon Boltzmann transport equation have found that monolayer MS_2 is able to achieve thermal conductivity as high as 142 W m^{-1} K^{-1} at RT, then followed by MoS_2 (103 W m^{-1} K^{-1}) and $MoSe_2$ (54 W m^{-1} K^{-1}) [232]. However, the measurement results are not in line with the theoretical calculation so far. Lee *et al* measured the in-plane thermal conductivity of monolayer, bilayer and multilayer MoS_2 by a non-invasive Raman spectroscopy method. Their results show that the in-plane thermal conductivities for the monolayer, bilayer, and multilayer MoS_2 are 13.3 ± 1.4, 15.6 ± 1.5, and 43.4 ± 9.1 W m^{-1} K^{-1}, respectively. Reduced phonon boundary scattering was used to explain the increase in thermal conductivity with the increased number of MoS_2 layers [233]. It has been reported that a 4-layer-thick MoS_2 exhibited a thermal conductivity of 44–50 W m^{-1} K^{-1} at RT, while a 7-layer-thick MoS_2 exhibited 48–52 W m^{-1} K^{-1} as reported by Shi *et al* [234]. Therefore, various phonon properties such as interatomic bonding and anharmonic vibrations, and their

Table 2. Different forms of 2D materials for thermal management applications.

Materials/structures	Application area	Thermal conductivity (W m^{-1} K^{-1})	Heat transport direction
Mono- and few layer graphene	Heat spreader (micro-scale)	>2000 (suspended) [18, 19, 23] 600 (attached) [23, 81]	In-plane
Graphene films	Heat spreader	1000–3000 [40, 82, 85, 90–93]	In-plane
LPE graphene	Heat spreader	120 [112]	In-plane
h-BN films	Heat spreader	390 [248]	In-plane
Graphene foam	TIM	<2 (pristine) [177] 90 (compressed) [176, 181]	Isotropic
h-BN foam	TIM	60 (compressed) [176]	
Vertically aligned graphene	TIM	100–600 [185, 186]	Through-plane, in-plane unidirectional
Graphene enhanced composite	TIM, thermal composites, coatings	3–15 [25, 34, 39]	Isotropic
h-BN enhanced composite	TIM, thermal composites, coatings	1–6 [44, 45, 124, 249]	Isotropic
Graphene fibers	Flexible heat spreader, smart textiles	1200–1600 (single fiber) [158, 160]	Unidirectional

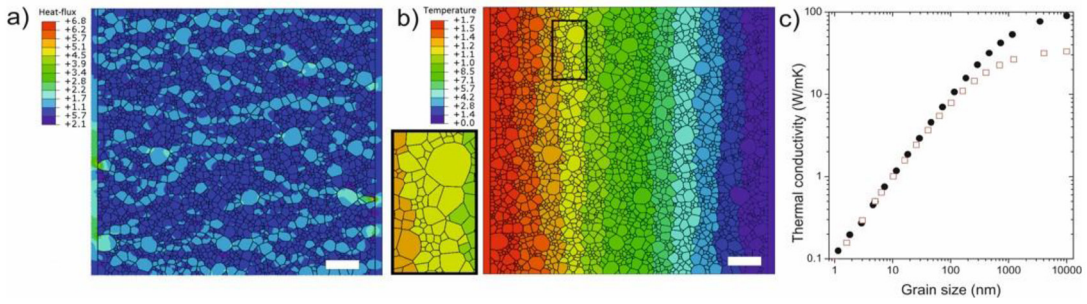

Figure 15. (a) Simulated heat flux in the sample. Scale bar corresponds to 30 nm. (b) Temperature distribution in the sample. Scale bar is 30 nm. Inset: detail of the marked region. (c) Thermal conductivity as a function of the average grain size assuming two values of single-crystalline thermal conductivity of MoS_2: 100 W m^{-1} K^{-1} (full circles) and 34 W m^{-1} K^{-1} (open squares). Reproduced with permission from [235].

roles in heat transport, still need further investigation to understand the thermal performance of TMDs.

Heat conduction in 2D materials can be effectively engineered by means of controlling nanoscale grain structure. It was experimentally shown that 5 nm-thick polycrystalline MoS_2 with grains of about 5 nm size the thermal conductivity decreased to below 1 W m^{-1} K^{-1} [235]. Finite element method simulations on a sample resembling the experimental one has shown that the grain boundary conductance was the limiting factor for the heat transfer. In the polycrystalline sample the significant temperature changes occur across the grain boundaries and the majority of the heat flux is conveyed by the large grains that are percolating together. Consequently, the heat-flux is mainly transferred along percolation paths, which minimizes the crossing with grain boundaries. The calculation yields an effective grain boundary conductance of 87.5 ± 1.5 MW m^{-2} K^{-1} for the polycrystalline MoS_2 films [235].

In the same work [235] thermal conductivity as a function of grainsize was calculated, assuming two values of the thermal conductivities of 100 W m^{-1} K^{-1} (full circle) or 34.5 W m^{-1} K^{-1} (full square) for single-crystalline MoS_2, as shown in figure 15. In the small grain size limit (below 100 nm) the grain boundaries play the major role in the heat transport and the both assumptions lead to similar values of the effective thermal conductivity. Only by increasing the grain sizes, the effect of the grain on thermal conductivity increases and the predictions start to differ.

The importance of grain boundaries in heat transport was also shown for polycrystalline MoS_2 in which thermal conductivity of 0.27 W m^{-1} K^{-1}, was obtained in a sample formed by a combination of horizontally and vertically oriented grains in similar proportion. Analysis by means of molecular dynamics and finite element method simulations confirmed that such a grain arrangement leads to the lowest grain boundary conductance [236].

MXenes are another class of 2D materials consisting of few-atom thick of transition metal carbides, nitrides, or carbonitrides. Until now, the research on MXenes for thermal management is still limited. Ananthakumar *et al* added 2D Ti_3SiC_2 MXene nanosheets into fluid to improve the thermal conductivity to 0.276 W m^{-1} K^{-1}, an increase

of 45% with a loading of 0.25 Vol% MAXene [237]. Lin *et al* measured the effective thermal conductivity of $Ti_3C_2T_x$ MXene films and results showed that the effective thermal conductivity of $Ti_3C_2T_x$ MXene films increased from 1.26 W m^{-1} K^{-1} at 80 K to 2.84 W m^{-1} K^{-1} at 290 K [238].

Theoretical calculations have been performed to investigate the thermal properties of silicene by Green-Kubo method, non-quilibrium MD and first-principle approach, and thermal conductivity values of 20 W m^{-1} K^{-1} [239], 14.6–65 W m^{-1} K^{-1} [240–243], and 9.4 W m^{-1} K^{-1} [244], were predicted respectively. First-principle method has also been applied by Peng *et al* and Zaveh *et al* to investigate stanene and a thermal conductivity of 11.6 W m^{-1} K^{-1} was reported [245, 246]. MD simulations have been performed by Balatero *et al* to investigate Germanene nanoribbons with armchair and zigzag chirality, and length dependent thermal conductivity values ranging from 14 to 52 W m^{-1} K^{-1} have been found [247]. Experimental measurements are yet to be performed to verify these theoretical calculations.

3.8. Summary

The different graphene, graphene derivatives and other 2D materials for thermal applications are summarized in table 2, and compared in terms of thermal conductivity, heat transfer direction and application areas. The main application areas for these materials within thermal management is heat spreading and TIM. In table 2, we can see that the thermal conductivity of mono- and few-layer graphene approaches to the theoretical maximum value, but their performance drops quickly when attached onto a substrate surface. In addition, the low thickness of mono- and few-layer graphene heat spreaders means that the total heat transfer may be relatively small despite of a high thermal conductivity. Nonetheless, we may see use in specific applications owing to the small size and the possibility of placing it extremely close to the heat source.

Macro-scale graphene heat spreaders can transfer heat at a scale relevant for many applications, such as mobile phone cooling. Compared to graphene films, LPE graphene offers closer adherence to substrates, but suffer in terms of thermal conductivity. Although it is possible to improve the thermal conductivity through high-temperature annealing and pressing, such methods will be incompatible with most substrates. On the other hand, graphene films can be treated separately from the substrate, which gives potential processing possibilities that lead very high thermal conductivity.

Nonetheless, graphene films may be the first application area where graphene based materials reaches a widespread commercial use, for instance, in the mobile of Mate 20. Here, the graphene assembled film is used for a quick heat spreading from the battery, RF and CPU modules to the casing. The efficient heat spreading can bring down the perceived temperature of the casing in a hand. In order to decrease the temperature further, drastic quality improvement of the graphene film is needed. Promising avenues are increased grain size and reducing interlayer binding energy, as well as a combination of various concepts of graphene alignment structures.

For TIM applications, the two main tracks are graphene and *h*-BN enhanced composites and pure 2D based monolithic structures. Graphene enhances composites are advantageous in that the polymer matrix can reduce the thermal contact resistance and can be created with a variety of form factors, as with most currently commercially available TIMs. Composites with a high loading of graphene can have a higher thermal conductivity than commercial alternatives, although it is overall much lower than for pure graphene materials. Graphene monolithic structures such as graphene foam or vertically aligned graphene can achieve significantly higher thermal conductivity, but are limited by the thermal contact resistance in TIM applications. Nonetheless, both tracks offer significant improvement over existing TIM within certain applications.

In addition to these main application areas, there are additional application areas where graphene and 2D-materials may play a role. For instance, graphene and *h*-BN enhanced composites may find application in coating or other thermal composites, and graphene fibers may be interesting for smart textiles.

4. Modeling of thermal transport in graphene

Carbon being one of the most studied element and taking a central part in key domains such as life or energy, the modeling of graphene is not a recent story, especially if considered as a brick element of graphite. Tight binding models and then density functional theory computations can be traced back to several decades [250]. Those quantum descriptions are able to qualify structure, electronic properties and their derivatives as well as chemical combinations. But they remain limited to the zero temperature condition and include a small number of atoms.

More recently, with the uprising of fullerenes and then graphene, several teams from nanophysics have investigated the thermal properties of graphene by using Molecular Dynamic technique. Molecular Dynamics is a classical description of the atomic motion based on a fair description of the force field. In graphene, interatomic forces have to involve the fifth neighbor, to describe phonons, which are the main heat carriers.

This method allows for the simulation of systems of millions of thermally active atoms. However, its classical nature forbids it to predict behaviors at temperature below the third of the Debye temperature. This condition is challenging when considering the sp^2 hybridized bonded orbitals of graphene, generating extremely stiff links between atoms. This stiff bond is at the origin of the extremely high, and maybe diverging, thermal conductivity of graphene [18]. Conse-

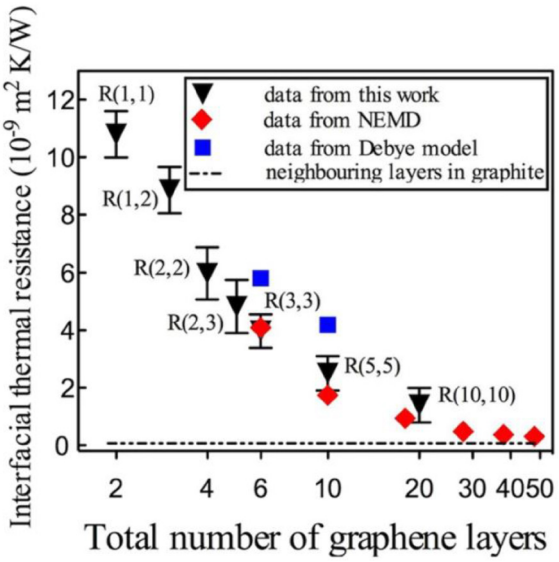

Figure 16. The calculated inter-FLG thermal resistance as a function of layer number at 300 K. Reproduced with permission from [252].

quently, Debye temperature of graphene is larger than 1000 K. However, the flexural (ZA) modes are the predominant phonon modes involved in heat transport and those are characterized by low frequencies and can be considered safely as classical [30].

Covering a substrate with graphene or few layer graphene has been proven to efficiently spread heat [62]. Thermal management of nanodevices can hence be efficiently performed by the adequate integration of graphene based multilayers or composites. In this section, thermal properties of graphene and few layer graphene will be investigated when in direct contact with a substrate and then when the contact is functionalized.

4.1. Molecular dynamics simulations of interfacial thermal resistance involving graphene

Understanding and controlling the interfacial thermal resistance involving graphene and few layer graphene (FLG) are crucial to the development and performance of FLG-based films in thermal management. Several factors govern the interfacial thermal resistance involving graphene, including but not limited to the layer number, the substrate property, and the interfacial coupling. In this section, we review the advances in the molecular dynamics simulations of interfacial thermal resistance involving graphene, aiming to provide a clear picture of how these important factors affect the interfacial thermal property.

4.1.1. The impact of graphene layer number

The layer number of graphene has large impact on the inter-layer thermal resistance of few layer graphene (FLG), as well as the resistance between FLG and the substrate. Due to the experimental inaccuracy, it is difficult to measure the layer number-induced thermal resistance variation directly from conventional experimental approaches. Fortunately, computer simulations such as molecular dynamics simulations provide an accurate and fast way for such tasks.

4.1.1.1.Layer number dependent inter-layer thermal resistance in few layer graphene

By using non-equilibrium molecular dynamics (NEMD) simulations, Wei *et al* [251] calculated the layer number dependent interfacial thermal resistance between two neighboring graphene layers. The interfacial thermal resistance R_{inter} was obtained according to the following formula

$$(N-1)\cdot R_{\text{inter}} = \frac{N\cdot L}{\kappa_{\text{C}}}$$

where L is the layer thickness (i.e. 0.34 nm), N is the layer number and κ_{c} is the effective cross-plane thermal conductivity of multilayer graphene. The value of the interfacial thermal resistance for $N = 48$ is almost one order magnitude smaller than that for $N = 6$. The decreasing trend for the interfacial thermal resistance with the layer number was explained by the size effects. It is the hot and cold reservoirs that limit the phonon mean free path, which causes the interfacial thermal resistance decreases almost linearly with the layer number.

To eliminate the size effect in NEMD, Ni *et al* [252, 253] adopted an approach based on equilibrium molecular dynamics (EMD) simulations. The thermal resistance R_{int} between two systems with temperature difference ΔT could be calculated by the following equation proposed by Volz *et al* [254]:

$$R_{\text{int}}k_{\text{B}} = \int_0^{\infty} \frac{\langle T(0)\,\Delta T(t)\rangle}{\langle T(0)^2\rangle} dt \left(\frac{1}{N_1}+\frac{1}{N_2}\right),$$

where k_{B} is the Boltzmann constant, N_1 and N_2 refer to the number of degrees of freedom of the two subsystems in interaction. This method is not constrained by the thermal reservoirs and allows for

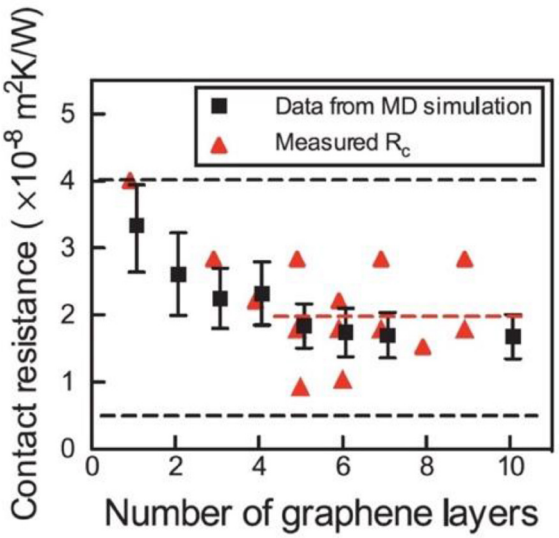

Figure 17. Contact resistance between FLG and SiO_2 substrate versus layer number at 300 K: a comparison between MD simulations and measurements. Reproduced with permission from [257]. The red dashed line is the averaged value of the experimental results. Reproduced with permission from [256].

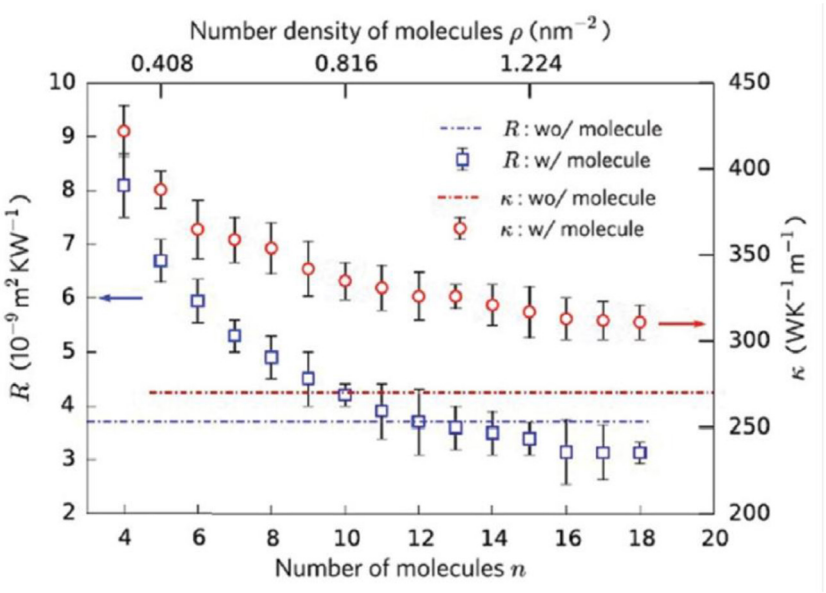

Figure 18. In-plane thermal conductivity (red circles) of the graphene based film and its associated thermal resistance R (blue rectangles) with the functionalized graphene substrate as a function of the number of molecules and the equivalent molecule number density in the functionalized graphene substrate. Reproduced with permission from [110].

the calculation of the thermal resistance between two single layers of graphene. The calculated resistances from different methods shown in figure 16 agree in that the interfacial resistance decreases as the number of FLG increases. The interfacial resistance finally reaches the graphite limit at large layer numbers.

Unlike in suspended FLG, no significant layer dependence is found for R_{int} in supported FLG SiO_2 substrate [255], indicating that it is less sensitive to the layer number due to the existence of the substrate. At small layer numbers, R_{int} in supported FLG is much lower than that in the suspended configuration. These results suggest that one can reduce R_{int} in suspended FLG either by increasing the graphene layer number or by adding a substrate.

4.1.1.2.Layer number dependent interfacial thermal resistance between few layer graphene and a substrate

The thermal contact between graphene and the substrate is known to be impeded by the weak Van der Waals interactions at play. Despite a large number of studies on the SLG-substrate and FLG-substrate contact resistances, the latter has always been considered as independent to the layer number, since no correlation between resistance and layer number could be observed due to experimental inaccuracy. However, equilibrium

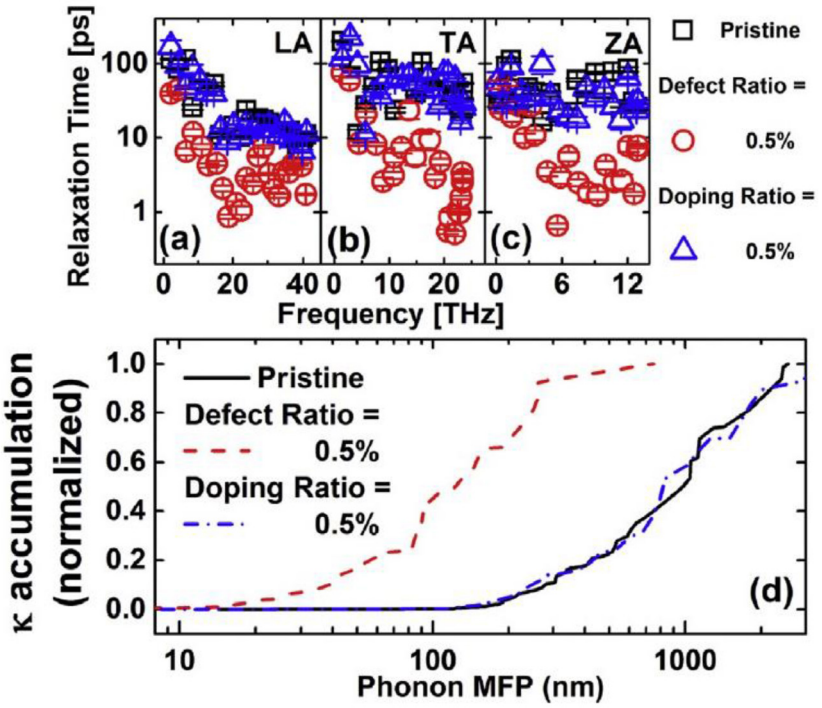

Figure 19. Comparison of the effects of defect and doping on thermal transport properties of graphene. Reproduced with permission from [268].

molecular dynamics calculations reveal that the contact resistance between FLG and SiO_2 decreases with layer number and converges for six graphene layers [256]. Figure 17 shows that the MD data are in satisfactory agreement with the experimental values [257], especially for FLGs with layer number from 1 to 4. When the layer number is larger than 4, the measurement gave a range of the resistances due to the limited experimental accuracy, but the averaged value of 2×10^{-8} m^2 KW^{-1} (red dashed line) is quite close to the MD data 1.7×10^{-8} m^2 KW^{-1}.

4.1.2. The effects of interfacial coupling and substrate property

The interfacial thermal resistance (R_{int}) between graphene/FLG and the substrate is a crucial limiting factor to their thermal performance in devices. Covalent functionalization has been proved to efficiently promote heat transfer between interfaces by introducing additional thermal pathways through the functionalizing molecule. Zhang [110] and Han [258] *et al* studied the thermal performance of a supported graphene-based film with the addition of silane-functionalized molecules. Their molecular dynamics simulations show that both the thermal conductivity and R_{int} decrease with respect to the number density of the silane-based molecules (figure 18). Wang *et al* [259] reported that the interfacial thermal transfer can be engineered by intercalating guest atoms such as argon, which modulates the interfacial thermal conductivity, and insulates the supported graphene sheet electronically. Luo *et al* [260] used steady-state NEMD to calculate interfacial thermal resistance of graphene/graphite-polymer systems. They found that long wavelength phonons in graphene play important roles in thermal transport across the graphene-polymer interfaces. The existence of the low frequency modes (2–16 THz), due to out-of-plane motions, enables strong coupling between graphene spectra and polymer spectra and thus facilitates interfacial thermal transport. Using MD simulations, Chen *et al* [261] found that thermal conductivity of supported FLG increases rapidly with the layer thickness, reaching about 90% of that of the bulk graphite limit at 6 layers, and eventually saturates at the thickness of 13.4 nm (40 layers).

Phonon transmission through graphene interfaces is affected not only by the atomic interactions but also by the structure of substrate. In traditional understanding, amorphous solids transport heat far slower than its crystalline forms due to the short phonon mean free path. However, when it comes to the interfacial thermal transport where the intrinsic phonon mean free path of one component at the interface does not dominate the thermal conductance, the situation can be different. With NEMD simulations, Li *et al* [262] studied the effect of the crystallinity of SiC substrate, and found that the R_{int} across amorphous interface is smaller than crystalline interfaces. This phenomenon is presumably due to rough surface feature of amorphous solids and the wide phonon channels opened by the smooth phonon density of states of amorphous SiC. Nevertheless, Zhang *et al* [263] reported that the heat removal ability in 2D transistors does rely heavily on the thermal conductivity of the substrate, and it is difficult to largely reduce the

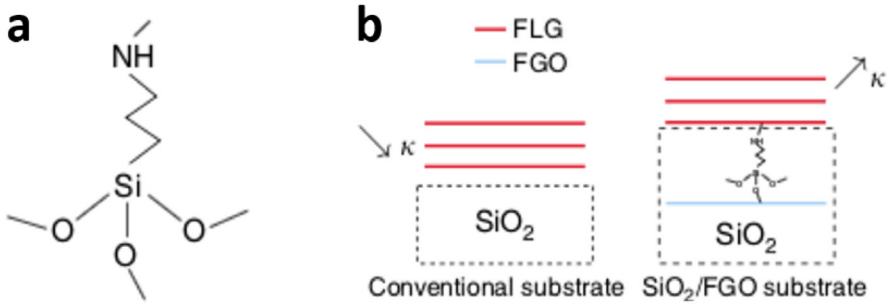

Figure 20. (a) Sketch of the chemical bonds of the silane molecule. (b) Schematic of a graphene film on different supports. Left: conventional silica substrate. Right: the proposed silica/FGO substrate. Reproduced with permission from [62].

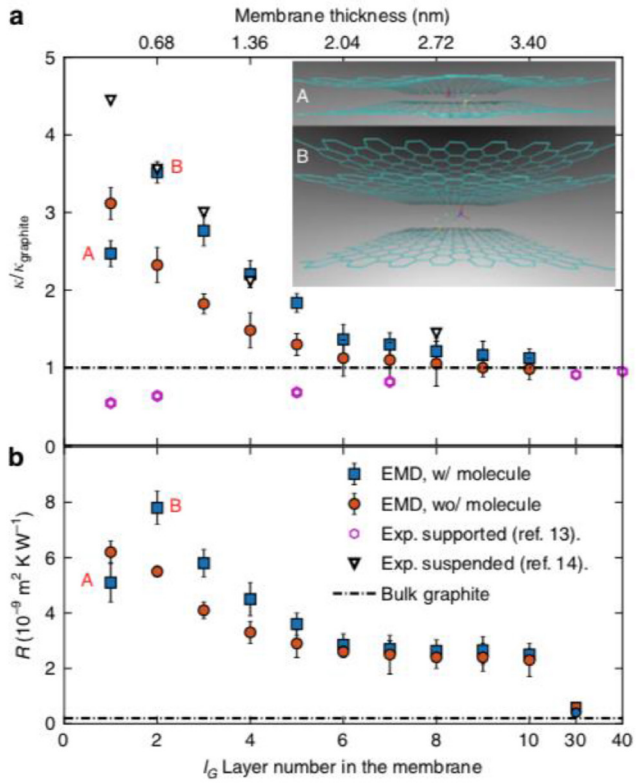

Figure 21. (a) Molecular dynamics simulation results of in-plane thermal conductivity k of the graphene film and (b) interfacial thermal resistance R between the FGO substrate and the graphene film versus the graphene layer number l_G in the film. The molecule density is $r = 0.081\,\mathrm{nm}^{-2}$. Reproduced with permission from [258].

hot-spot temperature by tuning the 2D material–substrate interface resistance.

Apart from the above mentioned factors, the thermal property of graphene can also be affected by other means, such as strain engineering [264], and by creating phononic crystal structures [265].

4.1.3. The effects of doping on graphene thermal performance

Doping is the most feasible method to open a sizeable and well-tuned bandgap in graphene. The B and N atoms are the natural candidates for doping in graphene because of their similar atomic size as that of C and of their hole acceptor and electron donor characters for substitutional B- and N-doping, respectively [266]. However, the thermal performance of graphene can be affected by doping. Using NEMD, the interfacial thermal resistance and thermal rectification of nitrogen-doped zigzag graphene (NDZG) are investigated by Shi *et al* [267]. It is found that the interfacial thermal resistance at the location of nitrogen-doping causes severe reduction in thermal conductivity of the NDZG. Thermal rectification of the triangular single-nitrogen-doped graphene (SNDG) decreases with increasing temperature. Chen *et al* investigated the effects of defect and isotopic doping with different ratios on the thermal conductivity of graphene by NEMD [268, 269], as shown in figure 19. The spectral phonon relaxation time and normalized accumulation thermal conductivity with respect to the phonon mean free path (MFP) reveal that the long-MFP phonon modes are strongly suppressed in the defected and doped

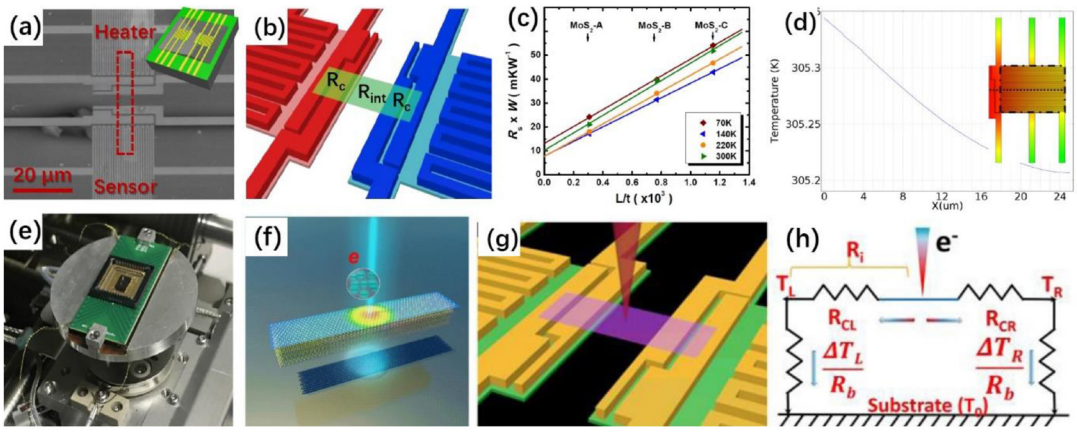

Figure 22. (a) SEM image of suspended MEMS devices, the rectangle in red color is the 2D materials ready to be measured, the scale bar is 20 μm. Insert: schematic of a prefabricated suspended thermal bridge device. (b) Schematic of the thermal contact resistance R_c and the intrinsic thermal resistance R_{int}; R_c comes from the contacting point between sample and suspended membranes. (c) Length-dependent thermal resistance of suspended few-layer MoS_2, from which R_c can be extracted. (d) Temperature profile crossing the Sensor (Finite Element Simulations: COMSOL Multiphysics 5.2)). (e) Picture of the measurement stage (Electron-beam self-heating method) and chip carrier adapted on the SEM sample holder. (f) Schematic of high-energy electron beam pathing though sample. (g) Schematic diagram of the focused electron-beam self-heating technique. (h) The equivalent thermal resistance circuit for the electron-beam self-heating method, showing the $R_i(x)$ from the left sensor to the local heat spot, the thermal contact resistance (R_{CL} and R_{CR}), temperature rise of the left (ΔT_L) and right (ΔT_R) sensor. Reproduced with permission from [95, 273].

graphene, resulting in the suppressed size dependence and the weaker temperature dependence of the thermal conductivity compared to the pristine graphene.

4.2. Functionalization of graphene to increase heat spreading performances

Graphene in-plane heat conduction can be increased by intercalating chemical bonding between graphene and substrate. Accordingly, thermal management of a micro heater can be considerably improved via introducing alternative heat-spreading channels implemented with graphene assembled film (GF) bonded to functionalized graphene oxide (FGO) through amino-silane molecules. A GF bonded to the FGO substrate through silane molecules is shown in figures 20(a) and (b). 3-Aminopropyltriethoxysilane (APTES) has three –Si–O– groups and one $–NH_2$ end, as shown in figure 4(a). Owing to the simple chemistry of APTES, it can easily bind two different substrates. The –Si–O end of APTES binds to the GO substrate. The crosslinked Si–O structure acts as a strong bonding layer between the substrate and GFs. On the other hand, the $–NH_2$ end of APTES binds onto carboxyl groups on the functionalized graphene film.

To explore the effect of functional APTES molecules on the in-plane thermal conductance of the graphene film, molecular dynamics simulations were implemented to study a nanoscale molecular junction between two stacks of multilayer graphene nanoflakes.

The in-plane thermal conductivity k of the film and its interfacial thermal resistance R with the FGO substrate is plotted as a function of the graphene layer number l_G in the film in figures 21(a) and (b), respectively.

It is clearly seen from figure 21(a) that the critical layer number for the in-plane thermal conductivity switch is $l_c = 2$.

The microscopic origin of the thermal conductivity k enhancement in the graphene film was investigated by probing the mode-wise phonon relaxation time. By inserting the APTES molecule, the relaxation time of the acoustic flexural modes ZA largely increase at low frequencies, whereas the longitudinal and transverse modes undergo a slight decrease. The notable increase for the ZA modes accounts for the enhancement in k of the graphene film bonded to the substrate since the ZA modes contribute considerably to k as much as 77% at 300 K [30].

The cross-plane heat conduction between the top graphene films and the lower FGO layers is governed by the competing effects of (i) the intercalation of the molecules that tends to weaken the interlayer coupling of graphene therefore increasing the cross-plane thermal resistance and (ii) the additional heat channels introduced by the molecules covalently bonding the graphene sheets that tend to facilitate the cross-plane thermal coupling.

Molecular dynamics simulations and *ab initio* calculations reveal that the functionalization constrains the cross-plane scattering of low-frequency phonons, which in turn enhances in-plane heat conduction of the bonded graphene film by recovering the long flexural phonon lifetime. Those results provide evidence that a graphene film deposited on a FGO substrate provides a very attractive platform for thermal management applications.

5. Thermal characterization

There are various thermal characterization methods. Each method can give very different results even for the same material. This puts the characterization into a central and critical role as graphene based

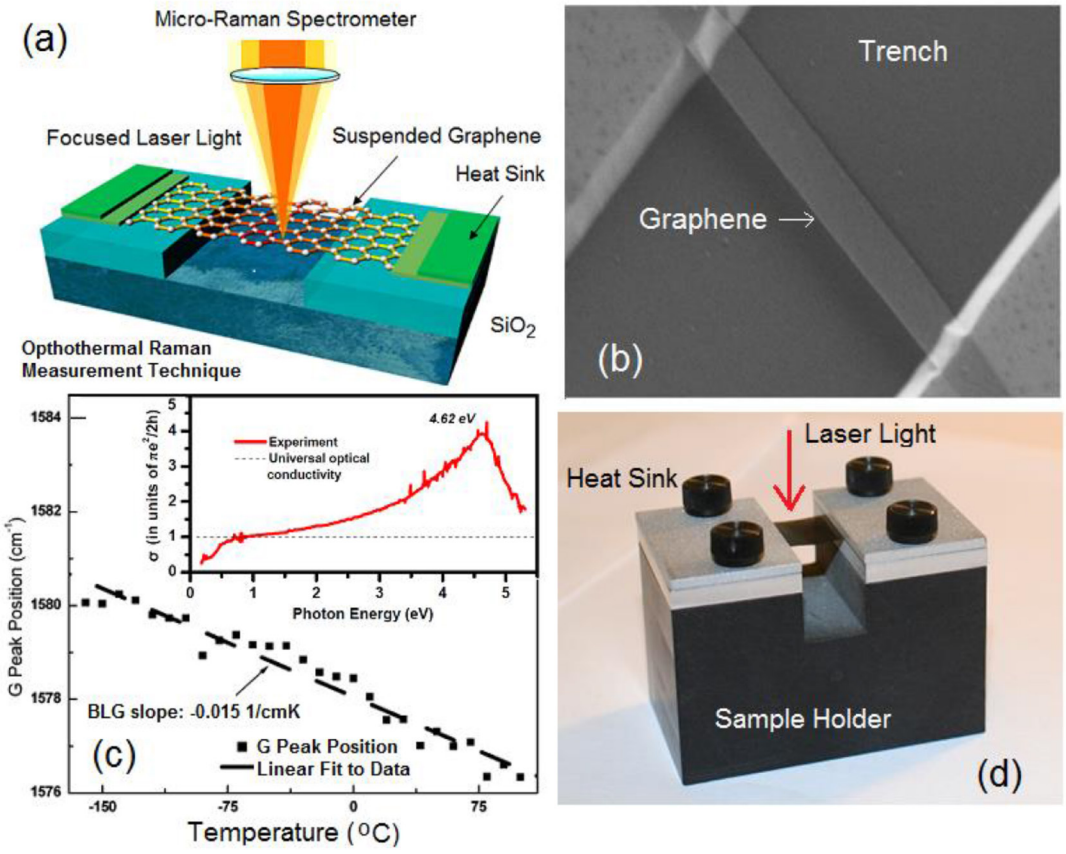

Figure 23. Illustration of the optothermal Raman technique. The first experimental study of thermal conductivity of graphene was made possible with an optothermal Raman technique (panel (a)). The heating power ΔP was provided by a laser light focused on a suspended graphene layer connected to heat sinks at its ends. Scanning electron microscopy image shows bilayer graphene of rectangular shape suspended across a 3 μm-wide trench in a Si wafer (panel (b)). Temperature rise, ΔT, in response to changing excitation power, ΔP, is determined with a micro-Raman spectrometer. The G peak in graphene's Raman spectrum exhibits strong temperature dependence (panel (c)). The inset shows that the optical absorption in graphene is a function of the light wavelength. The calibration of the spectral position of the G peak with temperature is performed by changing the sample temperature while using very low laser power to avoid local heating. The optothermal Raman technique has been extended to other suspended films (panel (d)). The images are reproduced with permission from the Nature Publishing Group.

materials for real use often exists in micro-thick dimensions. Below is a summary of the state-of the art of the thermal measurement techniques used for the graphene and other 2D materials.

5.1. Thermal bridge

The thermal bridge method was firstly introduced/invented by Kim *et al* to measure the thermal conductivity of individual multi-walled CNTs in year 2001, before which time thermal conductivity of nanotubes/nanowires were measured in the form of pallet or bundles using one-heater two-sensors method and the measured thermal conductivity in not intrinsic due to the dominated inter-tube scatterings [270]. Complex electron beam lithography was introduced to fabricate microdevices suitable for thermal measurement, in which two suspended microelectromechanical system (MEMS) were fabricated and used to suspend low-dimensional samples and detect temperature changes at microscale. This thermal bridge method is considered to be one the most successful techniques in measuring thermal conductivity and thermopower of nanotubes, nanowires and 2D materials [271, 272].

Thermal bridge method was firstly used by Xu *et al* to measure the thermal conductivity and thermal power of suspended single layer graphene [31, 95, 274]. Figure 22(a) is the scanning electron microscope image of a typical MEMS device. The MEMS consists of two 25 μm $\times$ 20 μm low-strain SiN_x membranes, each is suspended by six 400 μm to 600 μm long beams. A platinum or gold resistive coil is prepatterned on top of each SiN_x membranes and beams, which serves as both heater (R_h) and temperature sensor (R_s), depending on the direction of heat flow. The suspended single layer graphene thermally connects these two membranes and is electrically isolated from the resistive coil. The device should be mounted in chamber with vacuum condition better than 1×10^{-5} pa, to eliminate background gas convection and thermal radiation between membranes. An AC current (usually with amplitude of 100 nA to few μA and frequency of few thousand hertz) with a biased DC voltage is applied to the heater, and another AC current with the same amplitude/frequency is applied to the sensor. The DC current (I) is used to apply micro-watt Joule heat into heater and increase its temperature (T_h) and the AC current is used to measure the resistance of R_h/R_s, corresponding

to T_h/T_s since resistive coil can be used as temperature monitor. The Joule heat at the heater R_h will partly dissipate through the six beams. The rest of them will dissipate through sample which connecting the two membranes, gradually increases the temperature T_s at sensor R_s. In the steady state, the thermal conduction of sample σ_s and the suspended SiN_x beams σ_l, can be obtained from $\sigma_l = (Q_h + Q_l)/(\Delta T_h + \Delta T_s)$ and $\sigma_s = \Delta T_s \sigma_l/(\Delta T_h - \Delta T_s)$, where Q_h, Q_l, ΔT_h, and ΔT_s are heating power on heater, heating power on one SiN_x beam, temperature rise at R_h and R_s, respective. The thermal conductivity κ of sample can be obtained by $\kappa = L \times \sigma_s/S = L/(R \times S)$, where L, S and R are the sample length, cross-section area and total thermal resistance.

Thermal bridge method is commonly used in measuring thermal conductivity of suspended single or multiple layer 2D materials including graphene [31, 95, 275–277], boron nitride [248, 278, 279], black phosphorus [280–282], transition-metal dichalcogenides [273, 283–285] and etc. However, there are many problems and challenges. For example, thermal conductivity of graphene and MoS_2 scatters several folds randomly, leaving the intrinsic thermal conductivity unsolved with hot debate and disagreement persisting [31, 95, 273, 275–277, 283–285].

The primary challenge lies in the thermal contact resistance R_c at the two ends of samples, which contributes unavoidably to the total measured thermal resistance R, i.e. $R = R_{int} + 2R_c$, where R_{int} is the intrinsic thermal resistance of sample (figure 22(b)). To reduce the influence from the R_c, Xu *et al* deposited metal bars at two ends of graphene to create additional heat path, however the length-dependent thermal resistance of suspended graphene shows that the contact cannot be eliminated to below the negligible level [31]. Therefore, systematic measurement of length-dependent thermal resistance is always required to extract the R_c at every temperature measured (figure 22(c)) [283, 286]. Alternatively, Liu *et al* and Adil *et al* used a brand-new method, i.e. electron-beam self-heating technique, to measure the R_c directly, which will be discussed in details later in this manuscript (section 5.2) [276, 287].

The secondary challenge is related to the uneven temperature distribution inside the SiN_x membrane. The measured T_h and T_s, corresponding to R_h and R_s, are the averaged temperature of membranes, however the temperature at contact point between sample and membrane are required to calculate thermal conductivity. This mismatch obscures the intrinsic thermal conductivity especially at the situation when σ_s and σ_l are in the same order of magnitude. To solve this problem, a finite element simulation is required to simulate the exact temperature rise at the contact point (figure 22(d)) [277, 278].

Some other minor challenges are: (a) the geometric asymmetry of heater and sensor beams, due to electron beam lithography and etching processes, could introduce further measurement uncertainty or thermal rectification [288]; (b) background thermal radiation between membranes should be further measured and substracted when sample hold extremely low thermal conductance [289]; (c) the absorbed particles, in particular the polymer residues, can reduce the thermal conductivity of suspended 2D materials to be at a comparable level to that in supported ones, which obscures the intrinsic thermal conduction of the 2D phonons [275].

Improved thermal bridge (ITB) method can be used to measure much thicker materials. Instead of placing mono- to few-layer 2D materials on the microfabricated heaters and temperature sensors, thick 2D material strips can be suspended between two homemade resistors to measure the in-plane thermal conductivity of the target material [40].

5.2. Electron beam self-heating method

Electron-beam self-heating method provides a direct measurement of thermal contact resistance, and therefore the intrinsic thermal conductivity [273, 276, 287]. This method is modified based on the thermal bridge method and the sample is mounted inside the SEM chamber for measurement (figure 22(e)). Different from thermal bridge method where R_h acts as heating source and R_s as temperature sensor, the two membranes are both regarded as temperature sensor and the electron beam is used as the heating source. During measurement, the electron beam is scanned along the length of sample, during which the energy of electrons is absorbed and therefore heats the local spot (figures 22(f) and (g)).

The local heat generated by absorbed electrons flows towards the two membranes and increases their temperature. The measured thermal resistance ($R_i(x)$) from one membrane to the heating spot is given by: $R_i(x) = R_l\left[\frac{\alpha_0 - \alpha_i(x)}{1+\alpha_i(x)}\right]$, $\alpha_0 = \frac{\Delta T_{L0}}{\Delta T_{R0}}$ and $\alpha_i = \frac{\Delta T_L}{\Delta T_R}$, where R_l is the equivalent thermal resistance of the supporting beams, x is the distance from one membrane to heating spot. ΔT_{L0} and ΔT_{R0} are the temperature rises of the left and right membranes measured by thermal bridged method. ΔT_L and ΔT_R are corresponding temperature rise when the focused electron beam is scanned along the length of the samples. The thermal conductivity of the samples is calculated by: $\kappa = \frac{1}{(dR_i/dx)\cdot A}$, where A is the cross-section area of the samples (figure 22(h)).

Electron-beam self-heating method is considered to be the rare techniques which can measure the thermal contact resistance and interfacial thermal resistance of heterostructure directly. However, this technique is still quite challenging. The primary challenge lies in the difficulty in fabricating clean and suspended sample suitable for the measurement, since any polymer residue, defects, rough edges etc could affect the path of high-energy electrons and results in fluctuation in $R_i(x)$ curves. More importantly, this

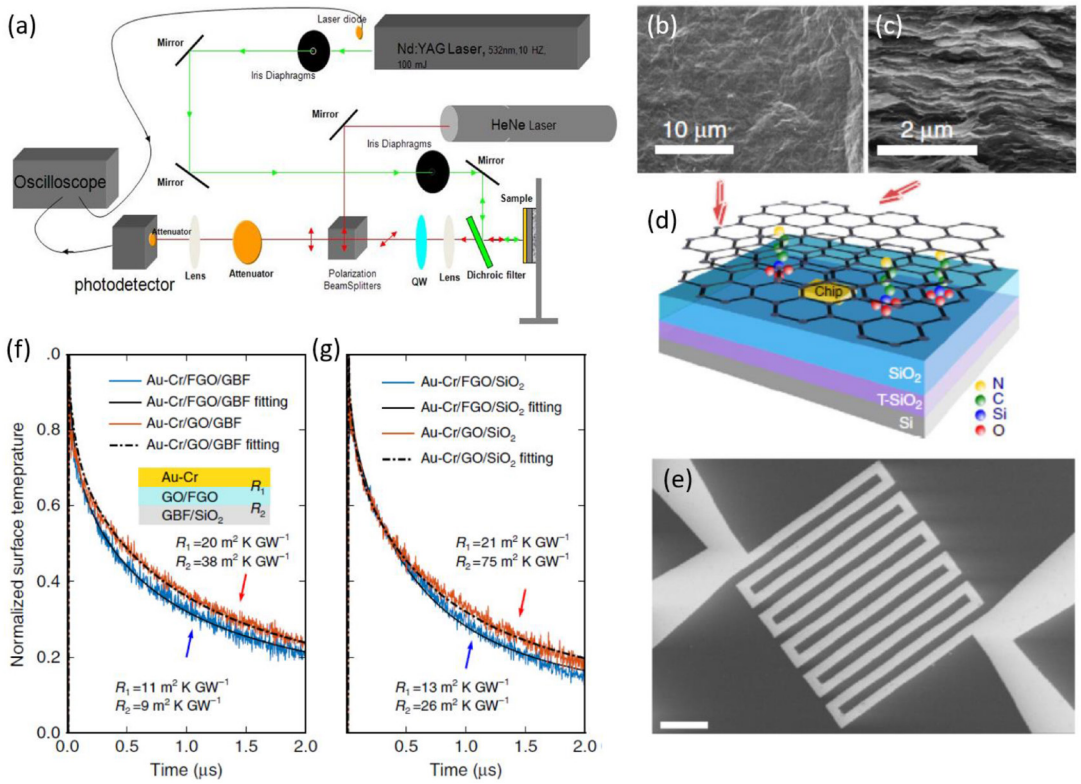

Figure 24. (a) Schematic diagram of the pulsed photothermal reflectance technique. (b) Top view of the graphene film. (c) Cross-section of the graphene film. (d) Schematic of the functionalization interface. (e) Hotspot structure. (f) Normalized surface temperature of PPR measurmenet of the thermal interface resistance at the Au-Cr/FGO/GF and Au-Cr/GO/GF samples. (g) Normalized surface temperature of PPR measurmenet of the thermal interface resistance at the Au-Cr/FGO/SiO_2 and Au-Cr/GO/SiO_2 samples. Reproduced with permission from [258].

technique is limited to thick samples in which there are relatively long path for the focused electron beam to go through and more atoms and electrons to interact with each other, introducing more heat in sample and increasing the signal to noise ratio [273]. This is probably the reason that the extension of such a technique to suspended single-layer 2D materials has not been reported yet.

5.3. Scanning thermal microscopy

Scanning thermal microscopy (SThM), modified from atomic force microscopy (AFM), is a type of scanning probe microscopy that maps the local temperature with nanoscale resolution and the thermal conduction of the samples. Instead of a sharp probe in AFM, a thermal resistance probe or thermocouple probe is used to detect the local temperature. This technique has been used to measure heat dissipation, local heat spot, grain boundaries of graphene and other 2D materials electronic devices [52,224,290–293]. However, directly measuring thermal conductivity of 2D materials or other nanomaterial is nearly impossible due to the unknown heat loss from cantilever, air conduction/convection, tip-sample interfacial thermal resistance, heat radius and etc [271].

Recently a crossover from ballistic to diffusive thermal transport in suspended graphene membranes was measured using the SThM technique. Suspended single-layer graphene membranes with radius between 150 nm and 1.6 μm were measured in a high-vacuum SThM with 17 nm thermal spatial resolution. The dependence on the thermal contact resistance between tip and graphene as a function of the membrane radius was obtained, with values between 1.15 and 1.52 $\times$ 10^8 KW^{-1} [294].

For the samples with radius below 775 nm the variation of the contact resistance was explained in terms of ballistic phonon transport, while in the larger samples a transition from ballistic to diffusive thermal transport was observed. This study also emphasized the role of the surface quality of the graphene sample and the thermal resistance between the graphene and the substrate on thermal transport.

5.4. Optothermal Raman spectroscopy

The optothermal Raman spectroscopy technique for measurements of the thermal conductivity has been developed and popularized by Balandin and coworkers in the context of graphene research [18, 19, 21, 22, 28, 57, 295–297]. This steady-state technique was first used to measure the thermal conductivity of the suspended graphene flakes, and later extended to a range of other 2D materials and macroscopic thin films. In the optothermal Raman technique, the excitation laser acts simultaneously as a local heat source and temperature sensor [18, 19, 21, 22, 295,

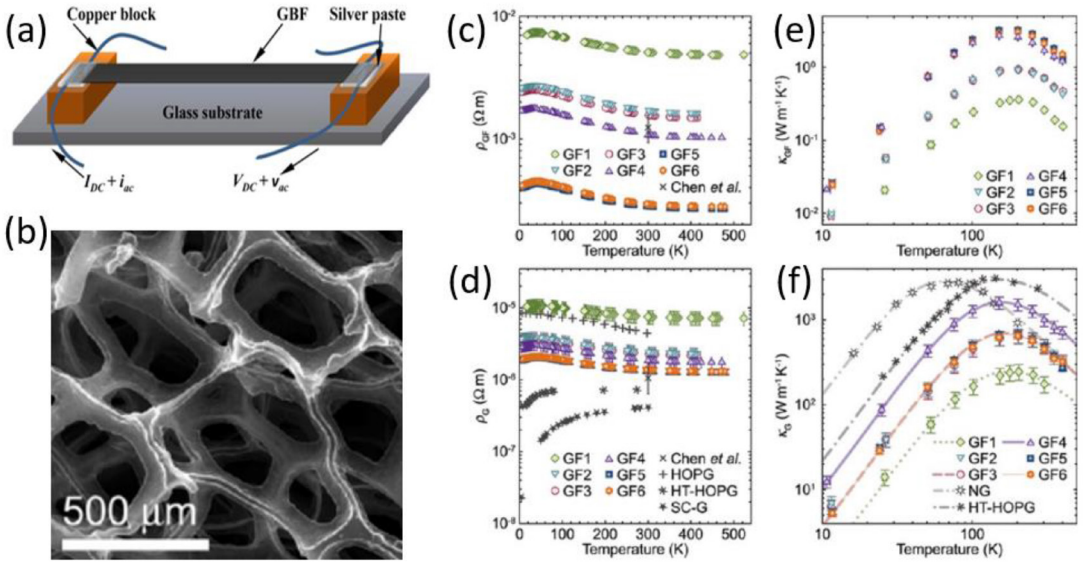

Figure 25. (a) Schematic diagram of the DRT method for the measurement of thermal conductivity. (b) 3D graphene based foam architecture. (c) Effective electrical resistivity of the graphene based foam. (d) Solid electrical resistivity of the FLG and ultrathin graphite within the graphene based foam. (e) Measured effective thermal conductivity of the graphene based foam. (f) Solid thermal conductivity of FLG and ultrathin graphite. Images (b)–(f) are reproduced with permission from [177].

296]. The method requires the material under study to have a pronounced phonon Raman peak. As the first step, one establishes the temperature dependence of the Raman peak. It is done using the low power laser excitation to avoid local heating of the sample with the laser. The sample temperature is controlled externally by placing the sample to the cold-hot cell. The temperature dependence of the Raman peaks constitutes the calibration characteristic, which can be used for determining the local temperature. As the second step, one starts to increase the power of the excitation laser in order to produce local heating on the sample. The resulting temperature is calculated from the shift in the Raman peak position and known calibration characteristic. The measurement procedure also requires the knowledge of the dissipated power in the sample. In the original experiments by the Balandin and co-workers for investigation of the thermal conductivity of graphene, the dissipated power was determined by comparing the measured integrated Raman intensity of the G peak of graphene and graphite [18]. In the follow up works, whenever the sample geometry allowed, the methods was modified to measure the transmitted power by a detector placed under the sample [19]. It is important to determine the absorbed power of the laser light under the conditions of the experiment. For example, the optical absorption of graphene can be higher than 2.3% per atomic plane at higher photon energies (shorter wavelength), and be affected by the surface contaminations, sample bending and near-field optical effects due to reflectance from the substrates [19, 295]. Figure 23 illustrates Balandin´s method of measuring the thermal conductivity using Raman spectroscopy on the example of graphene and macroscopic thin film.

Since the development of this technique by Balandin and co-workers [18], this non-contact technique has been used for measuring thermal conductivity of various graphene based films [19, 20, 26, 121, 298] and a wide range of other 2D materials [299–303]. The application of this technique is not limited to quasi-2D materials, and has been extended to relatively thick films [90, 113]. More details of the technique can be found in a few dedicated reviews [19, 96, 295, 304].

Recently, a variation of the Raman based technique, namely two-laser Raman thermometry was introduced [305]. The basic idea of this method is to use two lasers: one high power laser fixed in the centre of the membrane, which serves as a steady state heater (405 nm wavelength), and another, low power, probing laser (488 nm wavelength), which probes the Raman shift on the sample. For both heating and probe laser the absorbed power is measured, and the probing laser power is kept to the minimum to avoid sample heating.

Either temperature profiles or the full temperature maps of suspended samples can be obtained with this technique, allowing for the direct solution of the Fourier heat equation. This is an improvement compared to the techniques based on one laser, were only the temperature of the hotspot is probed. The technique has been succesfully applied for measuring the thermal conductivity of 2D materials, such as MoS_2 [235].

5.5. Pulsed photothermal reflectance

Figure 24 shows the schematic diagram of pulsed photothermal reflectance (PPR) experimental setup. In this approach, thermal conductivity of the materials (bulk or film) is characterized in nanosecond regime by thermoreflectance technique. Keading *et al* were the first to apply the PPR technique to measure the thermal conductivity of SiO_2 thin films [306]. This technique is

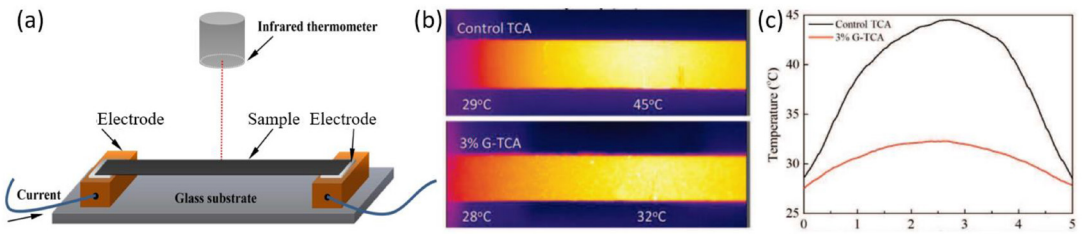

Figure 26. (a) Sketch of the Joule heating set-up. (b) Suspended graphene enhanced conductive adhesives measured by the Joule heating method. (c) Temperature profiles of the graphene based conductive adhesives as shown in (b). Reproduced with permission from [313].

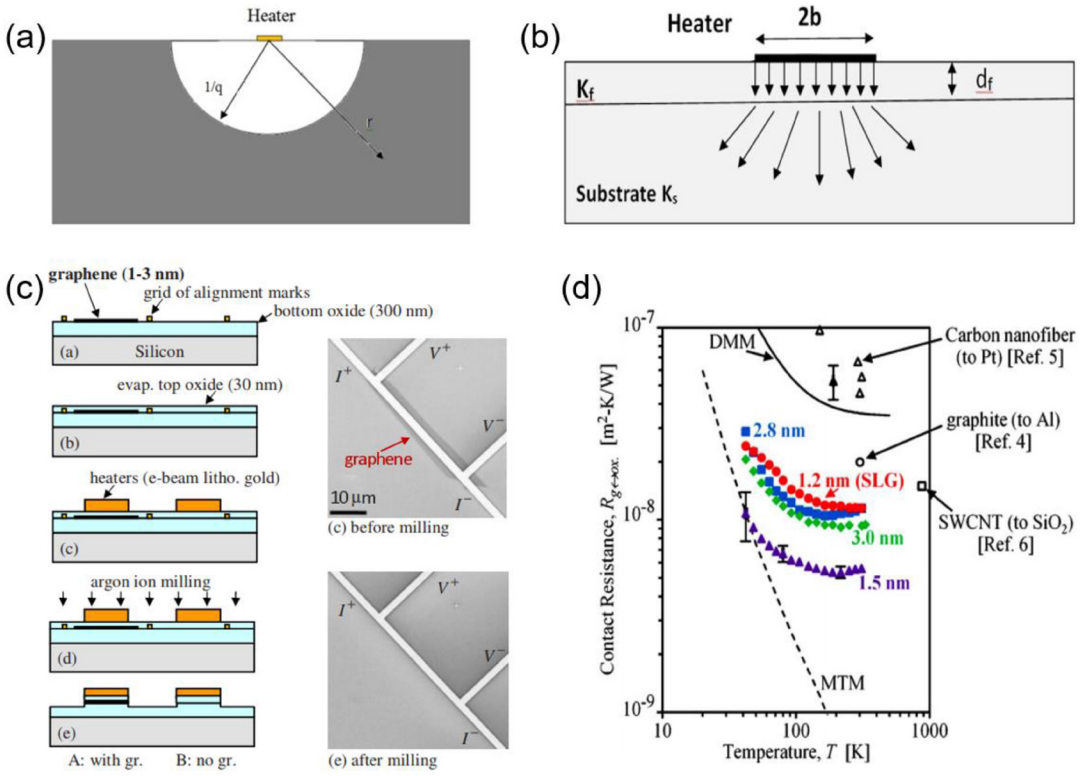

Figure 27. (a) Schematic diagram of conductive wire deposited on top of the surface for thermal conductivity measurement of bulk materials. This wire acts as a heater and thermometer. (b) Heat flow for a low thermal conductivity film on high thermal conductivity substrate. In this case $K_f \ll K_s$ and $d_f \ll 2b$. (c) Sample fabrication using 3ω method to measure the thermal contact resistance between graphene and SiO_2 substrate. Reproduced with permission from [322]. (d) Experimental measurements of the thermal contact resistance between graphene and SiO_2, for four samples of different thicknesses. Reproduced with permission from [322].

an optical and noncontact method consisting a pump laser and a probe laser. Before the measurement of thermal conductivity, a metal film, preferably gold is deposited on top of the sample surface for the purpose of enhancing heat absorption and capturing surface temperature by thermoreflectance technique.

Han *et al* applied the PPR method to measure the interfacial thermal resistance between rGO films (with and without chemical functionalization) and the supporting substrate [258]. They used a Nd:YAG laser pulse with a full width at half maximum of 7 ns, pulse repetition rate of 10 Hz, and pulse energy of 5 mJ. The measurement started with the pump laser pulse with spot size of 3 mm incident on the sample surface that induces the sample's surface temperature change over time. The heated surface induces a change in refractive index on the surface [307]. The probe laser is a 1 mW He–Ne laser focused at the center of the pump spot with a 20 μm spot size to monitor the changes in the beam reflected from the gold surface. The temperature excursion of metal surface is measured through the temperature dependence of metal's reflectivity. Since for most metals, the thermo-reflectance coefficient $C_{tr} = \Delta R/(R_0 \Delta T)$ where R_0 and T are a reference reflectivity and the metal temperature respectively) is about constant [307], the intensity of reflected probe beam is inversely proportional to the gold surface temperature. Temperature excursion profile depends on the thermal properties of the underlying layers and thermal resistance between the layers. By

solving the heat diffusion equation analytically, the thermal properties of a film can be extracted from its thermal response captured by the PPR technique [198, 308, 309].

5.6. Dependence of resistance on temperature

In this method, the suspended sample is heated by running the alternating current (AC) and DC current through the sample and temperature of the sample was measured by dependence of the resistance on the temperature (DRT) of the sample. In this case, the temperature coefficient of resistance of the sample was measured as well. The film was suspended between two copper heat sinks and placed in a vacuum chamber and electrodes were attached in a four-point differential resistance configuration. The sample has to be cut into slices with the ratio of length/width less than 0.1. Therefore, the heat conduction along the GF can be considered as 1D heat transfer. Figure 25(a) shows the schematic diagram of the self-heating (DRT) method. In the AC method, a $i_{ac,rms} = 1$ mA current with a frequency of 2000 Hz coupled with the DC current was run into the sample, raising its temperature through Joule heating. Then the resistance of the sample at different values of I_{DC} is obtained by $R_{sample}(I_{DC}) = v_{ac,rms}/i_{ac,rms}$ where $v_{ac,rms}$ is the first harmonic voltage drop across the sample measured by lock-in amplifier. During self-electrical-heating of the sample, the change in electrical resistance of the UGF was measured and used to determine the average temperature rise. The thermal conductivity of the sample is then obtained by using the applied Joule heating power and corresponding average temperature rise as inputs to a combined heat conduction [40, 177, 310]. Figures 25(b)–(f) shows an example of using the DRT method to measure the thermal conductivity of 3D graphene based foam architecture.

5.7. Joule heating

Nanomaterials such as graphene and CNTs show clear temperature dependent Joule heating effect [311, 312]. In this method, the suspended graphene films are heated by running a direct current (DC) and the temperature rise of the sample is measured by inferred radiation (IR). The sketch of the Joule heating set-up and samples are shown in figure 26(a).

During the measurement, the material is suspended and fixed across two electrodes. A DC current will be run through the material and the temperature of the material would correspondingly change. The DC current is adjusted to have a temperature rise of less than 10 °C on the target material so that the radiation and convection loss can be neglected. The volumetric heat generation due to Joule heating, $Q = VI/(Lwt)$, is uniform, where w, t and L are the width, thickness and length of the sample, and V, I are the voltage across the contacts and the current, respectively.

Due to the difference in the heat capacity of the target material and the heat sink, the temperature profile along the film will reach a steady state within several micro-seconds after heating. All the experiments were conducted in an airtight testing environment in order to prevent the effect of airflow. During the measurement heat sink temperature was maintained in constant temperature $T_{L/2} = T_{-L/2} = T_o$. Temperature profile of the target material is distributed symmetrically with respect to the center of the sample.

The maximum temperature T_M was achieved in the center of the sample. By considering the temperature at the edge (T_0) and middle point (T_M) of the sample, the thermal conductivity of the target material is defined by the following equation:

$$k = \frac{VIL/2}{4wt(T_M - T_0)}. \quad (3)$$

Where k is the in-plane thermal conductivity of target material. By measuring the temperature at the edge and center of the material by IR detector, together with the voltage across the sample and applied current and the dimensions of the sample, the thermal conductivity can be calculated. For instance, Wang *et al* used the Joule heating method to measure the thermal conductivity of graphene enhanced thermal conductive adhesives and they found that the thermal conductivity of conductive adhesive with 3 wt% graphene is 8 W m^{-1} K^{-1}, which is about 4 times higher than the reference conductive adhesive without graphene [313]. The IR image and temperature profile of the graphene enhanced conductive adhesive sample is shown in figures 26(b) and (c).

5.8. 3ω method

Corbino [314, 315] in 1911 noticed that when a current at frequency ω runs through a resistor, in addition to a voltage across the resistor at frequency ω, the third-harmonic voltage (3ω) appears in the resistor. This effect is a consequence of the temperature dependence of resistivity. Later, it was found that the third-harmonic voltage has a practical application to measure the thermal properties of solids and liquids [316]. In this technique, a thin metal wire is used to heat the specimen indirectly and the same wire serves both as a heater and thermometer. The 3ω technique, was developed by Cahill and Pohl in 1987 [317] and now it is a widely used technique for thermal conductivity measurement on bulk and thin film [109, 318–320]. The method used is based on heat diffusion in a semi-infinite solid as shown in figure 27(a). A thin electrically conductive wire is deposited on top of solid-state specimen whose thermal conductivity needs to be measured. Figure 27(b) shows the cross section of the heat flow in a typical thin film sample.

In most thermal conductivity measurement techniques, heat is applied at a known rate and the temperature is monitored to deduct the thermal conductivity. In the 3ω method, the deposited wire acts as a heater and thermometer simultaneously when a sinusoidal

current at frequency (ω) is running in the wire. The heater frequency is adjusted in such a way that the penetration depth of heat is smaller than the thickness of the solid.

There are two ways to measure thermal conductivity of thin film on substrate. One is the slope method and the other one is the differential method [321]. In both methods, heat conduction across the film is assumed to be 1D. To satisfy this assumption, several requirements have to be established as follow:

- Wire width should be larger than the film thickness, but should be smaller than the thermal penetration depth for line heat source approximation.
- Substrate's thermal conductivity should be higher than that of the thin film.
- Heating frequency should be adjusted in such a way that thermal penetration depth is much larger than the thickness of the film.

Chen *et al* used the differential 3ω method to measure the contact thermal resistance between graphene and SiO_2 substrate over a temperature range from 42 K to 310 K [322]. As shown in figure 27(c), they firstly deposited mechanically-exfoliated graphene on oxidized Si wafer, and then the graphene samples were annealed at 400 °C for 1 h to get rid of the residues. Afterwards a thin SiO_2 insulating layer was covered on graphene so that the heating elements can be deposited on top. Finally Ar ion beam was used to pattern the graphene sample to ensure 1D heat flow through the graphene flake. The measurement results (figure 27(d)) showed that the contact thermal resistance between graphene and the underneath SiO_2 layer is in the range of 5.6×10^{-9}–1.2×10^{-8} m^2 K W^{-1} at RT, and the contact thermal resistance is independent of the graphene thickness.

5.9. Transient plane source

The transient plane source (TPS) technique is hot wire based transient method, first developed by S E Gustafsson [323]. The TPS method consists of a thin spiral circuit sandwiched between thin polymer substrates, which is placed in a sandwich structure between two surfaces of a bulk material to be tested. The spiral acts as both heater and sensor for the measurement. A current through the circuit heats the sample, and the transient temperature response is measured through a resistance change in the circuit. The method can be used to extract both thermal conductivity and specific heat capacity.

In its basic configuration, the TPS method relies on the assumption that the material to be tested can be modeled as infinite, i.e. that the thickness of the material is larger than the penetration depth of the transient heating pulse. However, adaptations of the technique has allowed for the measurement of thinner samples [324]. Due to these limitations however, the method is primarily suited to measurement of bulk samples, and has been used to characterized graphene filled composites [325, 326].

In the case of measuring highly thermal conductive graphite/graphene thin-film structures, there are some limitations that need to be addressed carefully. For example: the sample size might have to be very large (up to 120 mm for graphite) in order to increase the time of the transient. The thickness of the testing sample is also preferred to be larger than the radius of hot disk sensor to achieve high accuracy. Moreover, many important parameters, like heating power, measuring time, and radius of disk, must be selected carefully in order to obtain reasonable results.

5.10. Laser flash

The Laser Flash technique is a widely used method to measure the thermal diffusivity and thermal conductivity of materials due to a few important features, such as high precision and reproducibility, short measurement times, and well-defined testing atmospheres. The laser flash technique determines the through-plane thermal diffusivity of millimeter thin plane samples [327]. During a measurement, the lower surface of the sample is firstly heated by a short laser pulse. The resulting temperature change on the upper surface of the sample is then measured by an infrared detector. In its most simple adiabatic configuration, the thermal diffusivity a of the sample is related to the thickness l and the time to half of the maximum temperature t_{50} rise according to [327]:

$$a = 0.1388 \frac{l^2}{t_{50}}.$$

More complicated models allows for corrections due to finite pulse lengths and heat losses [328, 329]. It is also possible to measure multilayer structures of either three layers [330] or two layers with a contact resistance between [331], as long as the properties of all but one layer is known beforehand. Such a non-contact method of Laser Flash benefits on eliminating the effect of contact thermal resistance and shows directly about the material's bulk thermal properties. To measure in-plane thermal properties, a special in-plane sample holder is designed so that the position for the energy input on the bottom side of the sample and the position for measuring the temperature increase on the top side of the sample (energy output) are located at different lateral positions [332]. Thus, the measured temperature increase of the sample shows the thermal diffusivity in a horizontal direction (in-plane). In spite of all merits of Laser Flash technique, there are some potential limitations when measuring highly thermal conductive graphene/graphite thin film structures. For example, the testing samples must always be coated by a layer of graphite with a thickness of a few micrometers in order to enhance the absorption of laser energy and the emission of IR radiation to the detector. The thinner testing samples are, the greater

Table 3. Summary of different thermal measurement methods.

Method	Material geometry	Material size (lateral)	Material preparation	Measurement	Advantages	Limitations/challenges
Thermal bridge	Suspended single-layer to thin film of 2D materials	~Few μm—tens of μm	2D material flakes suspended on micro-fabricated heaters and temperature sensors	In-plane thermal conductivity of 2D materials	High accuracy, being able to measure thin film down to single atomic layer	Complex sample preparation and influence of contact thermal resistance from sample to contact electrodes
Electron beam self-heating	Suspended few-layer to membrane of 2D materials	~Few μm—tens of μm	Modified from thermal bridge method, material mounted in SEM chamber	In-plane thermal conductivity, contact thermal resistance, interfacial thermal resistance in heterostructures	High accuracy	Difficult to fabricate clean and suspended sample suitable for the measurement and limited to relatively thick samples
Scanning thermal microscopy	Single-layer to thin film of 2D material flakes	~Few μm—tens of μm	2D material flakes placed on insulating substrate	Heat dissipation, local heat spot, grain boundaries of 2D materials, extremely difficult to measure thermal conductivity	Easy sample preparation, nanoscale mapping of local temperature and heat conduction	Extremely difficult to measure thermal conductivity due to unknown heat loss from cantilever, air conduction/convention, tip-sample interfacial thermal resistance, heat radius and etc
Optothermal Raman spectroscopy	Suspended single-layer 2D materials up to thick films	~Few μm—few cm	Materials suspended between two electrodes	In-plane thermal conductivity of materials	Easy sample preparation, high accuracy, freedom in material size	Complex sample preparation for atomically thin materials
Pulsed photothermal reflectance	Nanoscale thin film up to bulk 2D materials	Millimeter size	Thin metal film deposited on target material on substrate	Cross plane thermal conductivity and contact thermal resistance	Easy sample preparation, high accuracy, freedom in material size	Not possible to measure in-plane thermal conductivity
Dependence of resistance on temperature	Suspended thin strips up to bulk 2D materials	Millimeter size	Material length/width ratio <0.1	In-plane thermal conductivity, temperature coefficient of resistance	Low cost, easy sample preparation	Only applicable to conductive materials, measurement must be performed in vacuum
Joule heating-IR	Suspended thin strips up to bulk 2D materials	Millimeter size	Material length/width ratio <0.1	In-plane thermal conductivity	Low cost, easy sample preparation	Only applicable to conductive materials
3ω	Nanoscale thin film up to microscale 2D materials	Millimeter size	Thin metal film deposited on target material	In-plane and cross-plane thermal conductivity	Low cost, high accuracy	For thin film measurement the substrate's thermal conductivity should be higher than that of the thin film
Transient plane source	Microscale up to bulk 2D materials	Millimeter size	Materials with flat surface	In-plane and cross-plane thermal conductivity, thermal diffusivity, specific heat capacity	Fast, easy sample preparation	Unproven measurement of very thin, small-sized and very high-thermal conductivity materials
Laser flash	Microscale up to bulk 2D materials	Millimeter size	Materials with flat surface	In-plane and cross-plane thermal conductivity	Easy sample preparation	Not possible to measure very thin and small-sized materials

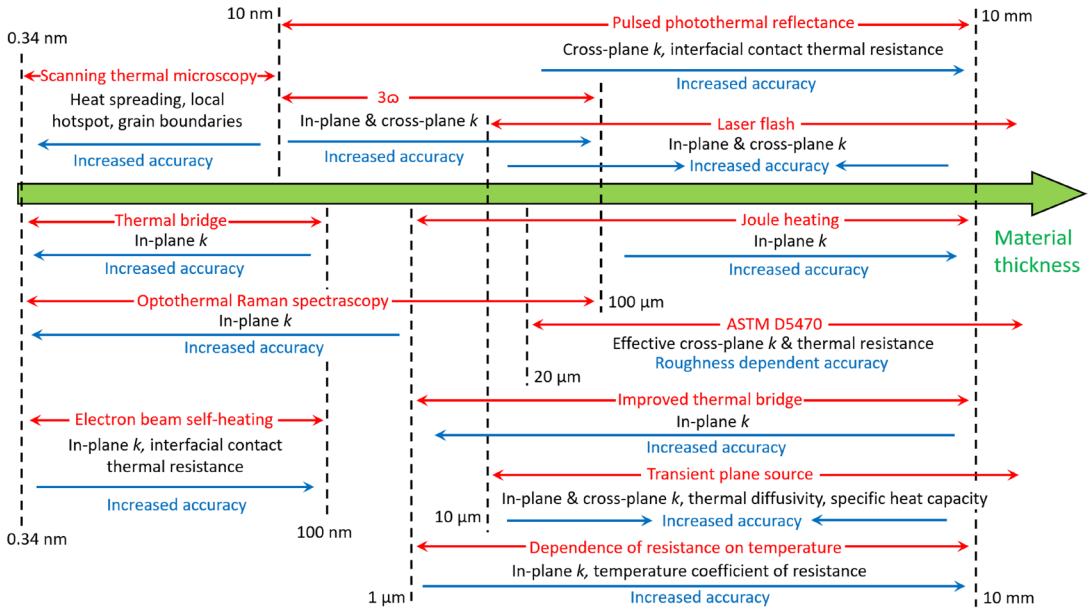

Figure 28. Diagram of thermal characterization methods used for measurement of 2D materials with different thicknesses.

influence of graphite coating layer will be. Therefore, samples with a thickness less than 10 μm are hard to be measured accurately by laser flash equipment. In addition, the time resolution of input laser and detector also has strong effect to the accuracy of the testing results, especially for ultra-high thermal conductive materials (above than 1000 mm^2 s^{-1}). Various graphene based composite films measured by Laser Flash method have been reported [325, 333–337].

5.11. Summary

As presented above, there are many different methods that can be used to evaluate the thermal performance of 2D materials. Depending on the geometry and required properties of the materials, the method has to be carefully selected so that the measurement can be performed by the simplest method with reasonable accuracy. Table 3 shows a summary of all methods with remarks on their advantages and limitations.

A diagram for different thermal characterization methods used for different thickness of materials is shown in figure 28. Generally speaking, it is difficult to point out which method should be used to get best accuracy and most exact value regarding the thermal performance. Every method has accuracy issues which are related to intrinsic, equipment set up and geometric factors. Scanning Thermal Microscopy method cannot generate direct values of thermal conductivity but rather give the temperature distribution/gradient, often in submicron length scale, for instance across the grain boundary, thus providing very useful information when studying thermal transport properties. Thermal bridging method often requests MEMS based technology with clean room skills. Therefore, it is not very commonly used for engineering purposes. However, ITB method is also very attractive and is based on the same idea as ASTM 5470 standard, but it requires tedious time for setting up the experiments. However, it can give quite good accuracy, often in the range of 10%–20% [40]. Electron beam self-heating method requires similar sample fabrication as the thermal bridge method. Additionally, it utilizes the electron beam in SEM chamber to heat up the sample for thermal measurement. Although the setup is very complex, the method offers direct measurement of contact thermal resistance. Optothermal Raman spectroscopy needs information of calibration coefficient in different temperatures which can be very different to obtain with high accuracy, therefore affecting its trustiness of the data produced. PPR or Time domain time reflectance method is recommended for the measurement of cross-plane thermal conductivity and interfacial contact thermal resistance of 2D materials and combined structures with thickness of 10 nm to 10 mm, but materials/structures with a few nanometer thickness is still possible to be measured by this method, as it becomes much more difficult to prepare the sample with such a small thickness. With 3ω method for the 2D materials of graphene, it needs to create an insulation layer between the graphene and substrate adding on additional sample preparation effort and cost. Transient plane source is a convenient method to quickly measure various thermal properties of 2D materials, but it is limited to relatively thick and big-sized samples. Laser flash is very useful for a generic purpose of the thermal measurement as it does not require specific sample preparation, but it is not useful for sample thickness less than for instance 10 μm. Joule heating method offers simple and quick measurement based on Fourier's Law and it gives reasonable accuracy with less than 20% in most cases. The

key issue is here, to determine the emissivity factor as function of temperature for the sample measured. The DRT method, especially carried out in vacuum, is interesting but it takes quite long time for the sample preparation. To conclude, it seems that Joule heating is the most versatile and easy-to-use method for quick screening purpose of graphene based films with different thicknesses from a few micrometers up to millimeters.

6. Current and future potential applications

Up to date, a few applications have been demonstrated to use graphene and related 2D materials for thermal management on commercial products. For example, graphene was used to coat LED filaments and it was claimed that graphene can facilitate the heat dissipation in the LED bulb, therefore extending the lifetime and improving the efficiency of the LEDs [338]. Graphene based heat spreader can be supplied with different thicknesses varying from 20 μm to 100 μm with thermal conductivity up to 3200 W m^{-1} K^{-1} [339–341]. In addition, vertically aligned graphene based TIM is available to offer thermal conductivity up to 1000 W m^{-1} K^{-1} in the Z direction [341]. Furthermore, it is claimed that graphene based thermal grease with thermal conductivity >10 W m^{-1} K^{-1} can be provided [342].

A real commercial application of graphene film seems to be in the mobile of Mate 20. It seems that the graphene assembled film can bring down the perception temperature efficiently. In order to decrease the temperature further, drastic quality improvement of the graphene film is needed.

7. Concluding remarks

The large-scale production of high quality 2D materials has been considered as the major obstacle for their industrial application. Thanks to the very strong interest in graphene and related 2D materials, great progress has been achieved to produce 2D materials over the past years. Roll-to-roll system has been developed to fabricate continuous large-area graphene by CVD method. The LPE method makes the mass production of graphene and other 2D materials inexpensive, which makes it practical to use graphene and related 2D materials as fillers in composites, as well as use graphene and BN films as heat spreaders. These enabling technologies paved the way for 2D materials for thermal management application in the industry.

This review paper serves as a critical analysis and summary of the state of the art of the various aspects of graphene and other 2D materials from science to engineering and to final applications. It is also our sincere hope that it will trigger furthermore scientific studies as well as develop more commercial applications in this area. And we are sure that so will happen.

Acknowledgments

YF, JH, YL, AZ, MK and JL acknowledge the financial support from The Swedish National Science Foundation (VR under the contract No 621-2007-4660), The Swedish Foundation for Strategic Research (SSF) under contract (No SE13-0061), the Swedish Board for innovation under the Siografen program and from the Production Area of Advance at Chalmers University of Technology, Sweden. SC, YZ and JL acknowledge the financial support by the Key R&D Development Program from the Ministry of Science and Technology of China with the contract No: 2017YFB040600 and the National Natural Science Foundation of China (No. 51872182). XX is supported the National Natural Science Foundation of China (No. 11674245 & No. 11890703). MS and CMST acknowledge financial support from the CERCA programme/Generalitat de Catalunya, the Severo Ochoa Centres of Excellence programme, funded by the Spanish Research Agency (AEI, Grant No. SEV-2017-0706).

ORCID iDs

Yifeng Fu https://orcid.org/0000-0001-7783-8766
Josef Hansson https://orcid.org/0000-0003-1278-946X
Yuxiang Ni https://orcid.org/0000-0001-8567-6998
Yan Zhang https://orcid.org/0000-0002-2461-060X
Zhi-Bin Zhang https://orcid.org/0000-0003-0244-8565
Marianna Sledzinska https://orcid.org/0000-0001-8592-1121
Alexander A Balandin https://orcid.org/0000-0002-9944-7894
Xiangfan Xu https://orcid.org/0000-0001-7163-4957
Johan Liu https://orcid.org/0000-0001-9931-1439

References

[1] Manno M, Yang B, Khanna S, McCluskey P and Bar-Cohen A 2015 Microcontact-enhanced thermoelectric cooling of ultrahigh heat flux hotspots *IEEE Trans. Compon. Packag. Manuf. Technol.* **5** 1775–83
[2] Novoselov K S, Geim A K, Morozov S V, Jiang D, Zhang Y, Dubonos S V, Grigorieva I V and Firsov A A 2004 Electric field effect in atomically thin carbon films *Science* **306** 666–9
[3] Novoselov K S, Fal'ko V I, Colombo L, Gellert P R, Schwab M G and Kim K 2012 A roadmap for graphene *Nature* **490** 192–200
[4] Geim A K and Novoselov K S 2007 The rise of graphene *Nat. Mater.* **6** 183–91
[5] Nika D L, Yan Z and Balandin A A 2015 Thermal properties of graphene and few-layer graphene: applications in electronics *IET Circuits Devices Syst.* **9** 4–12
[6] Neugebauer P, Orlita M, Faugeras C, Barra A-L and Potemski M 2009 How perfect can graphene be? *Phys. Rev. Lett.* **103** 136403
[7] Banszerus L, Schmitz M, Engels S, Dauber J, Oellers M, Haupt F, Watanabe K, Taniguchi T, Beschoten B and Stampfer C 2015 Ultrahigh-mobility graphene devices from chemical vapor deposition on reusable copper *Sci. Adv.* **1** e1500222

[8] Alonso E T *et al* 2018 Graphene electronic fibres with touch-sensing and light-emitting functionalities for smart textiles *Npj Flex. Electron.* **2** 25
[9] Molina J 2016 Graphene-based fabrics and their applications: a review *RSC Adv.* **6** 68261–91
[10] Li N, Chen Z, Ren W, Li F and Cheng H-M 2012 Flexible graphene-based lithium ion batteries with ultrafast charge and discharge rates *Proc. Natl Acad. Sci. USA* **109** 17360
[11] Huang Y *et al* 2018 Flexible high energy density zinc-ion batteries enabled by binder-free MnO_2/reduced graphene oxide electrode *Npj Flex. Electron.* **2** 21
[12] La Notte L, Cataldi P, Ceseracciu L, Bayer I S, Athanassiou A, Marras S, Villari E, Brunetti F and Reale A 2018 Fully-sprayed flexible polymer solar cells with a cellulose-graphene electrode *Mater. Today Energy* **7** 105–12
[13] Sim J-K, Kang S, Nandi R, Jo J-Y, Jeong K-U and Lee C-R 2018 Implementation of graphene as hole transport electrode in flexible CIGS solar cells fabricated on Cu foil *Sol. Energy* **162** 357–63
[14] Song Y, Chang S, Gradecak S and Kong J 2016 Visibly-transparent organic solar cells on flexible substrates with all-graphene electrodes *Adv. Energy Mater.* **6** 1600847
[15] Gibertini M, Koperski M, Morpurgo A F and Novoselov K S 2019 Magnetic 2D materials and heterostructures *Nat. Nanotechnol.* **14** 408
[16] Ashworth C 2018 2D materials: the thick and the thin *Nat. Rev. Mater.* **3** 18019
[17] Schaibley J R, Yu H, Clark G, Rivera P, Ross J S, Seyler K L, Yao W and Xu X 2016 Valleytronics in 2D materials *Nat. Rev. Mater.* **1** 16055
[18] Balandin A A, Ghosh S, Bao W, Calizo I, Teweldebrhan D, Miao F and Lau C N 2008 Superior thermal conductivity of single-layer graphene *Nano Lett.* **8** 902–7
[19] Balandin A A 2011 Thermal properties of graphene and nanostructured carbon materials *Nat. Mater.* **10** 569–81
[20] Cai W, Moore A L, Zhu Y, Li X, Chen S, Shi L and Ruoff R S 2010 Thermal transport in suspended and supported monolayer graphene grown by chemical vapor deposition *Nano Lett.* **10** 1645–51
[21] Ghosh S, Bao W, Nika D L, Subrina S, Pokatilov E P, Lau C N and Balandin A A 2010 Dimensional crossover of thermal transport in few-layer graphene *Nat. Mater.* **9** 555–8
[22] Ghosh S, Calizo I, Teweldebrhan D, Pokatilov E P, Nika D L, Balandin A A, Bao W, Miao F and Lau C N 2008 Extremely high thermal conductivity of graphene: prospects for thermal management applications in nanoelectronic circuits *Appl. Phys. Lett.* **92** 151911
[23] Seol J H *et al* 2010 Two-dimensional phonon transport in supported graphene *Science* **328** 213–6
[24] Jauregui L A *et al* 2010 Thermal transport in graphene nanostructures: experiments and simulations *ECS Trans.* **28** 73–83
[25] Renteria J, Legedza S, Salgado R, Balandin M P, Ramirez S, Saadah M, Kargar F and Balandin A A 2015 Magnetically-functionalized self-aligning graphene fillers for high-efficiency thermal management applications *Mater. Des.* **88** 214–21
[26] Chen S *et al* 2011 Raman measurements of thermal transport in suspended monolayer graphene of variable sizes in vacuum and gaseous environments *ACS Nano* **5** 321–8
[27] Yoon K, Hwang G, Chung J, Kim H G, Kwon O, Kihm K D and Lee J S 2014 Measuring the thermal conductivity of residue-free suspended graphene bridge using null point scanning thermal microscopy *Carbon* **76** 77–83
[28] Nika D L, Pokatilov E P, Askerov A S and Balandin A A 2009 Phonon thermal conduction in graphene: role of Umklapp and edge roughness scattering *Phys. Rev.* B **79** 155413
[29] Fugallo G, Cepellotti A, Paulatto L, Lazzeri M, Marzari N and Mauri F 2014 Thermal conductivity of graphene and graphite: collective excitations and mean free paths *Nano Lett.* **14** 6109–14
[30] Lindsay L, Broido D A and Mingo N 2010 Flexural phonons and thermal transport in graphene *Phys. Rev.* B **82** 115427
[31] Xu X *et al* 2014 Length-dependent thermal conductivity in suspended single-layer graphene *Nat. Commun.* **5** 3689
[32] Nika D L, Askerov A S and Balandin A A 2012 Anomalous size dependence of the thermal conductivity of graphene ribbons *Nano Lett.* **12** 3238–44
[33] Chen S, Wu Q, Mishra C, Kang J, Zhang H, Cho K, Cai W, Balandin A A and Ruoff R S 2012 Thermal conductivity of isotopically modified graphene *Nat. Mater.* **11** 203–7
[34] Shahil K M F and Balandin A A 2012 Graphene–multilayer graphene nanocomposites as highly efficient thermal interface materials *Nano Lett.* **12** 861–7
[35] Goyal V and Balandin A A 2012 Thermal properties of the hybrid graphene-metal nano-micro-composites: applications in thermal interface materials *Appl. Phys. Lett.* **100** 073113
[36] Eda G and Chhowalla M 2009 Graphene-based composite thin films for electronics *Nano Lett.* **9** 814–8
[37] Huang X, Yin Z, Wu S, Qi X, He Q, Zhang Q, Yan Q, Boey F and Zhang H 2011 Graphene-based materials: synthesis, characterization, properties, and applications *Small Weinh. Bergstr. Ger.* **7** 1876–902
[38] Wu Z-S, Ren W, Gao L, Zhao J, Chen Z, Liu B, Tang D, Yu B, Jiang C and Cheng H-M 2009 Synthesis of graphene sheets with high electrical conductivity and good thermal stability by hydrogen arc discharge exfoliation *ACS Nano* **3** 411–7
[39] Goli P, Legedza S, Dhar A, Salgado R, Renteria J and Balandin A A 2014 Graphene-enhanced hybrid phase change materials for thermal management of Li-ion batteries *J. Power Sources* **248** 37–43
[40] Wang N *et al* 2018 Tailoring the thermal and mechanical properties of graphene film by structural engineering *Small* **14** 1801346
[41] Zhong J, Sun W, Wei Q, Qian X, Cheng H-M and Ren W 2018 Efficient and scalable synthesis of highly aligned and compact two-dimensional nanosheet films with record performances *Nat. Commun.* **9** 3484
[42] Liu Z, Li Z, Xu Z, Xia Z, Hu X, Kou L, Peng L, Wei Y and Gao C 2014 Wet-spun continuous graphene films *Chem. Mater.* **26** 6786–95
[43] Ouyang T, Chen Y, Xie Y, Yang K, Bao Z and Zhong J 2010 Thermal transport in hexagonal boron nitride nanoribbons *Nanotechnology* **21** 245701
[44] Jang I, Shin K-H, Yang I, Kim H, Kim J, Kim W-H, Jeon S-W and Kim J-P 2017 Enhancement of thermal conductivity of BN/epoxy composite through surface modification with silane coupling agents *Colloids Surf. Physicochem. Eng. Asp.* **518** 64–72
[45] Wang Z, Iizuka T, Kozako M, Ohki Y and Tanaka T 2011 Development of epoxy/BN composites with high thermal conductivity and sufficient dielectric breakdown strength partI–sample preparations and thermal conductivity *IEEE Trans. Dielectr. Electr. Insul.* **18** 1963–72
[46] Lei Y, Han Z, Ren D, Pan H, Xu M and Liu X 2018 Design of *h*-BN-filled cyanate/epoxy thermal conductive composite with stable dielectric properties *Macromol. Res.* **26** 602–8
[47] Kuo D H, Lin C Y, Jhou Y C, Cheng J Y and Liou G S 2013 Thermal conductive performance of organosoluble polyimide/BN and polyimide/(BN + ALN) composite films fabricated by a solution-cast method *Polym. Compos.* **34** 252–8
[48] Wattanakul K, Manuspiya H and Yanumet N 2011 Thermal conductivity and mechanical properties of BN-filled epoxy composite: effects of filler content, mixing conditions, and BN agglomerate size *J. Compos. Mater.* **45** 1967–80
[49] Wattanakul K, Manuspiya H and Yanumet N 2011 Effective surface treatments for enhancing the thermal conductivity of BN-filled epoxy composite *J. Appl. Polym. Sci.* **119** 3234–43
[50] Sun S, Bao J, Mu W, Fu Y, Zhang Y, Ye L and Liu J 2015 Cooling hot spots by hexagonal boron nitride heat spreaders *2015 IEEE 65th Electronic Components and Technology Conf. (ECTC)* pp 1658–63
[51] Bao J, Edwards M, Huang S, Zhang Y, Fu Y, Lu X, Yuan Z, Jeppson K and Liu J 2016 Two-dimensional hexagonal boron nitride as lateral heat spreader in electrically insulating packaging *J. Phys. D: Appl. Phys.* **49** 265501

[52] Choi D, Poudel N, Park S, Akinwande D, Cronin S B, Watanabe K, Taniguchi T, Yao Z and Shi L 2018 Large reduction of hot spot temperature in graphene electronic devices with heat-spreading hexagonal boron nitride *ACS Appl. Mater. Interfaces* **10** 11101–7
[53] Pop E, Varshney V and Roy A K 2012 Thermal properties of graphene: fundamentals and applications *MRS Bull.* **37** 1273–81
[54] Jung H *et al* 2015 High through-plane thermal conduction of graphene nanoflake filled polymer composites melt-processed in an L-shape kinked tube *ACS Appl. Mater. Interfaces* **7** 15256–62
[55] Mahajan R, Chia-Pin C and Chrysler G 2006 Cooling a microprocessor chip *Proc. IEEE* **94** 1476–86
[56] Mahajan R and For E D 2002 Emerging directions for packaging technologies *Intel Technol. J.* **6** 62–75
[57] Nika D L, Ghosh S, Pokatilov E P and Balandin A A 2009 Lattice thermal conductivity of graphene flakes: comparison with bulk graphite *Appl. Phys. Lett.* **94** 203103
[58] Fujii M, Zhang X, Xie H, Ago H, Takahashi K, Ikuta T, Abe H and Shimizu T 2005 Measuring the thermal conductivity of a single carbon nanotube *Phys. Rev. Lett.* **95** 065502
[59] Yu C, Shi L, Yao Z, Li D and Majumdar A 2005 Thermal conductance and thermopower of an individual single-wall carbon nanotube *Nano Lett.* **5** 1842–6
[60] Slack G A 1962 Anisotropic thermal conductivity of pyrolytic graphite *Phys. Rev.* **127** 694–701
[61] Slack G A 1964 Thermal conductivity of pure and impure silicon, silicon carbide, and diamond *J. Appl. Phys.* **35** 3460–6
[62] Yan Z, Liu G, Khan J M and Balandin A A 2012 Graphene quilts for thermal management of high-power GaN transistors *Nat. Commun.* **3** 827
[63] Subrina S, Kotchetkov D and Balandin A A 2009 Heat removal in silicon-on-insulator integrated circuits with graphene lateral heat spreaders *IEEE Electron Device Lett.* **30** 1281–3
[64] Gao Z, Zhang Y, Fu Y, Yuen M M F and Liu J 2013 Thermal chemical vapor deposition grown graphene heat spreader for thermal management of hot spots *Carbon* **61** 342–8
[65] Gao Z, Zhang Y, Fu Y, Yuen M and Liu J 2012 Graphene heat spreader for thermal management of hot spots in electronic packaging *18th Int. Workshop on Thermal Investigation of ICs and Systems* pp 1–4
[66] Bae S, Shabani R, Lee J, Baeck S, Cho H J and Ahn J 2014 Graphene-based heat spreader for flexible electronic devices *IEEE Trans. Electron Devices* **61** 4171–5
[67] Shih M-H, Li L-J, Yang Y-C, Chou H-Y, Lin C-T and Su C-Y 2013 Efficient heat dissipation of photonic crystal microcavity by monolayer graphene *ACS Nano* **7** 10818–24
[68] Lee P-H, Tu W-M and Tseng H-C 2018 Graphene heat spreaders for thermal management of InGaP/GaAs collector-up HBTs *IEEE Trans. Electron Devices* **65** 352–5
[69] Polsen E S, McNerny D Q, Viswanath B, Pattinson S W and John Hart A 2015 High-speed roll-to-roll manufacturing of graphene using a concentric tube CVD reactor *Sci. Rep.* **5** 10257
[70] Shivayogimath A *et al* 2019 Do-it-yourself transfer of large-area graphene using an office laminator and water *Chem. Mater.* **31** 2328–36
[71] Luo D *et al* Adlayer-free large-area single crystal graphene grown on a Cu(1 1 1) foil *Adv. Mater.* **31** 1903615
[72] Lee W, Kihm K D, Kim H G, Shin S, Lee C, Park J S, Cheon S, Kwon O M, Lim G and Lee W 2017 In-plane thermal conductivity of polycrystalline chemical vapor deposition graphene with controlled grain sizes *Nano Lett.* **17** 2361–6
[73] Lee J-H *et al* 2014 Wafer-scale growth of single-crystal monolayer graphene on reusable hydrogen-terminated germanium *Science* **344** 286–9
[74] Wu T *et al* 2016 Fast growth of inch-sized single-crystalline graphene from a controlled single nucleus on Cu–Ni alloys *Nat. Mater.* **15** 43–7
[75] Vlassiouk I V *et al* 2018 Evolutionary selection growth of two-dimensional materials on polycrystalline substrates *Nat. Mater.* **17** 318
[76] Hao Y *et al* 2013 The role of surface oxygen in the growth of large single-crystal graphene on copper *Science* **342** 720–3
[77] Gnisci A, Faggio G, Messina G, Kwon J, Lee J-Y, Lee G-H, Dikonimos T, Lisi N and Capasso A 2018 Ethanol-CVD growth of sub-mm single-crystal graphene on flat Cu surfaces *J. Phys. Chem.* C **122** 28830–8
[78] Xu X *et al* 2017 Ultrafast epitaxial growth of metre-sized single-crystal graphene on industrial Cu foil *Sci. Bull.* **62** 1074–80
[79] Deng B *et al* 2017 Wrinkle-free single-crystal graphene wafer grown on strain-engineered substrates *ACS Nano* **11** 12337–45
[80] Lin L *et al* 2019 Towards super-clean graphene *Nat. Commun.* **10** 1912
[81] Qiu B and Ruan X 2012 Reduction of spectral phonon relaxation times from suspended to supported graphene *Appl. Phys. Lett.* **100** 193101
[82] Song N-J, Chen C-M, Lu C, Liu Z, Kong Q-Q and Cai R 2014 Thermally reduced graphene oxide films as flexible lateral heat spreaders *J. Mater. Chem.* A **2** 16563–8
[83] Dikin D A, Stankovich S, Zimney E J, Piner R D, Dommett G H B, Evmenenko G, Nguyen S T and Ruoff R S 2007 Preparation and characterization of graphene oxide paper *Nature* **448** 457–60
[84] Chen H, Müller M B, Gilmore K J, Wallace G G and Li D 2008 Mechanically strong, electrically conductive, and biocompatible graphene paper *Adv. Mater.* **20** 3557–61
[85] Xin G, Sun H, Hu T, Fard H R, Sun X, Koratkar N, Borca-Tasciuc T and Lian J 2014 Large-area freestanding graphene paper for superior thermal management *Adv. Mater.* **26** 4521–6
[86] Wang X, Zhi L and Müllen K 2008 Transparent, conductive graphene electrodes for dye-sensitized solar cells *Nano Lett.* **8** 323–7
[87] Li J, Ye F, Vaziri S, Muhammed M, Lemme M C and Östling M 2013 Efficient inkjet printing of graphene *Adv. Mater.* **25** 3985–92
[88] Becerril H A, Mao J, Liu Z, Stoltenberg R M, Bao Z and Chen Y 2008 Evaluation of solution-processed reduced graphene oxide films as transparent conductors *ACS Nano* **2** 463–70
[89] Aboutalebi S H, Gudarzi M M, Zheng Q B and Kim J-K 2011 Spontaneous formation of liquid crystals in ultralarge graphene oxide dispersions *Adv. Funct. Mater.* **21** 2978–88
[90] Renteria J D, Ramirez S, Malekpour H, Alonso B, Centeno A, Zurutuza A, Cocemasov A I, Nika D L and Balandin A A 2015 Strongly anisotropic thermal conductivity of free-standing reduced graphene oxide films annealed at high temperature *Adv. Funct. Mater.* **25** 4664–72
[91] Shen B, Zhai W and Zheng W 2014 Ultrathin flexible graphene film: an excellent thermal conducting material with efficient EMI shielding *Adv. Funct. Mater.* **24** 4542–8
[92] Teng C, Xie D, Wang J, Yang Z, Ren G and Zhu Y 2017 Ultrahigh conductive graphene paper based on ball-milling exfoliated graphene *Adv. Funct. Mater.* **27** 1700240
[93] Peng L, Xu Z, Liu Z, Guo Y, Li P and Gao C 2017 Ultrahigh thermal conductive yet superflexible graphene films *Adv. Mater.* **29** 1700589
[94] Mu X, Wu X, Zhang T, Go D B and Luo T 2014 Thermal transport in graphene oxide—from ballistic extreme to amorphous limit *Sci. Rep.* **4** 3909
[95] Xu X, Chen J and Li B 2016 Phonon thermal conduction in novel 2D materials *J. Phys.: Condens. Matter* **28** 483001
[96] Nika D L and Balandin A A 2017 Phonons and thermal transport in graphene and graphene-based materials *Rep. Prog. Phys.* **80** 036502
[97] Zhang J, Yang H, Shen G, Cheng P, Zhang J and Guo S 2010 Reduction of graphene oxide viaL-ascorbic acid *Chem. Commun.* **46** 1112–4
[98] Moon I K, Lee J, Ruoff R S and Lee H 2010 Reduced graphene oxide by chemical graphitization *Nat. Commun.* **1** 73
[99] Pei S, Zhao J, Du J, Ren W and Cheng H-M 2010 Direct reduction of graphene oxide films into highly conductive and flexible graphene films by hydrohalic acids *Carbon* **48** 4466–74

[100] Mattevi C, Eda G, Agnoli S, Miller S, Mkhoyan K A, Celik O, Mastrogiovanni D, Granozzi G, Garfunkel E and Chhowalla M 2009 Evolution of electrical, chemical, and structural properties of transparent and conducting chemically derived graphene thin films *Adv. Funct. Mater.* **19** 2577–83
[101] Liu J and Wang N 2017 Method for manufacturing a graphene based thermally conductive film *Patent no.* PCT/SE2017/050185
[102] Rozada R, Paredes J I, Villar-Rodil S, Martínez-Alonso A and Tascón J M D 2013 Towards full repair of defects in reduced graphene oxide films by two-step graphitization *Nano Res.* **6** 216–33
[103] Ma T *et al* 2017 Tailoring the thermal and electrical transport properties of graphene films by grain size engineering *Nat. Commun.* **8** 14486
[104] Malard L M, Pimenta M A, Dresselhaus G and Dresselhaus M S 2009 Raman spectroscopy in graphene *Phys. Rep.* **473** 51–87
[105] Wei Z, Ni Z, Bi K, Chen M and Chen Y 2011 In-plane lattice thermal conductivities of multilayer graphene films *Carbon* **49** 2653–8
[106] Hishiyama Y, Yoshida A, Kaburagi Y and Inagaki M 1992 Graphite films prepared from carbonized polyimide films *Carbon* **30** 333–7
[107] Evans W J, Hu L and Keblinski P 2010 Thermal conductivity of graphene ribbons from equilibrium molecular dynamics: effect of ribbon width, edge roughness, and hydrogen termination *Appl. Phys. Lett.* **96** 203112
[108] Hummers W S and Offeman R E 1958 Preparation of graphitic oxide *J. Am. Chem. Soc.* **80** 1339
[109] Zhang Y, Edwards M, Samani M K, Logothetis N, Ye L, Fu Y, Jeppson K and Liu J 2016 Characterization and simulation of liquid phase exfoliated graphene-based films for heat spreading applications *Carbon* **106** 195–201
[110] Zhang Y, Han H, Wang N, Zhang P, Fu Y, Murugesan M, Edwards M, Jeppson K, Volz S and Liu J 2015 Improved heat spreading performance of functionalized graphene in microelectronic device application *Adv. Funct. Mater.* **25** 4430–5
[111] Han N *et al* 2013 Improved heat dissipation in gallium nitride light-emitting diodes with embedded graphene oxide pattern *Nat. Commun.* **4** 1452
[112] Liang Q, Yao X, Wang W, Liu Y and Wong C P 2011 Three-dimensional vertically aligned functionalized multilayer graphene architecture: an approach for graphene-based thermal interfacial materials *ACS Nano* (ACS Publications) **5** 2392
[113] Malekpour H, Chang K-H, Chen J-C, Lu C-Y, Nika D L, Novoselov K S and Balandin A A 2014 Thermal conductivity of graphene laminate *Nano Lett.* **14** 5155–61
[114] Tortello M *et al* 2016 Effect of thermal annealing on the heat transfer properties of reduced graphite oxide flakes: a nanoscale characterization via scanning thermal microscopy *Carbon* **109** 390–401
[115] Xin G 2014 Large-area freestanding graphene paper for superior thermal management *Adv. Mater.* (Wiley Online Library) **26** 4521
[116] Goli P, Ning H, Li X, Lu C Y, Novoselov K S and Balandin A A 2014 Thermal properties of graphene–copper–graphene heterogeneous films *Nano Lett.* **14** 1497–503
[117] Saadah M, Hernandez E and Balandin A A 2017 Thermal management of concentrated multi-junction solar cells with graphene-enhanced thermal interface materials *Appl. Sci.* **7** 589
[118] Fu Y-X, He Z-X, Mo D-C and Lu S-S 2014 Thermal conductivity enhancement of epoxy adhesive using graphene sheets as additives *Int. J. Therm. Sci.* **86** 276–83
[119] Shtein M, Nadiv R, Buzaglo M and Regev O 2015 Graphene-based hybrid composites for efficient thermal management of electronic devices *ACS Appl. Mater. Interfaces* **7** 23725–30
[120] Aksamija Z and Knezevic I 2011 Lattice thermal conductivity of graphene nanoribbons: anisotropy and edge roughness scattering *Appl. Phys. Lett.* **98** 141919
[121] Li H, Ying H, Chen X, Nika D L, Cocemasov A I, Cai W, Balandin A A and Chen S 2014 Thermal conductivity of twisted bilayer graphene *Nanoscale* **6** 13402–8
[122] Bae M-H, Li Z, Aksamija Z, Martin P N, Xiong F, Ong Z-Y, Knezevic I and Pop E 2013 Ballistic to diffusive crossover of heat flow in graphene ribbons *Nat. Commun.* **4** 1734
[123] Chen L, Xie H, Yu W, Wang B and Wu Z 2015 Thermal transport behaviors of suspended graphene sheets with different sizes *Int. J. Therm. Sci.* **94** 221–7
[124] Kargar F, Barani Z, Salgado R, Debnath B, Lewis J S, Aytan E, Lake R K and Balandin A A 2018 Thermal percolation threshold and thermal properties of composites with high loading of graphene and boron nitride fillers *ACS Appl. Mater. Interfaces* **10** 37555–65
[125] Bujard P 1988 Thermal conductivity of boron nitride filled epoxy resins: temperature dependence and influence of sample preparation *InterSociety Conf. on Thermal Phenomena in the Fabrication and Operation of Electronic Components. I-THERM '88* pp 41–9
[126] Shenogina N, Shenogin S, Xue L and Keblinski P 2005 On the lack of thermal percolation in carbon nanotube composites *Appl. Phys. Lett.* **87** 133106
[127] Bonnet P, Sireude D, Garnier B and Chauvet O 2007 Thermal properties and percolation in carbon nanotube-polymer composites *Appl. Phys. Lett.* **91** 201910
[128] Zheng R, Gao J, Wang J, Feng S-P, Ohtani H, Wang J and Chen G 2012 Thermal percolation in stable graphite suspensions *Nano Lett.* **12** 188–92
[129] Shtein M, Nadiv R, Buzaglo M, Kahil K and Regev O 2015 Thermally conductive graphene-polymer composites: size, percolation, and synergy effects *Chem. Mater.* **27** 2100–6
[130] Gu J, Xie C, Li H, Dang J, Geng W and Zhang Q 2014 Thermal percolation behavior of graphene nanoplatelets/polyphenylene sulfide thermal conductivity composites *Polym. Compos.* **35** 1087–92
[131] Choi S U S, Zhang Z G, Yu W, Lockwood F E and Grulke E A 2001 Anomalous thermal conductivity enhancement in nanotube suspensions *Appl. Phys. Lett.* **79** 2252–4
[132] Ding Y, Alias H, Wen D and Williams R A 2006 Heat transfer of aqueous suspensions of carbon nanotubes (CNT nanofluids) *Int. J. Heat Mass Transf.* **49** 240–50
[133] Stankovich S, Dikin D A, Dommett G H B, Kohlhaas K M, Zimney E J, Stach E A, Piner R D, Nguyen S T and Ruoff R S 2006 Graphene-based composite materials *Nature* **442** 282–6
[134] Biercuk M J, Llaguno M C, Radosavljevic M, Hyun J K, Johnson A T and Fischer J E 2002 Carbon nanotube composites for thermal management *Appl. Phys. Lett.* **80** 2767–9
[135] Pang H, Chen T, Zhang G, Zeng B and Li Z-M 2010 An electrically conducting polymer/graphene composite with a very low percolation threshold *Mater. Lett.* **64** 2226–9
[136] Zhang H-B, Zheng W-G, Yan Q, Yang Y, Wang J-W, Lu Z-H, Ji G-Y and Yu Z-Z 2010 Electrically conductive polyethylene terephthalate/graphene nanocomposites prepared by melt compounding *Polymer* **51** 1191–6
[137] Martin C A, Sandler J K W, Shaffer M S P, Schwarz M-K, Bauhofer W, Schulte K and Windle A H 2004 Formation of percolating networks in multi-wall carbon-nanotube–epoxy composites *Compos. Sci. Technol.* **64** 2309–16
[138] Awasthi K, Awasthi S, Srivastava A, Kamalakaran R, Talapatra S, Ajayan P M and Srivastava O N 2006 Synthesis and characterization of carbon nanotube–polyethylene oxide composites *Nanotechnology* **17** 5417–5422
[139] Potts J R, Dreyer D R, Bielawski C W and Ruoff R S 2011 Graphene-based polymer nanocomposites *Polymer* **52** 5–25
[140] Li A, Zhang C and Zhang Y-F 2017 Thermal conductivity of graphene-polymer composites: mechanisms, properties, and applications *Polymers* **9** 437
[141] Shahil K M F and Balandin A A 2012 Thermal properties of graphene and multilayer graphene: applications in thermal interface materials *Solid State Commun.* **152** 1331–40
[142] Bar-Cohen A, Matin K and Narumanchi S 2015 Nanothermal interface materials: technology review and recent results *J. Electron. Packag.* **137** 040803

[143] Hansson J, Zandén C, Ye L and Liu J 2016 Review of current progress of thermal interface materials for electronics thermal management applications *2016 IEEE 16th Int. Conf. on Nanotechnology (IEEE-NANO)* pp 371–4
[144] Hernandez Y *et al* 2008 High-yield production of graphene by liquid-phase exfoliation of graphite *Nat. Nanotechnol.* **3** 563–8
[145] Lotya M *et al* 2009 Liquid phase production of graphene by exfoliation of graphite in surfactant/water solutions *J. Am. Chem. Soc.* **131** 3611–20
[146] Allen M J, Tung V C and Kaner R B 2010 Honeycomb carbon: a review of graphene *Chem. Rev.* **110** 132–45
[147] Nethravathi C and Rajamathi M 2008 Chemically modified graphene sheets produced by the solvothermal reduction of colloidal dispersions of graphite oxide *Carbon* **46** 1994–8
[148] Stankovich S, Dikin D A, Piner R D, Kohlhaas K A, Kleinhammes A, Jia Y, Wu Y, Nguyen S T and Ruoff R S 2007 Synthesis of graphene-based nanosheets via chemical reduction of exfoliated graphite oxide *Carbon* **45** 1558–65
[149] Kargar F, Barani Z, Balinskiy M, Magana A S, Lewis J S and Balandin A A 2019 Dual-functional graphene composites for electromagnetic shielding and thermal management *Adv. Electron. Mater.* **5** 1800558
[150] Norley J, Tzeng J-W and Klug J 2003 Graphite-based heat sink *Google Patents*
[151] Getz G Jr and Burkett T W 2004 Heat sink made from longer and shorter graphite Sheets *Google Patents*
[152] Hsieh C-T, Chen Y-F, Lee C-E, Chiang Y-M, Hsieh K-Y and Wu H-S 2017 Heat transport enhancement of heat sinks using Cu-coated graphene composites *Mater. Chem. Phys.* **197** 105–12
[153] Lin Y-F, Hsieh C-T and Wai R-J 2015 Facile synthesis of graphene sheets for heat sink application *Solid State Sci.* **43** 22–7
[154] Hu J, Xu J, Zhu C, Li Q, Ullah Z, Liu F, Li W, Guo Y, Zhao X and Liu L 2017 Significant enhancement of metal heat dissipation from mechanically exfoliated graphene nanosheets through thermal radiation effect *AIP Adv.* **7** 055315
[155] Torres C A, North T C and Aurgonzeb D M 2017 Graphene based conformal heat sink and method therefor *Google Patents*
[156] Shih Y-M and Hsu H-Y 2018 Graphite heat sink *Google Patents*
[157] Xu Z and Gao C 2015 Graphene fiber: a new trend in carbon fibers *Mater. Today* **18** 480–92
[158] Xin G, Yao T, Sun H, Scott S M, Shao D, Wang G and Lian J 2015 Highly thermally conductive and mechanically strong graphene fibers *Science* **349** 1083–7
[159] Xu Z *et al* 2016 Ultrastiff and strong graphene fibers via full-scale synergetic defect engineering *Adv. Mater.* **28** 6449–56
[160] Xin G, Zhu W, Deng Y, Cheng J, Zhang L T, Chung A J, De S and Lian J 2019 Microfluidics-enabled orientation and microstructure control of macroscopic graphene fibres *Nat. Nanotechnol.* **14** 168–75
[161] Naito K, Tanaka Y, Yang J-M and Kagawa Y 2008 Tensile properties of ultrahigh strength PAN-based, ultrahigh modulus pitch-based and high ductility pitch-based carbon fibers *Carbon* **46** 189–95
[162] Adams P M, Katzman H A, Rellick G S and Stupian G W 1998 Characterization of high thermal conductivity carbon fibers and a self-reinforced graphite panel *Carbon* **36** 233–45
[163] Li Z, Xu Z, Liu Y, Wang R and Gao C 2016 Multifunctional non-woven fabrics of interfused graphene fibres *Nat. Commun.* **7** 13684
[164] Sun P, Chen Q, Li X, Liu H, Wang K, Zhong M, Wei J, Wu D, Ma R and Sasaki T 2015 Highly efficient quasi-static water desalination using monolayer graphene oxide/titania hybrid laminates *NPG Asia Mater.* **7** e162
[165] Su Y, Kravets V G, Wong S L, Waters J, Geim A K and Nair R R 2014 Impermeable barrier films and protective coatings based on reduced graphene oxide *Nat. Commun.* **5** 4843
[166] Aqeeli M, Leng T, Huang X, Chen J C, Chang K H, Alburaikan A and Hu Z 2015 Electromagnetic interference shielding based on highly flexible and conductive graphene laminate *Electron. Lett.* **51** 1350–2
[167] Wang N, Chen S, Nkansah A, Darmawan C C, Ye L and Liu J 2018 Highly thermally conductive and light weight copper/graphene film laminated composites for cooling applications *2018 19th Int. Conf. on Electronic Packaging Technology (ICEPT)* (IEEE) pp 1588–92
[168] Preston D J, Mafra D L, Miljkovic N, Kong J and Wang E N 2015 Scalable graphene coatings for enhanced condensation heat transfer *Nano Lett.* **15** 2902–9
[169] Li X *et al* 2009 Large-area synthesis of high-quality and uniform graphene films on copper foils *Science* **324** 1312–4
[170] Liu G, Jin W and Xu N 2015 Graphene-based membranes *Chem. Soc. Rev.* **44** 5016–30
[171] Mortazavi B and Rabczuk T 2015 Multiscale modeling of heat conduction in graphene laminates *Carbon* **85** 1–7
[172] Xie Y, Yuan P, Wang T, Hashemi N and Wang X 2016 Switch on the high thermal conductivity of graphene paper *Nanoscale* **8** 17581–97
[173] Papageorgiou D G, Kinloch I A and Young R J 2017 Mechanical properties of graphene and graphene-based nanocomposites *Prog. Mater. Sci.* **90** 75–127
[174] Huang Y, Ouyang Q, Guo Q, Guo X, Zhang G and Zhang D 2016 Graphite film/aluminum laminate composites with ultrahigh thermal conductivity for thermal management applications *Mater. Des.* **90** 508–15
[175] Wang Z, Mao B, Wang Q, Yu J, Dai J, Song R, Pu Z, He D, Wu Z and Mu S 2018 Ultrahigh conductive copper/large flake size graphene heterostructure thin-film with remarkable electromagnetic interference shielding effectiveness *Small* **14** 1704332
[176] Loeblein M, Tsang S H, Pawlik M, Phua E J R, Yong H, Zhang X W, Gan C L and Teo E H T 2017 High-density 3D-boron nitride and 3D-graphene for high-performance nano-thermal interface material *ACS Nano* **11** 2033–44
[177] Pettes M T, Ji H, Ruoff R S and Shi L 2012 Thermal transport in three-dimensional foam architectures of few-layer graphene and ultrathin graphite *Nano Lett.* **12** 2959–64
[178] Calmidi V V and Mahajan R L 1999 The effective thermal conductivity of high porosity fibrous metal foams *J. Heat Transf.* **121** 466–71
[179] Zhang X *et al* 2014 Exceptional thermal interface properties of a three-dimensional graphene foam *Carbon* **66** 201–9
[180] Kuang J, Liu L, Gao Y, Zhou D, Chen Z, Han B and Zhang Z 2013 A hierarchically structured graphene foam and its potential as a large-scale strain-gauge sensor *Nanoscale* **5** 12171–7
[181] Lv P, Tan X-W, Yu K-H, Zheng R-L, Zheng J-J and Wei W 2016 Super-elastic graphene/carbon nanotube aerogel: a novel thermal interface material with highly thermal transport properties *Carbon* **99** 222–8
[182] Zeng X, Yao Y, Gong Z, Wang F, Sun R, Xu J and Wong C-P 2015 Ice-templated assembly strategy to construct 3D boron nitride nanosheet networks in polymer composites for thermal conductivity improvement *Small* **11** 6205–13
[183] An F, Li X, Min P, Liu P, Jiang Z-G and Yu Z-Z 2018 Vertically aligned high-quality graphene foams for anisotropically conductive polymer composites with ultrahigh through-plane thermal conductivities *ACS Appl. Mater. Interfaces* **10** 17383–92
[184] Zhamu A and Jang B Z 2017 Chemical-free production of 3D graphene-carbon hybrid foam *Google Patents*
[185] Liang Q, Yao X, Wang W, Liu Y and Wong C P 2011 A three-dimensional vertically aligned functionalized multilayer graphene architecture: an approach for graphene-based thermal interfacial materials *ACS Nano* **5** 2392–401
[186] Zhang Y-F, Han D, Zhao Y-H and Bai S-L 2016 High-performance thermal interface materials consisting of vertically aligned graphene film and polymer *Carbon* **109** 552–7

[187] Wang N, Chen S, Nkansah A, Ye L and Liu J 2018 Light-weight compressible and highly thermal conductive graphene-based thermal interface material *2018 7th Electronic System-Integration Technology Conf. (ESTC)* pp 1–5
[188] Wang N, Chen S, Nkansah A, Wang Q, Wang X, Chen M, Ye L and Liu J 2018 Vertically aligned graphene-based thermal interface material with high thermal conductivity *2018 24rd Int. Workshop on Thermal Investigations of ICs and Systems (THERMINIC)* pp 1–4
[189] Zhang J, Shi G, Jiang C, Ju S and Jiang D 2015 3D Bridged carbon nanoring/graphene hybrid paper as a high-performance lateral heat spreader *Small* **11** 6197–204
[190] Dai W *et al* 2019 A paper-like inorganic thermal interface material composed of hierarchically structured graphene/silicon carbide nanorods *ACS Nano* **13** 1547–54
[191] Hansson J, Nilsson T M J, Ye L and Liu J 2018 Novel nanostructured thermal interface materials: a review *Int. Mater. Rev.* **63** 22–45
[192] Varshney V, Patnaik S S, Roy A K, Froudakis G and Farmer B L 2010 Modeling of thermal transport in pillared-graphene architectures *ACS Nano* **4** 1153–61
[193] Lee J, Varshney V, Brown J S, Roy A K and Farmer B L 2012 Single mode phonon scattering at carbon nanotube-graphene junction in pillared graphene structure *Appl. Phys. Lett.* **100** 183111
[194] Park J and Prakash V 2014 Phonon scattering and thermal conductivity of pillared graphene structures with carbon nanotube-graphene intramolecular junctions *J. Appl. Phys.* **116** 014303
[195] Xu L, Wei N, Zheng Y, Fan Z, Wang H-Q and Zheng J-C 2011 Graphene-nanotube 3D networks: intriguing thermal and mechanical properties *J. Mater. Chem.* **22** 1435–44
[196] Zhu Y *et al* 2012 A seamless three-dimensional carbon nanotube graphene hybrid material *Nat. Commun.* **3** 1225
[197] Tang C, Zhang Q, Zhao M-Q, Tian G-L and Wei F 2014 Resilient aligned carbon nanotube/graphene sandwiches for robust mechanical energy storage *Nano Energy* **7** 161–9
[198] Sun S, Samani M K, Fu Y, Xu T, Ye L, Satwara M, Jeppson K, Nilsson T, Sun L and Liu J 2018 Improving thermal transport at carbon hybrid interfaces by covalent bonds *Adv. Mater. Interfaces* **5** 1800318
[199] Hansson J, Samani M K, Nylander A, Ye L, Wang N, Nilsson T and Liu J 2018 Synthesis of a graphene carbon nanotube hybrid film by joule self-heating CVD for Thermal Applications *2018 IEEE 68th Electronic Components and Technology Conf. (ECTC)* pp 2450–6
[200] Buongiorno J *et al* 2009 A benchmark study on the thermal conductivity of nanofluids *J. Appl. Phys.* **106** 94312
[201] Ghozatloo A, Rashidi A and Shariaty-Niassar M 2014 Convective heat transfer enhancement of graphene nanofluids in shell and tube heat exchanger *Exp. Therm. Fluid Sci.* **53** 136–41
[202] Imani-Mofrad P, Zeinali Heris S and Shanbedi M 2018 Experimental investigation of the effect of different nanofluids on the thermal performance of a wet cooling tower using a new method for equalization of ambient conditions *Energy Convers. Manag.* **158** 23–35
[203] Theres Baby T and Ramaprabhu S 2011 *Enhanced Convective Heat Transfer Using Graphene Dispersed Nanofluids Nanoscale Res. Lett.* **6** 289
[204] Sadeghinezhad E, Mehrali M, Rosen M A, Akhiani A R, Tahan Latibari S, Mehrali M and Metselaar H S C 2016 Experimental investigation of the effect of graphene nanofluids on heat pipe thermal performance *Appl. Therm. Eng.* **100** 775–87
[205] Nazari M A, Ghasempour R, Ahmadi M H, Heydarian G and Shafii M B 2018 Experimental investigation of graphene oxide nanofluid on heat transfer enhancement of pulsating heat pipe *Int. Commun. Heat Mass Transf.* **91** 90–4
[206] Nayak V U and Prabhu N K 2016 Wetting behavior and heat transfer of aqueous graphene nanofluids *J. Mater. Eng. Perform.* **25** 1474–80
[207] Cabaleiro D, Colla L, Barison S, Lugo L, Fedele L and Bobbo S 2017 Heat transfer capability of (ethylene glycol + water)-based nanofluids containing graphene nanoplatelets: design and thermophysical profile *Nanoscale Res. Lett.* **12** 53
[208] Kole M and Dey T K 2013 Investigation of thermal conductivity, viscosity, and electrical conductivity of graphene based nanofluids *J. Appl. Phys.* **113** 84307
[209] Bahaya B, Johnson D W and Yavuzturk C C 2018 On the effect of graphene nanoplatelets on water–graphene nanofluid thermal conductivity, viscosity, and heat transfer under laminar external flow conditions *J. Heat. Transf.* **140** 064501
[210] Anoop K B, Kabelac S, Sundararajan T and Das S K 2009 Rheological and flow characteristics of nanofluids: influence of electroviscous effects and particle agglomeration *J. Appl. Phys.* **106** 034909
[211] Rodríguez-Laguna M R *et al* 2018 Mechanisms behind the enhancement of thermal properties of graphene nanofluids *Nanoscale* **10** 15402–9
[212] Khan N S, Zuhra S, Shah Z, Bonyah E, Khan W and Islam S 2018 Slip flow of Eyring-Powell nanoliquid film containing graphene nanoparticles *AIP Adv.* **8** 115302
[213] Pollack G L 1969 Kapitza resistance *Rev. Mod. Phys.* **41** 48–81
[214] Swartz E T and Pohl R O 1989 Thermal boundary resistance *Rev. Mod. Phys.* **61** 605–68
[215] Kim B H, Beskok A and Cagin T 2008 Thermal interactions in nanoscale fluid flow: molecular dynamics simulations with solid–liquid interfaces *Microfluid. Nanofluidics* **5** 551–9
[216] Kim B H, Beskok A and Cagin T 2008 Molecular dynamics simulations of thermal resistance at the liquid-solid interface *J. Chem. Phys.* **129** 174701
[217] Kim B H, Beskok A and Cagin T 2010 Viscous heating in nanoscale shear driven liquid flows *Microfluid. Nanofluidics* **9** 31–40
[218] Thekkethala J F and Sathian S P 2015 The effect of graphene layers on interfacial thermal resistance in composite nanochannels with flow *Microfluid. Nanofluidics* **18** 637–48
[219] Yazid M N A W M, Sidik N A C and Yahya W J 2017 Heat and mass transfer characteristics of carbon nanotube nanofluids: a review *Renew. Sustain. Energy Rev.* **80** 914–41
[220] Albojamal A and Vafai K 2017 Analysis of single phase, discrete and mixture models, in predicting nanofluid transport *Int. J. Heat Mass Transf.* **114** 225–37
[221] Sadri R, Mallah A R, Hosseini M, Ahmadi G, Kazi S N, Dabbagh A, Yeong C H, Ahmad R and Yaakup N A 2018 CFD modeling of turbulent convection heat transfer of nanofluids containing green functionalized graphene nanoplatelets flowing in a horizontal tube: comparison with experimental data *J. Mol. Liq.* **269** 152–9
[222] Sajjad M, Kamran M S, Shaukat R and Zeinelabdeen M I M 2018 Numerical investigation of laminar convective heat transfer of graphene oxide/ethylene glycol-water nanofluids in a horizontal tube *Eng. Sci. Technol. Int. J.* **21** 727–35
[223] Cassabois G, Valvin P and Gil B 2016 Hexagonal boron nitride is an indirect bandgap semiconductor *Nat. Photon.* **10** 262–6
[224] Liu D *et al* 2019 Conformal hexagonal-boron nitride dielectric interface for tungsten diselenide devices with improved mobility and thermal dissipation *Nat. Commun.* **10** 1188
[225] Yang N, Zeng X, Lu J, Sun R and Wong C-P 2018 Effect of chemical functionalization on the thermal conductivity of 2D hexagonal boron nitride *Appl. Phys. Lett.* **113** 171904
[226] Ren L, Zeng X, Sun R, Xu J-B and Wong C-P 2019 Spray-assisted assembled spherical boron nitride as fillers for polymers with enhanced thermally conductivity *Chem. Eng. J.* **370** 166–75
[227] Zhang T, Sun J, Ren L, Yao Y, Wang M, Zeng X, Sun R, Xu J-B and Wong C-P 2019 Nacre-inspired polymer composites with high thermal conductivity and enhanced mechanical strength *Compos. Part Appl. Sci. Manuf.* **121** 92–9
[228] Sun N, Sun J, Zeng X, Chen P, Qian J, Xia R and Sun R 2018 Hot-pressing induced orientation of boron nitride in polycarbonate composites with enhanced thermal conductivity *Compos. Part Appl. Sci. Manuf.* **110** 45–52

[229] Sun J, Yao Y, Zeng X, Pan G, Hu J, Huang Y, Sun R, Xu J-B and Wong C-P 2017 Preparation of boron nitride nanosheet/nanofibrillated cellulose nanocomposites with ultrahigh thermal conductivity via engineering interfacial thermal resistance *Adv. Mater. Interfaces* **4** 1700563
[230] Shen H, Guo J, Wang H, Zhao N and Xu J 2015 Bioinspired modification of *h*-BN for high thermal conductive composite films with aligned structure *ACS Appl. Mater. Interfaces* **7** 5701–8
[231] He J, Li D, Ying Y, Feng C, He J, Zhong C, Zhou H, Zhou P and Zhang G 2019 Orbitally driven giant thermal conductance associated with abnormal strain dependence in hydrogenated graphene-like borophene *Npj Comput. Mater.* **5** 47
[232] Peng B, Zhang H, Shao H, Xu Y, Zhang X and Zhu H 2016 Thermal conductivity of monolayer MoS_2, $MoSe_2$, and WS_2: interplay of mass effect, interatomic bonding and anharmonicity *RSC Adv.* **6** 5767–73
[233] Bae J J, Jeong H Y, Han G H, Kim J, Kim H, Kim M S, Moon B H, Lim S C and Lee Y H 2017 Thickness-dependent in-plane thermal conductivity of suspended MoS_2 grown by chemical vapor deposition *Nanoscale* **9** 2541–7
[234] Jo I, Pettes M T, Ou E, Wu W and Shi L 2014 Basal-plane thermal conductivity of few-layer molybdenum disulfide *Appl. Phys. Lett.* **104** 201902
[235] Sledzinska M *et al* 2016 Thermal conductivity of MoS_2 polycrystalline nanomembranes *2D Mater.* **3** 035016
[236] Sledzinska M *et al* 2017 Record low thermal conductivity of polycrystalline MoS_2 films: tuning the thermal conductivity by grain orientation *ACS Appl. Mater. Interfaces* **9** 37905
[237] Mahesh K V, Linsha V, Mohamed A P and Ananthakumar S 2016 Processing of 2D-MAXene nanostructures and design of high thermal conducting, rheo-controlled MAXene nanofluids as a potential nanocoolant *Chem. Eng. J.* **297** 158–69
[238] Chen L, Shi X, Yu N, Zhang X, Du X and Lin J 2018 Measurement and analysis of thermal conductivity of $Ti_3C_2T_x$ MXene films *Mater.* **11** 1701
[239] Li H and Zhang R 2012 Vacancy-defect–induced diminution of thermal conductivity in silicene *EPL Europhys. Lett.* **99** 36001
[240] Hu M, Zhang X and Poulikakos D 2013 Anomalous thermal response of silicene to uniaxial stretching *Phys. Rev.* B **87** 195417
[241] Pei Q-X, Zhang Y-W, Sha Z-D and Shenoy V B 2013 Tuning the thermal conductivity of silicene with tensile strain and isotopic doping: a molecular dynamics study *J. Appl. Phys.* **114** 033526
[242] Ng T Y, Yeo J and Liu Z 2013 Molecular dynamics simulation of the thermal conductivity of shorts strips of graphene and silicene: a comparative study *Int. J. Mech. Mater. Des.* **9** 105–14
[243] Das D and Sarkar J 2018 Multiscale modeling of thermal properties of silicene using molecular dynamics *Mod. Phys. Lett.* B **32** 1–10
[244] Xie H, Hu M and Bao H 2014 Thermal conductivity of silicene from first-principles *Appl. Phys. Lett.* **104** 131906
[245] Peng B, Zhang H, Shao H, Xu Y, Zhang X and Zhu H 2016 Low lattice thermal conductivity of stanene *Sci. Rep.* **6** 20225
[246] Jomehpour Zaveh S, Roknabadi M R, Morshedloo T and Modarresi M 2016 Electronic and thermal properties of germanene and stanene by first-principles calculations *Superlattices Microstruct.* **91** 383–90
[247] Balatero M, Paylaga G, Paylaga N and Bantaculo R 2015 Molecular dynamics simulations of thermal conductivity of germanene nanoribbons (GeNR) with armchair and zigzag chirality *Appl. Mech. Mater.* **772** 67–71
[248] Jo I, Pettes M T, Kim J, Watanabe K, Taniguchi T, Yao Z and Shi L 2013 Thermal conductivity and phonon transport in suspended few-layer hexagonal boron nitride *Nano Lett.* **13** 550–4
[249] Lin Z, Liu Y, Raghavan S, Moon K, Sitaraman S K and Wong C 2013 Magnetic alignment of hexagonal boron nitride platelets in polymer matrix: toward high performance anisotropic polymer composites for electronic encapsulation *ACS Appl. Mater. Interfaces* **5** 7633–40
[250] Aoki H and Dresselhaus M S 2014 *Physics of Graphene* (Cham: Springer)
[251] Wei Z, Ni Z, Bi K, Chen M and Chen Y 2011 Interfacial thermal resistance in multilayer graphene structures *Phys. Lett.* A **375** 1195–9
[252] Ni Y, Chalopin Y and Volz S 2013 Significant thickness dependence of the thermal resistance between few-layer graphenes *Appl. Phys. Lett.* **103** 061906
[253] Ni Y, Chalopin Y and Volz S 2012 Calculation of inter-plane thermal resistance of few-layer graphene from equilibrium molecular dynamics simulations *J. Phys.: Conf. Ser.* **395** 012106
[254] Rajabpour A and Volz S 2010 Thermal boundary resistance from mode energy relaxation times: case study of argon-like crystals by molecular dynamics *J. Appl. Phys.* **108** 094324
[255] Ni Y, Kosevich Y A, Xiong S, Chalopin Y and Volz S 2014 Substrate-induced cross-plane thermal propagative modes in few-layer graphene *Phys. Rev.* B **89** 205413
[256] Ni Y, Chalopin Y and Volz S 2013 Few layer graphene based superlattices as efficient thermal insulators *Appl. Phys. Lett.* **103** 141905
[257] Mak K F, Lui C H and Heinz T F 2010 Measurement of the thermal conductance of the graphene/SiO_2 interface *Appl. Phys. Lett.* **97** 221904
[258] Han H *et al* 2016 Functionalization mediates heat transport in graphene nanoflakes *Nat. Commun.* **7** 11281
[259] Wang H, Gong J, Pei Y and Xu Z 2013 Thermal transfer in graphene-interfaced materials: contact resistance and interface engineering *ACS Appl. Mater. Interfaces* **5** 2599–603
[260] Luo T and Lloyd J R 2012 Enhancement of thermal energy transport across graphene/graphite and polymer interfaces: a molecular dynamics study *Adv. Funct. Mater.* **22** 2495–502
[261] Chen J, Zhang G and Li B 2012 Substrate coupling suppresses size dependence of thermal conductivity in supported graphene *Nanoscale* **5** 532–6
[262] Li M, Zhang J, Hu X and Yue Y 2015 Thermal transport across graphene/SiC interface: effects of atomic bond and crystallinity of substrate *Appl. Phys. Mater. Sci. Process.* **119** 415–24
[263] Zhang H, Wang H, Xiong S, Han H, Volz S and Ni Y 2018 Multiscale modeling of heat dissipation in 2D transistors based on phosphorene and silicene *J. Phys. Chem.* C **122** 2641–7
[264] Chen J, Walther J H and Koumoutsakos P 2014 Strain engineering of kapitza resistance in few-layer graphene *Nano Lett.* **14** 819–25
[265] Yang L, Chen J, Yang N and Li B 2015 Significant reduction of graphene thermal conductivity by phononic crystal structure *Int. J. Heat Mass Transf.* **91** 428–32
[266] Guo B, Fang L, Zhang B and Gong J R 2011 Graphene doping: a review *Insciences J.* **1** 80–9
[267] Shi J H, Yang G, Li X L and Huang X 2015 Interfacial thermal resistance and thermal rectification in graphene with geometric variations of doped nitrogen: a molecular dynamics study *Adv. Mater. Res.* **1081** 338–42
[268] Hu S, Chen J, Yang N and Li B 2017 Thermal transport in graphene with defect and doping: phonon modes analysis *Carbon* **116** 139–44
[269] Li X, Chen J, Yu C and Zhang G 2013 Comparison of isotope effects on thermal conductivity of graphene nanoribbons and carbon nanotubes *Appl. Phys. Lett.* **103** 013111
[270] Han H *et al* 2016 Functionalization mediates heat transport in graphene nanoflakes *Nat. Commun.* **7** 11281
[271] Cahill D G, Ford W K, Goodson K E, Mahan G D, Majumdar A, Maris H J, Merlin R and Phillpot S R 2002 Nanoscale thermal transport *J. Appl. Phys.* **93** 793–818
[272] Cahill D G *et al* 2014 Nanoscale thermal transport. II. 2003–2012 *Appl. Phys. Rev.* **1** 011305
[273] Aiyiti A, Bai X, Wu J, Xu X and Li B 2018 Measuring the thermal conductivity and interfacial thermal resistance

of suspended MoS_2 using electron beam self-heating technique *Sci. Bull.* **63** 452–8
[274] Xu X *et al* 2010 Phonon transport in suspended single layer graphene (arXiv:1012.2937)
[275] Pettes M T, Jo I, Yao Z and Shi L 2011 Influence of polymeric residue on the thermal conductivity of suspended bilayer graphene *Nano Lett.* **11** 1195–200
[276] Wang Z, Xie R, Bui C T, Liu D, Ni X, Li B and Thong J T L 2011 Thermal transport in suspended and supported few-layer graphene *Nano Lett.* **11** 113–8
[277] Wang J, Zhu L, Chen J, Li B and Thong J T L 2013 Suppressing thermal conductivity of suspended tri-layer graphene by gold deposition *Adv. Mater.* **25** 6884–8
[278] Wang C, Guo J, Dong L, Aiyiti A, Xu X and Li B 2016 Superior thermal conductivity in suspended bilayer hexagonal boron nitride *Sci. Rep.* **6** 25334
[279] Guo J, Wang C-R, Dong L and Xu X-F 2017 Thickness-dependent thermal conductivity in suspended fewer-layer boron nitride *K. Cheng Je Wu Li Hsueh PaoJournal Eng. Thermophys.* **38** 2220–4
[280] Luo Z, Maassen J, Deng Y, Du Y, Garrelts R P, Lundstrom M S, Ye P D and Xu X 2015 Anisotropic in-plane thermal conductivity observed in few-layer black phosphorus *Nat. Commun.* **6** 8572
[281] Lee S *et al* 2015 Anisotropic in-plane thermal conductivity of black phosphorus nanoribbons at temperatures higher than 100 K *Nat. Commun.* **6** 8573
[282] Zhao Y *et al* 2018 Probing the physical origin of anisotropic thermal transport in black phosphorus nanoribbons *Adv. Mater.* **30** 1804928
[283] Aiyiti A *et al* 2018 Thermal conductivity of suspended few-layer MoS_2 *Nanoscale* **10** 2727–34
[284] Yarali M *et al* 2017 Effects of defects on the temperature-dependent thermal conductivity of suspended monolayer molybdenum disulfide grown by chemical vapor deposition *Adv. Funct. Mater.* **27** 1704357
[285] Yarali M, Brahmi H, Yan Z, Li X, Xie L, Chen S, Kumar S, Yoon M, Xiao K and Mavrokefalos A 2018 Effect of metal doping and vacancies on the thermal conductivity of monolayer molybdenum diselenide *ACS Appl. Mater. Interfaces* **10** 4921–8
[286] Guo J, Huang Y, Wu X, Wang Q, Zhou X, Xu X and Li B 2019 Thickness-dependent in-plane thermal conductivity and enhanced thermoelectric performance in p-Type $ZrTe_5$ nanoribbons *Phys. Status Solidi* **13** 1800529
[287] Liu D, Xie R, Yang N, Li B and Thong J T L 2014 Profiling nanowire thermal resistance with a spatial resolution of nanometers *Nano Lett.* **14** 806–12
[288] Aiyiti A, Zhang Z, Chen B, Hu S, Chen J, Xu X and Li B 2018 Thermal rectification in Y-junction carbon nanotube bundle *Carbon* **140** 673–9
[289] Dong L, Xi Q, Chen D, Guo J, Nakayama T, Li Y, Liang Z, Zhou J, Xu X and Li B 2018 Dimensional crossover of heat conduction in amorphous polyimide nanofibers *Natl Sci. Rev.* **5** 500–6
[290] Yu Y-J, Han M Y, Berciaud S, Georgescu A B, Heinz T F, Brus L E, Kim K S and Kim P 2011 High-resolution spatial mapping of the temperature distribution of a Joule self-heated graphene nanoribbon *Appl. Phys. Lett.* **99** 183105
[291] Grosse K L, Dorgan V E, Estrada D, Wood J D, Vlassiouk I, Eres G, Lyding J W, King W P and Pop E 2014 Direct observation of resistive heating at graphene wrinkles and grain boundaries *Appl. Phys. Lett.* **105** 143109
[292] Yalon E *et al* 2017 Energy dissipation in monolayer MoS_2 electronics *Nano Lett.* **17** 3429–33
[293] Pumarol M E, Rosamond M C, Tovee P, Petty M C, Zeze D A, Falko V and Kolosov O V 2012 Direct nanoscale imaging of ballistic and diffusive thermal transport in graphene nanostructures *Nano Lett.* **12** 2906–11
[294] Sachat A E, Köenemann F, Menges F, Corro E D, Garrido J A, Torres C M S, Alzina F and Gotsmann B 2019 Crossover from ballistic to diffusive thermal transport in suspended graphene membranes *2D Mater.* **6** 025034
[295] Ghosh S, Nika D L, Pokatilov E P and Balandin A A 2009 Heat conduction in graphene: experimental study and theoretical interpretation *New J. Phys.* **11** 095012
[296] Balandin A A, Ghosh S, Nika D L and Pokatilov E P 2010 Thermal conduction in suspended graphene layers *Fuller. Nanotub. Carbon Nanostructures* **18** 474–86
[297] Nika D L, Pokatilov E P and Balandin A A 2011 Theoretical description of thermal transport in graphene: the issues of phonon cut-off frequencies and polarization branches *Phys. Status Solidi* b **248** 2609–14
[298] Lee J-U, Yoon D, Kim H, Lee S W and Cheong H 2011 Thermal conductivity of suspended pristine graphene measured by Raman spectroscopy *Phys. Rev.* B **83** 081419
[299] Yan R, Simpson J R, Bertolazzi S, Brivio J, Watson M, Wu X, Kis A, Luo T, Hight Walker A R and Xing H G 2014 Thermal conductivity of monolayer molybdenum disulfide obtained from temperature-dependent Raman spectroscopy *ACS Nano* **8** 986–93
[300] Sahoo S, Gaur A P S, Ahmadi M, Guinel M J-F and Katiyar R S 2013 Temperature-dependent raman studies and thermal conductivity of few-layer MoS_2 *J. Phys. Chem.* C **117** 9042–7
[301] Peimyoo N, Shang J, Yang W, Wang Y, Cong C and Yu T 2015 Thermal conductivity determination of suspended mono- and bilayer WS_2 by Raman spectroscopy *Nano Res.* **8** 1210–21
[302] Zhang X, Sun D, Li Y, Lee G-H, Cui X, Chenet D, You Y, Heinz T F and Hone J C 2015 Measurement of lateral and interfacial thermal conductivity of single- and bilayer MoS_2 and $MoSe_2$ using refined optothermal raman technique *ACS Appl. Mater. Interfaces* **7** 25923–9
[303] Yan Z, Jiang C, Pope T R, Tsang C F, Stickney J L, Goli P, Renteria J, Salguero T T and Balandin A A 2013 Phonon and thermal properties of exfoliated $TaSe_2$ thin films *J. Appl. Phys.* **114** 204301
[304] Malekpour H and Balandin A A 2018 Raman-based technique for measuring thermal conductivity of graphene and related materials *J. Raman Spectrosc.* **49** 106–20
[305] Reparaz J S, Chavez-Angel E, Wagner M R, Graczykowski B, Gomis-Bresco J, Alzina F and Sotomayor Torres C M 2014 A novel contactless technique for thermal field mapping and thermal conductivity determination: two-laser Raman thermometry *Rev. Sci. Instrum.* **85** 034901
[306] Käding O W, Skurk H and Goodson K E 1994 Thermal conduction in metallized silicon-dioxide layers on silicon *Appl. Phys. Lett.* **65** 1629–31
[307] Ujihara K 1972 Reflectivity of metals at high temperatures *J. Appl. Phys.* **43** 2376–83
[308] Jing L *et al* 2017 Thermal conductivity enhancement of coaxial carbon@boron nitride nanotube arrays *ACS Appl. Mater. Interfaces* **9** 14555–60
[309] Samani M K, Ding X Z, Khosravian N, Amin-Ahmadi B, Yi Y, Chen G, Neyts E C, Bogaerts A and Tay B K 2015 Thermal conductivity of titanium nitride/titanium aluminum nitride multilayer coatings deposited by lateral rotating cathode arc *Thin Solid Films* **578** 133–8
[310] Zhang Q G, Cao B Y, Zhang X, Fujii M and Takahashi K 2006 Size effects on the thermal conductivity of polycrystalline platinum nanofilms *J. Phys.: Condens. Matter* **18** 7937–7950
[311] Ragab T and Basaran C 2009 Joule heating in single-walled carbon nanotubes *J. Appl. Phys.* **106** 063705
[312] Chu Y, Ragab T and Basaran C 2015 Temperature dependence of joule heating in zigzag graphene nanoribbon *Carbon* **89** 169–75
[313] Wang N, Logothetis N, Mu Wei, Shirong Huang, Lilei Ye and Johan Liu 2016 Development and characterization of graphene enhanced thermal conductive adhesives *2016 6th Electronic System-Integration Technology Conf. (ESTC)* pp 1–6

[314] Corbino O M 1911 Periodic variation of resistance of metallic filaments on alternating current *Atti Della R. Accad. Naz. Dei Lincei* **20** 222–8
[315] Corbino O M 1912 Measurement of specific heats of metals at high temperatures *Atti Della R. Accad. Naz. Dei Lincei* **21** 181–8
[316] Birge N O and Nagel S R 1987 Wide-frequency specific heat spectrometer *Rev. Sci. Instrum.* **58** 1464–70
[317] Cahill D G and Pohl R O 1987 Thermal conductivity of amorphous solids above the plateau *Phys. Rev.* B **35** 4067–73
[318] Cometto O, Samani M K, Liu B, Sun S, Tsang S H, Liu J, Zhou K and Teo E H T 2017 Control of nanoplane orientation in vobn for high thermal anisotropy in a dielectric thin film: a new solution for thermal hotspot mitigation in electronics *ACS Appl. Mater. Interfaces* **9** 7456–64
[319] Sun T, Samani M K, Khosravian N, Ang K M, Yan Q, Tay B K and Hng H H 2014 Enhanced thermoelectric properties of n-type $Bi_2Te_{2.7}Se_{0.3}$ thin films through the introduction of Pt nanoinclusions by pulsed laser deposition *Nano Energy* **8** 223–30
[320] Banerjee D, Vallin Ö, Samani K M, Majee S, Zhang S-L, Liu J and Zhang Z-B 2018 Elevated thermoelectric figure of merit of n-type amorphous silicon by efficient electrical doping process *Nano Energy* **44** 89–94
[321] Zeng Y and Marconnet A 2017 A direct differential method for measuring thermal conductivity of thin films *Rev. Sci. Instrum.* **88** 044901
[322] Chen Z, Jang W, Bao W, Lau C N and Dames C 2009 Thermal contact resistance between graphene and silicon dioxide *Appl. Phys. Lett.* **95** 161910
[323] Gustafsson S E 1991 Transient plane source techniques for thermal conductivity and thermal diffusivity measurements of solid materials *Rev. Sci. Instrum.* **62** 797–804
[324] Gustavsson M, Karawacki E and Gustafsson S E 1994 Thermal conductivity, thermal diffusivity, and specific heat of thin samples from transient measurements with hot disk sensors *Rev. Sci. Instrum.* **65** 3856–9
[325] Ramirez S, Chan K, Hernandez R, Recinos E, Hernandez E, Salgado R, Khitun A G, Garay J E and Balandin A A 2017 Thermal and magnetic properties of nanostructured densified ferrimagnetic composites with graphene—graphite fillers *Mater. Des.* **118** 75–80
[326] Wang S, Tambraparni M, Qiu J, Tipton J and Dean D 2009 Thermal expansion of graphene composites *Macromolecules* **42** 5251–5
[327] Parker W J, Jenkins R J, Butler C P and Abbott G L 1961 Flash method of determining thermal diffusivity, heat capacity, and thermal conductivity *J. Appl. Phys.* **32** 1679–84
[328] Cowan R D 1963 Pulse method of measuring thermal diffusivity at high temperatures *J. Appl. Phys.* **34** 926–7
[329] Cape J A and Lehman G W 1963 Temperature and finite pulse-time effects in the flash method for measuring thermal diffusivity *J. Appl. Phys.* **34** 1909–13
[330] Lee T Y R, Donaldson A B and Taylor R E 1978 Thermal diffusivity of layered composites *Thermal Conductivity* vol 15 ed V V Mirkovich (Boston, MA: Springer) pp 135–48
[331] Milošević N, Raynaud M and Maglić K 2002 Estimation of thermal Contact resistance between the materials of double-layer sample using the laser flash method *Inverse Problems Eng.* **10** 85–103
[332] Donaldson A B and Taylor R E 1975 Thermal diffusivity measurement by a radial heat flow method *J. Appl. Phys.* **46** 4584–9
[333] Jeon D, Kim S H, Choi W and Byon C 2019 An experimental study on the thermal performance of cellulose-graphene-based thermal interface materials *Int. J. Heat Mass Transf.* **132** 944–51
[334] Lin C-Y and Liu W-R 2019 Synthesis and characterizations of graphene-based composite film for thermal dissipation *J. Alloys Compd.* **790** 156–62
[335] Hsieh C-C and Liu W-R 2017 Synthesis and characterization of nitrogen-doped graphene nanosheets/copper composite film for thermal dissipation *Carbon* **118** 1–7
[336] Huang Y, Gong Q, Zhang Q, Shao Y, Wang J, Jiang Y, Zhao M, Zhuang D and Liang J 2017 Fabrication and molecular dynamics analyses of highly thermal conductive reduced graphene oxide films at ultra-high temperatures *Nanoscale* **9** 2340–7
[337] Zhao Y-H, Wu Z-K and Bai S-L 2016 Thermal resistance measurement of 3D graphene foam/polymer composite by laser flash analysis *Int. J. Heat Mass Transf.* **101** 470–5
[338] http://graphenelighting.co
[339] www.theglobalgraphenegroup.com/at1500
[340] Zhu Y, Ji H, Cheng H-M and Ruoff R S 2018 Mass production and industrial applications of graphene materials *Natl Sci. Rev.* **5** 90–101
[341] http://sht-tek.com/product/gf
[342] www.i-graphenelab.com/products-1/graphene-thermal-grease/